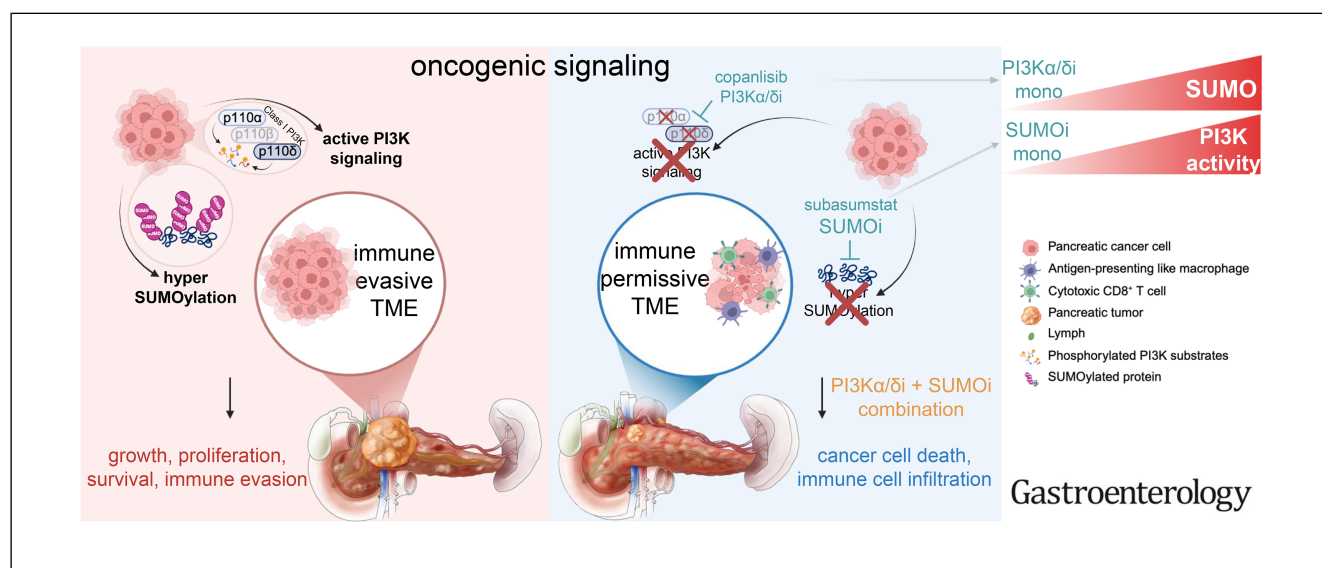


Targeting Mutual Dependence of Phosphatidylinositol-3-Kinase α/δ and Small Ubiquitin-Like Modifier Signaling in Pancreatic Cancer

Hazal Köse,^{1,2} Christian Schneeweis,³ Philipp Putze,³ Constanza Tapia Contreras,⁴ Laura Ferreiro,^{1,2} Leonie Witte,⁴ Ilaria Deidda,⁴ Frederik Herzberg,^{1,2} Sophie Ebert,⁴ Juraj Jakubik,^{5,6} Leoni Moldaner,^{5,6} Jovan Todorovic,⁷ Isabelle Träger,^{1,2} Chuanbing Zang,^{1,2} Uta M. Demel,^{1,2} Elisabeth Hessmann,^{8,9,10} Marieluise Kirchner,^{11,12} Simone Rhein,¹³ Jens Hoffmann,¹³ Zuzana Tatarova,^{5,6,14} Michael Ghadimi,⁴ Dieter Saur,^{3,15} Kai Kappert,¹⁶ Philipp Mertins,^{11,12} **Günter Schneider,**^{3,4,9,10,§} **Ulrich Keller,**^{1,2,17,§} and **Matthias Wirth**^{1,2,4,18,§}

¹Department of Hematology, Oncology and Cancer Immunology, Charité - Universitätsmedizin Berlin, corporate member of Freie Universität Berlin and Humboldt-Universität zu Berlin, Berlin, Germany; ²Max-Delbrück-Center for Molecular Medicine, Berlin, Germany; ³Institute for Translational Cancer Research and Experimental Cancer Therapy, Technical University Munich, Munich, Germany; ⁴Department of General, Visceral and Pediatric Surgery, University Medical Center Göttingen, Göttingen, Germany; ⁵Institute for Tumor Biology and Experimental Therapy, German Center for Translational Cancer Research (DKTK), Partner Site Frankfurt/Mainz, Georg-Speyer-Haus, Frankfurt, Germany; ⁶German Cancer Research Center (DKFZ), Heidelberg, Germany; ⁷Institute of Pathology, University Medical Center Göttingen, Göttingen, Germany; ⁸Department of Gastroenterology, Gastrointestinal Oncology and Endocrinology, University Medical Center Göttingen, Göttingen, Germany; ⁹CCC-N (Comprehensive Cancer Center Lower Saxony), Göttingen, Germany; ¹⁰Clinical Research Unit 5002, KFO5002, University Medical Center Göttingen, Göttingen, Germany; ¹¹Max Delbrück Center for Molecular Medicine, Berlin, Germany; ¹²Core Unit Proteomics, Berlin Institute of Health at Charité - Universitätsmedizin Berlin, Berlin, Germany; ¹³EPO, Experimental Pharmacology and Oncology Berlin-Buch GmbH, Berlin, Germany; ¹⁴Frankfurt Cancer Institute, Frankfurt, Germany; ¹⁵German Center for Translational Cancer Research (DKTK), Partner Site Munich, Munich, Germany; ¹⁶Institute of Diagnostic Laboratory Medicine, Clinical Chemistry and Pathobiochemistry, Charité - Universitätsmedizin Berlin, corporate member of Freie Universität Berlin and Humboldt-Universität zu Berlin, Berlin, Germany; ¹⁷Cluster of Excellence ImmunoPreCept, Berlin, Germany; and ¹⁸German Center for Translational Cancer Research (DKTK), Partner Site Berlin, Berlin, Germany



BACKGROUND & AIMS: Pancreatic ductal adenocarcinoma (PDAC) is a highly aggressive and lethal cancer, with a 5-year survival rate of <13%. Despite advances in diagnostics and treatments, the standard of care for PDAC remains inadequate, and most patients develop resistance to therapy. Targeted approaches, such as Kirsten rat sarcoma (KRAS) inhibition,

have shown promise in preclinical models, although clinical application remains challenged by the rapid development of resistance. The phosphatidylinositol-3-kinase (PI3K) signaling pathway is critical for PDAC development and maintenance, yet pharmacologic targeting has failed to yield significant clinical benefits. **METHODS:** To investigate the relationship

between the PI3K and small ubiquitin-like modifier (SUMO) pathways in PDAC, we used a comprehensive approach that included unbiased genome-wide clustered regularly interspaced short palindromic repeats/clustered regularly interspaced short palindromic repeats-associated protein 9 resistance screens, pharmacologic screens, transcriptomics, proteomics, and phosphoproteomics experiments. Genetic knockout models were applied to validate our findings. A novel molecularly targeted combination therapy was tested in pre-clinical mouse models. **RESULTS:** Using genetic and pharmacologic screenings, we discovered a mutual and targetable codependence between the PI3K and the SUMO pathways. Simultaneous inhibition of PIK3 α and PIK3 δ , combined with SUMO-activating E1 targeting, triggered synthetic lethality and cell death. In syngeneic orthotopic immune-competent PDAC models, this combination therapy reduced tumor growth and promoted immune cell infiltration and activity. **CONCLUSIONS:** Our study introduces a novel rational combination therapy in PDAC. Dual targeting of PI3K α/δ and SUMO signaling bears potential for clinical translation.

Keywords: Pancreatic Cancer; PI3K; SUMOylation; Regulated Cell Death; Combination Therapy.

Pancreatic ductal adenocarcinoma (PDAC) is one of the most aggressive and deadliest cancers, with a 5-year survival rate of just 13%. Despite its increasing incidence, including in younger patients, treatment options for PDAC remain limited and nonsatisfying.¹ PDAC is defined by a distinct genetic landscape, with frequent mutations in *KRAS*, *TP53*, *CDKN2A*, and *SMAD4*.² Activating *KRAS* mutations, present in 90% of cases, position the Kirsten rat sarcoma virus (*KRAS*)/mitogen-activated protein kinase signaling pathway as a central driver of tumor progression and a critical therapeutic target. Consequently, the recently developed rat sarcoma (RAS) inhibitors, including mutant-selective and pan-RAS inhibitors, have demonstrated promising early signs of clinical efficacy in PDAC.³ However, genetic and adaptive resistance to RAS inhibition remains challenging,³ underscoring the need of additional molecular targeted treatment strategies.

The phosphatidylinositol-3-kinase-(PI3K)-protein kinase B (AKT)-mechanistic target of rapamycin pathway has recently been implicated in resistance to RAS inhibitors.⁴ Furthermore, the finding that oncogenic PI3K-signaling can compensate *KRAS*-dependency to initiate and drive carcinogenesis and tumor progression in murine PDAC models^{5,6} highlights the PI3K pathway's significance as a therapeutic target. PI3K family kinases include 3 classes. Class Ia (p110 α /PIK3CA, p110 β /PIK3CB, and p110 δ /PIK3CD) and class Ib (p110 γ /PIK3CG) catalytic subunits are particularly relevant in clinical settings, with inhibitors targeting these isoforms available.⁷ PIK3CA mutations are the most common alterations within class I PI3Ks and may predict sensitivity to PI3K inhibition in preclinical PDAC models.⁷⁻⁹ Moreover, several isoform-specific PI3K inhibitors have been evaluated in clinical trials for solid tumors, including PDAC. Alpelisib (BYL-719), a PI3K α inhibitor (NCT02155088,

WHAT YOU NEED TO KNOW

BACKGROUND AND CONTEXT

Resistance to therapeutic interventions for pancreatic ductal adenocarcinoma remains challenging. Phosphatidylinositol-3-kinase signaling is critical for pancreatic ductal adenocarcinoma maintenance and progression, but pharmacologic targeting has failed to yield significant clinical benefits.

NEW FINDINGS

Simultaneous inhibition of phosphatidylinositol-3-kinase α/δ , combined with small ubiquitin-like modifier-activating E1 targeting, triggered synthetic lethality. In syngeneic immune-competent pancreatic ductal adenocarcinoma models, this combination therapy reduced tumor growth and promoted immune cell infiltration.

LIMITATIONS

Combining phosphatidylinositol-3-kinase α/δ and small ubiquitin-like modifier inhibitors triggered an immune-assisted anti-tumor response, marked by an unexpected immunophenotype, a phenomenon that requires further investigation in future studies.

CLINICAL RESEARCH RELEVANCE

The dual targeting of phosphatidylinositol-3-kinase α/δ and small ubiquitin-like modifier shows efficacy, manageable toxicity in mice and potential for clinical translation in pancreatic ductal adenocarcinoma, a cancer with significant unmet medical needs.

BASIC RESEARCH RELEVANCE

Blockade of the phosphatidylinositol-3-kinase pathway leads to the adaptive activation of the small ubiquitin-like modifier (SUMO)ylation machinery and vice versa. Only the combined inhibition of both phosphatidylinositol-3-kinase α and δ with a clinical-grade E1 small ubiquitin-like modifier inhibitor induced synergistic cell death in vitro and demonstrated synergy in an immunocompetent in vivo model. Our work highlights the unexpected requirement of phosphatidylinositol-3-kinase α and δ in the small ubiquitin-like modifier-ylation-associated stress response.

[§] Authors share co-senior authorship.

Abbreviations used in this paper: AKT, protein kinase B; Cas, clustered regularly interspaced short palindromic repeats-associated; CD, cluster of differentiation; CRISPR, clustered regularly interspaced short palindromic repeats; cyclIF, cyclic immunofluorescence; GSEA, gene set enrichment analysis; *KRAS*, Kirsten rat sarcoma viral oncogene homologue; MYC, myelocytomatosis oncogene; PDAC, pancreatic ductal adenocarcinoma; PDO, patient-derived organoid; PI3K, phosphatidylinositol-3-kinase; PI3Ki, phosphatidylinositol-3-kinase inhibitor; RAS, rat sarcoma; RCD, regulated cell death; RNAseq, RNA sequencing; SAE1, small ubiquitin-like modified-activating enzyme subunit 1; snRNA, single nuclei RNA; SOC, standard of care; SUMO, small ubiquitin-like modifier; SUMOi, small ubiquitin-like modifier E1 inhibitor; TME, tumor microenvironment.

© 2025 The Author(s). Published by Elsevier Inc. on behalf of the AGA Institute. This is an open access article under the CC BY license (<http://creativecommons.org/licenses/by/4.0/>).

0016-5085

<https://doi.org/10.1053/j.gastro.2025.08.018>

NCT02437318), has demonstrated tolerability in PDAC patients and efficacy in *PIK3CA*-mutated breast cancer.¹⁰ GSK2636771, a PI3K β inhibitor, is currently under investigation (NCT04439188) in patients with *PTEN* loss.¹¹ Eganalisib (IPI549), targeting PI3K γ (NCT02637531), has shown immune-modulation and antitumor activity when combined with nivolumab in solid tumors.¹² In contrast, idelalisib (CAL-101) and piasclisib (INCB050465), both targeting PI3K δ (NCT02468557, NCT02559492), have exhibited limited efficacy in solid tumors.^{13,14} These findings highlight the clinical potential of isoform-specific PI3K inhibitors; however, their role and targeting spectrum in the treatment of PDAC has yet to be established.

The small ubiquitin-like modifier (SUMO)ylation signaling pathway is a cellular process in which SUMOs are attached to target proteins, altering their function, stability, or localization. SUMOylation plays a crucial role in regulating processes such as transcription, DNA repair, the cell cycle, and stress responses.¹⁵ Pharmacologic targeting of the SUMO pathway has shown efficacy in PDAC and other malignancies in preclinical models.^{16,17}

To harness the therapeutic potential of PI3K-pathway inhibition in PDAC, we investigated pathway co-dependencies to inform translational strategies. We observed that blockade of the PI3K pathway leads to the adaptive activation of the SUMOylation machinery and furthermore observed a vice versa process. Only the combined inhibition of both PI3K α and PI3K δ with a clinical-grade SUMO-inhibitor induced synergistic cell death in vitro and demonstrated synergy in an immunocompetent in vivo model. Our work highlights the unexpected requirement of PI3K α and PI3K δ in the SUMO-associated stress response and unveils a novel combination therapy approach with the potential for clinical applicability.

Methods

Pharmacologic Screen

The drug library consisting of ≥ 99 inhibitors targeting various relevant cancer pathways in PDAC was purchased from Selleckchem. Subastumstat was kindly gifted by Takeda. Copanlisib (cat no HY-15346R) and pictilisib (cat no HY-50094) were purchased from MedChemExpress LLC. The drug screen was conducted in MiaPaCa-2, PSN-1, and 53631PPT cells, as recently described.¹⁸ After 72 hours of treatment, viability was measured. Plates were incubated at room temperature for 30 minutes. 25 μ L of CellTiter-Glo (Promega) was added to each well, incubated for 15 minutes, and luminescence was measured (FLUOstar-OPTIMA-microplate-reader, BMG-Labtech). Area under the curve and half-maximal growth inhibitory concentration values were calculated with RStudio (Posit Software) using a GRmetrics script.

Western Blot

Cells were treated with various conditions and harvested at different time points, and their protein lysates were analyzed by Western blot using specific primary antibodies and horseradish peroxidase-conjugated secondary antibodies.

The blots were developed using the OdysseyM imager (LI-COR Biotech), and the data were analyzed using EmpiriaStudio software (LI-COR Biotech).

Growth Curves by Cell-Live Imaging

Cells were seeded onto 96-well plates (5×10^3 cells/well), grown for 24 hours, and then treated with the indicated compounds. Confluency was determined by monitoring cells in real time with a confluency image mask, which was filtered for each cell line specifically. Cell confluency was quantified by 2024A version of the Incucyte software.

CRISPR/Cas9-based Gene Editing

Depletion of PI3K α a fragment from exon-2 and depletion of PI3K δ from exon-3 was mediated by clustered regularly interspaced short palindromic repeat (CRISPR)/clustered regularly interspaced short palindromic repeat associated protein 9 (Cas9). Then, 150,000 cells were transfected with 500 ng of single-guide (sg)RNA and 1 μ g of Cas9 protein (PNA-Bio) with a Neon-Transfection-System (Thermo Fisher/Invitrogen). A list of single-guide RNA sequences is available in the [Supplementary Material and Methods](#). Cleavage efficacy was tested 72 hours after transfection with Terra PCR Direct Card Kit (Takara Bio). Single cells were generated by serial dilution. Clones were screened for efficient gene editing, and selected clones were analyzed for protein expression by immunoblotting.

In Situ Resistance Assay

Cells were seeded onto a 96-well plate at a density of 250 cells/well on day 0. On day 1, treatment was added. Medium was changed and drugs refreshed weekly. Each week, cell confluency was analyzed using Incucyte (Live-Cell Imager, Sartorius). Wells reaching $>50\%$ confluency were scored as resistant. Data were plotted as a Kaplan-Meier plot.¹⁹

Toxicity Analysis in Mice

Serum samples of mice were isolated by postmortem cardiac puncture centrifuged at 2000g for 10 minutes. The concentrations of lactate dehydrogenase activity, albumin, calcium, urea, total protein, bilirubin, alanine aminotransferase, aspartate aminotransferase, alkaline phosphate, and inorganic phosphate were analyzed by photometry on a Roche cobas analyzer (Roche Diagnostics, Rotkreuz, Switzerland).

Detailed information on single-nuclei (sn)RNA sequencing (seq), RNAseq, processing, and analysis of gene expression data; CRISPR/Cas9-knockout screen; cell culture and treatment, chemicals, viral infection, and colony formation assay; cyclic immunofluorescence; in vivo drug efficacy analysis in mice and immunohistochemistry; patient-derived organoids; global and phosphoproteomics; and flow cytometry is available in the [Supplementary Material](#).

Statistics

Statistical analyses were performed using GraphPad Prism (GraphPad Software). *P* values $< .05$ were considered significant. All *P* values and tests are indicated in the figure legends.

Results

The SUMOylation Pathway Is Activated by PI3K Inhibition

PI3K-signaling is considerably involved in therapy resistance in multiple tumor entities.^{20–22} In PDAC, catalytic class-I PI3-kinase expression is increased (Supplementary Figure 1A). Both basal-like and mesenchymal subtypes, which overlap and are known to be more resistant to chemotherapy,²³ exhibit elevated PI3K/AKT-pathway activity, although mutations are rarely found (Figure 1A and B²⁴ and Supplementary Figure 1A and B). Mining data of patient-derived organoids (PDOs) isolated from treatment-naïve patients and patients after standard-of-care (SOC) chemotherapy²⁵ revealed a significant enrichment of the PI3K/AKT-signaling signatures in SOC-treated PDAC patients (Figure 1C). Furthermore, KRAS-knockout PDAC cells exhibited activated PI3K-dependent mitogen-activated protein kinase signaling and were sensitive to PI3K inhibition (Supplementary Figure 1C).²⁶ The combination of KRAS-inhibition by RMC-6236, a multiselective RAS^{on} inhibitor, and PI3K inhibition by pictilisib (a PIK3 α/δ inhibitor) acted synergistic in selected PDAC cell lines (Supplementary Figure 1D). Together, these data highlight the critical role of PI3K-dependent rewiring of oncogenic networks in cells with perturbed KRAS. Therefore, specifically in the context of PDAC, PI3K signaling plays a crucial role in adaptation to therapy and in treatment resistance.

To gain a deeper understanding of PI3K-controlled molecular networks, we analyzed a CRISPR^{knockout}-based PI3K-inhibitor (pictilisib) resistance screen²⁷ and identified SUMOylation-related pathways as synthetic lethal (Figure 1D). To causally test the relationship between PI3K-inhibition and changes in SUMOylation, we investigated the course of global protein SUMOylation upon PI3K inhibition with the formerly United States Food and Drug Administration–approved PIK3 α/δ inhibitor copanlisib. Indeed, over time, PI3K inhibition induced protein SUMOylation (Figure 1E and Supplementary Figure 1E), pointing to a role of SUMO in cells with inactivated PI3K signaling.

To extend our findings, we generated PI3K-inhibitor (copanlisib)–resistant PDAC cells (PI3K-R) and identified the induction of the SUMO-pathway core components SUMO1, SUMO2, SUMO3, and SUMO-activating enzyme subunit 1 (SAE1), ubiquitin-like modifier activating enzyme 2 (UBA2), and UBE2I (Figure 1F and Supplementary Figure 1E). We also examined the SUMOylation status after application of several selected SOC or targeted compounds. We observed induction of SUMOylation in some treatments, but not a general SUMO induction (Supplementary Figure 1F).

We next evaluated SUMOylation induction in PI3K inhibitor–treated MiaPaCa-2 by proteomics and phosphoproteomics (Figure 1G). Here, we found a significant induction of SUMO1 after 6 hours and SUMO2 after 24 hours (Figure 1H) upon PI3K inhibition. Additionally, various SUMOylation-related signatures were induced already after 6 hours, with some sustained after 24 hours (Figure 1I),

indicating early changes of protein SUMOylation in PI3K-inhibited cells. Sentrin/SUMO-specific proteases, which contribute to the maturation and homeostasis of SUMOylated proteins,²⁸ also showed a tendency toward induction after PI3K inhibition, with the SUMO2/3-specific deSUMOylase sentrin/SUMO-specific protease 3 being induced in particular (Supplementary Figure 1G). Phosphoproteomics and immunoblotting confirmed efficacy of PI3K inhibitor treatment as indicated by reduced phosphorylation of downstream targets (Figure 1J and Supplementary Figure 1H).

Together, these data show the induction of SUMOylation upon blockade of the PI3K pathway. Considering the synthetic lethal relation detected in the CRISPR screen (Figure 1D), the activation of SUMOylation pointed toward a functional relevance for PDAC cell survival.

SUMOylation Inhibition Induces PI3K Dependence

Observing the activation of SUMOylation in response to PI3K inhibition and in patients receiving SOC (Supplementary Figure 1I and J), we next sought to identify global PDAC dependencies in the context of SUMO pathway targeting. To this end we applied the highly specific clinical-grade SUMO E1 inhibitor (SUMOi) subasumstat²⁹ in a genome-wide CRISPR-knockout resistance screening in MiaPaCa-2 and PSN1 (Figure 2A). Indeed, we revealed that loss of genes associated with the PI3K/AKT pathway exhibited significant synthetic lethality in the context of SUMO blockade (Figure 2B and Supplementary Table 1). Complementary to the forward-directed genetic screen, we performed a subasumstat-anchored pharmacologic screen in human (MiaPaCa-2 and PSN1) and murine 53631PPT PDAC cell lines (Supplementary Table 2). Again, we identified a synthetic lethal relation between the SUMO and PI3K pathways (Figure 2C), which could be validated by multidose treatment with subasumstat (Figure 2D). In sum, these findings pointed toward a potential codependence of the 2 pathways in PDAC.

Pictilisib and copanlisib both exhibit equipotent inhibition of PIK3 α and PIK3 δ and less potent inhibition of PIK3 β and PIK3 γ isoforms.^{30,31} Owing to the ample (pre)clinical data, including some efficacy as well as toxicity and tolerability from clinical studies in lymphoma³² and other cancer entities,³³ we focused further studies on the formerly Food and Drug Administration–approved compound copanlisib. Combined treatment with copanlisib and subasumstat proved a targetable codependence between both pathways (Figure 2E and F). The synergistic effects of combined PI3K/SUMO targeting were confirmed in an expanded panel of PDAC cell lines (Supplementary Figure 2).

Taken together, these data indicate that SUMOylation inhibition provoked a cellular dependency on PI3K signaling. PI3K signaling thus represents a convergent node and specific vulnerability in PDAC cells lacking a functional SUMOylation machinery, and vice versa.

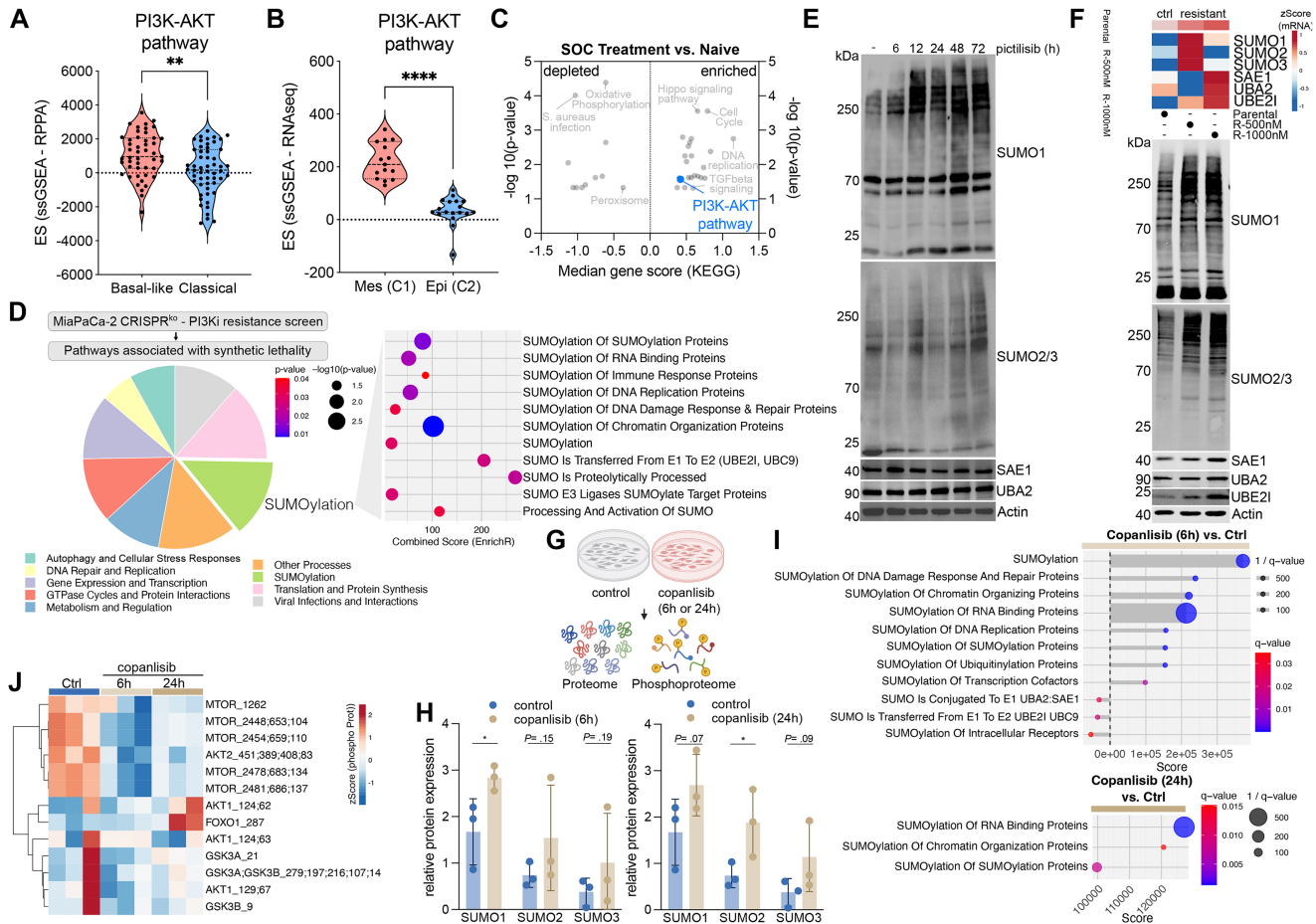


Figure 1. SUMOylation is enriched upon PI3K targeting in PDAC. (A) Distribution of single-sample (ss)GSEA enrichment scores for proteins of the Kyoto Encyclopedia of Genes and Genomes (KEGG) PI3K-AKT pathway in indicated PDAC subtypes. The large dashed lines inside the violin plot indicate the median and the smaller dashed lines indicate the interquartile range. (RPPA, Reverse Phase Protein Array, The Cancer Genome Atlas database). ** $P < .01$ by t test. (B). Distribution of ssGSEA enrichment score for messenger RNA of the KEGG PI3K-AKT pathway in mesenchymal (mes) C1 and epithelial (epi) C2 murine PDAC subtypes. **** $P < .0001$ by t test. (C) Top KEGG pathways enriched in post-chemotherapy PDOs shows an up-regulation of the PI3K-AKT pathway upon treatment. TGF, transforming growth factor. (D) Results from genome wide CRISPR-knockout PI3K-inhibition resistance screen performed in MiaPaCa-2. GSEA analysis (Reactome) of negatively selected genes revealed a synthetic lethal interaction between PI3K inhibition and SUMOylation inhibition. GTPase, guanosine-5'-triphosphatases. (E) Immunoblot analysis shows indicated proteins upon PI3K inhibition with pictilisib (1000 nmol/L) for indicated time points. β -Actin served as the loading control. UBA2, ubiquitin-like modifier activating enzyme 2. (F) Top: Transcript levels SUMO core components of MiaPaCa-2 cells—parental and resistant to copanlisib (R-500 nmol/L; R-1000 nmol/L). UBE2, ubiquitin-conjugating enzyme E2. Bottom: Immunoblot of SUMO core components in copanlisib resistant (R-500 nmol/L; R-1000 nmol/L) and parental MiaPaCa-2 cells. (G) Illustration of the global- and phosphoproteomics experimental setup. MiaPaCa-2 cells were treated for 6 or 24 hours with copanlisib (1000 nmol/L) or treated with dimethyl sulfoxide (vehicle-control). (H) Relative SUMO1/2/3 protein expression upon PI3K inhibition with copanlisib (1000 nmol/L, 6 or 24 hours; $n = 3$). P value by t test as indicated or * $P < .05$. The range bars designate standard deviation. (I) GSEA of SUMOylation-related gene sets (Reactome) upon PI3K inhibition with copanlisib (1000 nmol/L) for 6 or 24 hours compared with vehicle/dimethyl sulfoxide control in MiaPaCa-2. (J) Phosphorylation of indicated PI3K-Akt-mechanistic target of rapamycin (MTOR) downstream targets (mass spectrometry) upon PI3K-inhibition with copanlisib (1000 nmol/L) for 6 or 24 hours compared with vehicle/dimethyl sulfoxide control (MiaPaCa-2). GSKA, glycogen synthase kinase-3 alpha; FOXO1, forkhead box protein O1.

Simultaneous Inhibition of PIK3 α/δ and SUMO Is Required to Induce Synthetic Lethality

Our data indicate that inhibition of PIK3 α and PIK3 δ effectively induced susceptibility to SUMOylation inhibition, a crucial finding for clinical translation. To further

corroborate the dependency on specific PI3K isoforms and to provide robust data vital for clinical translation, we directly tested various PI3K inhibitors with known specificities for individual PI3K isoforms: alpelisib (PI3K α),¹⁰ GSK2636771 (PI3K β),¹¹ eganelisib (PI3K γ),¹² idelalisib

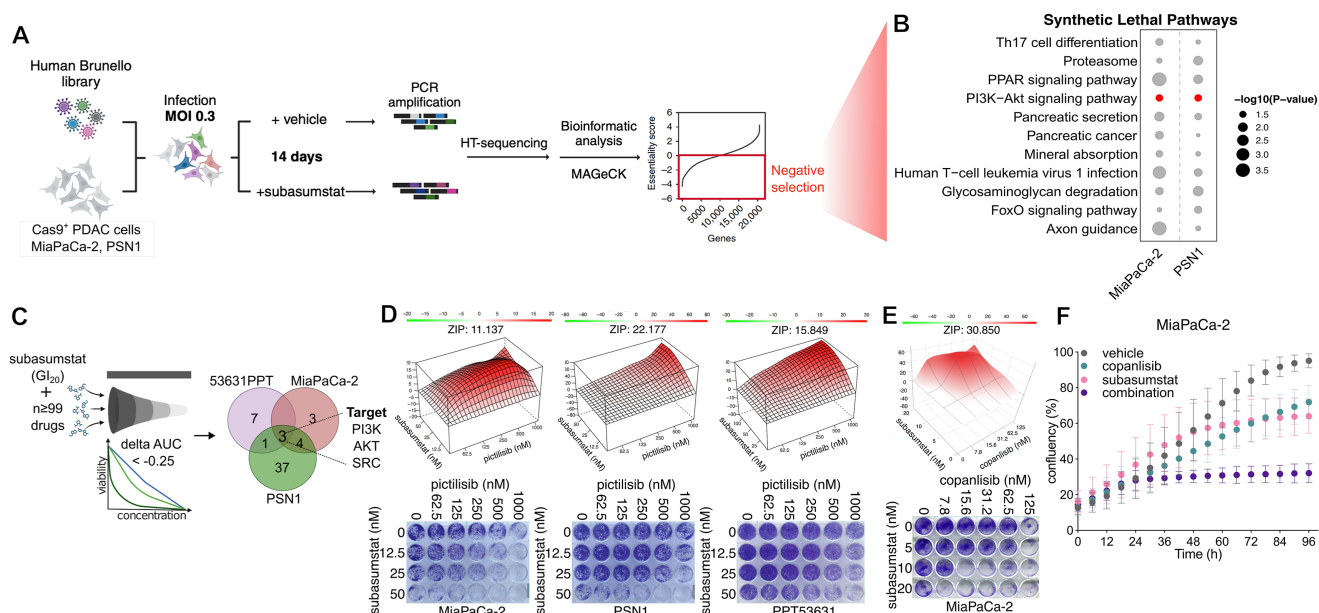


Figure 2. Synthetic lethal interaction between SUMO and PI3K pathways. (A) Schematic overview of the genome-wide CRISPR/Cas9 knockout subasumstat-resistance screen strategy conducted in MiaPaCa-2 and PSN1. HT, high throughput; MAGeCK, Model-based Analysis of Genome-wide CRISPR/Cas9 Knockout; MOI, multiplicity of infection; PCR, polymerase chain reaction. (B) Kyoto Encyclopedia of Genes and Genomes (KEGG) pathway analysis of negatively selected genes from CRISPR^{knockout} screens in the MiaPaCa-2 and PSN1 exposes the PI3K-Akt pathway as a common synthetic lethal pathway. PPAR, peroxisome proliferator-activated receptors; Th17, T helper 17. (C) Illustration/results of the subasumstat-anchored pharmacologic screen setup of subasumstat 20% growth inhibitory concentration (GI₂₀) and multidose treatment of n ≥ 99 compounds indicating in 3 indicated cell lines. AUC, area under the curve. (D) *Top*: Landscape plots depicting the synergistic area of concentrations of subasumstat and the PI3K inhibitor (pictilisib) in the 3 PDAC indicated cell lines. Synergy score was determined by SynergyFinder using the Zero Interaction Potency (ZIP) method. *Bottom*: Representative colony-growth images after treatment with subasumstat and pictilisib. (E) *Top*: Landscape plot depicting the synergistic area of concentrations of subasumstat and copanlisib in MiaPaCa-2. *Bottom*: Representative colony-growth image after treatment with subasumstat and copanlisib. (F) Proliferation of MiaPaCa-2 supplemented with subasumstat, copanlisib, or the combination of both. Cell confluency data were obtained by live cell imaging (n = 3). The range bars designate standard deviation.

(PI3K δ),³⁴ and parsacalisib (PI3K δ),¹⁴ all in combination with subasumstat. None of the isoform-specific PI3K inhibitors displayed synergism with subasumstat (Figure 3A and B, Supplementary Figure 3A). To substantiate these findings, we performed genetic knockouts of PIK3 α or PI3K δ isoforms by CRISPR/Cas9 (Figure 3C and Supplementary Figure 3B). Single knockout of the PIK3 α or PI3K δ isoforms did not exhibit synergism under subasumstat treatment. However, treating PI3K α knockout cells with a PI3K δ -specific inhibitor displayed synthetic lethality with the SUMO inhibitor subasumstat (Figure 3D and E). Confirming our previous data on SUMO pathway activation upon pharmacological PI3K-targeting (Figure 1) and supporting the codependence of the 2 pathways and in particular the specific PI3K isoforms, the SUMO state was increased in p110 δ /PI3K δ and p110 α /PI3K α knockout cells (Figure 3F, and Supplementary Figure 3B). In parental cells, the induction of a polySUMOylation high state upon PIK3 α / δ inhibition was blocked upon combination with subasumstat (Supplementary Figure 3C).

Together, these results show that highly specific PI3K α / δ inhibition or loss of PI3K α / δ induced profound activation of protein SUMOylation and created a targetable vulnerability. Consequently, inhibition of specifically PI3K α / δ is required

and sufficient for optimal synergy with SUMO-targeting by subasumstat.

Combined PI3K α / δ -SUMO Inhibition Induces Regulated Cell Death in Pancreatic Ductal Adenocarcinoma

To identify relevant pathways responsible for the fate of PDAC cells upon dual PI3K and SUMO inhibition, we examined the transcriptome and (phospho-)proteome upon monotreatment and combination treatment with copanlisib and subasumstat (Figure 4A). Single-sample gene set enrichment analysis (GSEA) revealed distinct patterns in the transcriptome (Figure 4B) and proteome (Figure 4C). PI3K signaling was significantly reduced and myelocytomatosis oncogene (MYC) signatures were depleted in both copanlisib monotherapy and combination with subasumstat, consistent with earlier observations.^{35,36} By analyzing hallmark signatures of the molecular signature database (MSigDb) enriched in the transcriptome and the proteome in the combination treatment, we identified 6 overlapping signatures, including metabolic, heme metabolism, and apoptosis signatures (Figure 4D). Therefore, we analyzed the expression of proteins related to apoptosis

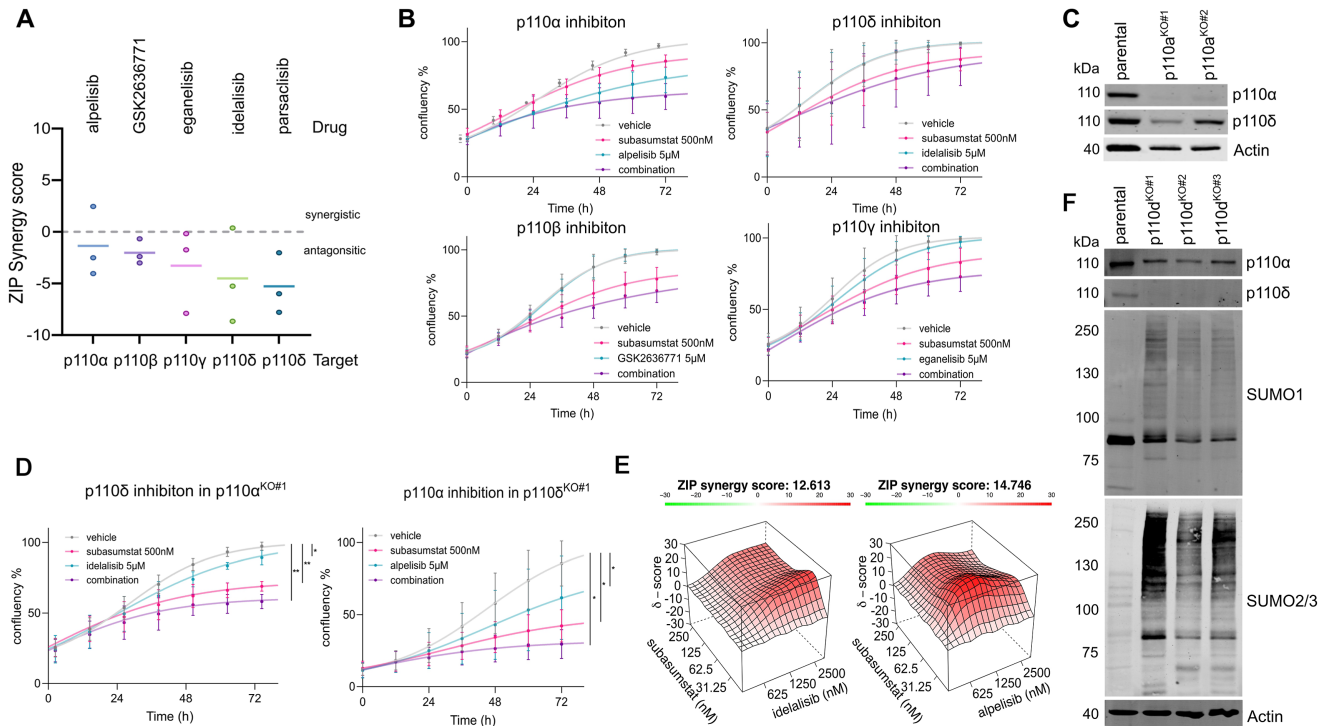


Figure 3. Double targeting of PI3K α /PI3K δ and SUMOylation induces synthetic interaction. (A) Zero Interaction Potency (ZIP) synergy scores upon combination of subasumstat and indicated PI3K inhibitors in MiaPaCa-2. Cells were treated with single and combination treatments using a 4 × 5 matrix. Cell confluency was assessed after 96 hours, and clonogenic assay quantification was imaged. Synergy score was determined by SynergyFinder using the ZIP method (n = 3). (B) Proliferation of MiaPaCa-2 supplemented with 500 nmol/L subasumstat, 5 μmol/L of indicated PI3K-specific inhibitors, or the combination of both. Cell confluency data were obtained by live cell imaging (12-hour intervals over 72 hours; n = 3). The range bars designate standard deviation. (C) Immunoblot analysis of p110 α / δ expression in MiaPaCa-2 harboring a CRISPR/Cas9-mediated PI3K α -de(p)letion. (D) Proliferation of p110 α -depleted MiaPaCa-2 supplemented with 500 nmol/L subasumstat, 5 μmol/L idelalisib, or the combination (left), and p110 δ -depleted MiaPaCa-2 supplemented with 500 nmol/L subasumstat, 5 μmol/L alpelisib, or the combination (right). Cell confluency data were obtained by live cell imaging (12-hour intervals over 72 hours; n = 3). **P < .01 by analysis of variance. The range bars designate standard deviation. (E) Landscape plots depict the synergistic area of concentrations of idelalisib and subasumstat combination treatment in p110 α -de(p)leted MiaPaCa-2 treated for 96 hours (left) and of concentrations of alpelisib and subasumstat combination treatment in p110 δ -depleted MiaPaCa-2 treated for 96 hours (right). Data (n = 3) were obtained by confluency measurement. (F) Immunoblot analysis of indicated proteins in MiaPaCa-2 harboring a CRISPR/Cas9-mediated PI3K δ -de(p)letion.

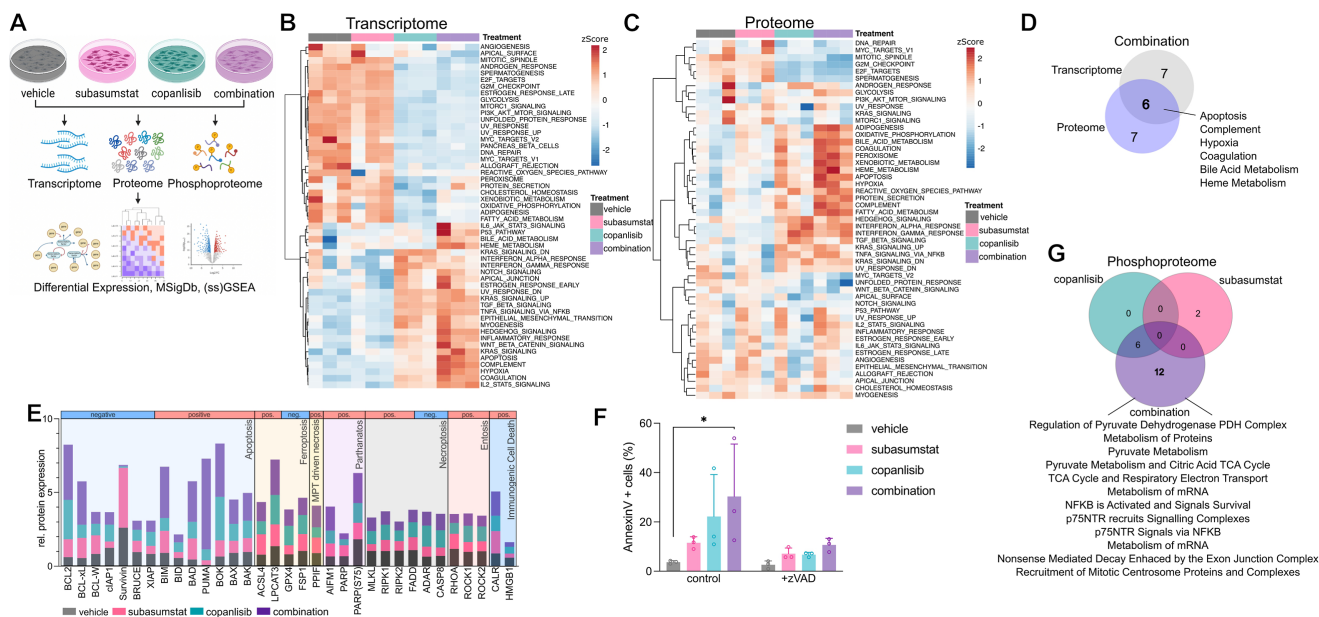
and other regulated cell death (RCD) modes (Figure 4E). Because we observed a trend for the regulation of proteins favoring apoptosis, we stained for cleaved caspase 3 and performed annexin-V/propidium iodide fluorescence-activated cell sorter. We observed an increase of cleaved caspase 3 (Supplementary Figure 4A) and annexin-V-positive cells upon combination treatment, which was blocked by a pan-caspase inhibitor (Figure 4F). However, the sole induction of apoptosis, which was relatively mild compared with the strong synergism observed, does not fully account for the cell-death mode. Analyses of cell-cycle profiles did not provide additional insights into the mode of action of the synergistic effects in the combination treatment (Supplementary Figure 4B). Considering the functional impact of SUMOylation on protein function and stability, we next investigated signatures and signaling pathways regulated at the protein level only. Applying phosphoproteomics, we identified that the SUMOi-PI3K inhibitor (PI3ki) combination specifically altered metabolic pathways, messenger RNA metabolism, and mitotic

regulation (Figure 4G), suggesting that affecting such pathways contribute to the strong synergism.

In summary, these data identified a multimodal induction of RCD by the combined inhibition of the PI3K α / δ and SUMOylation pathways.

Inhibition of PI3K α / δ and SUMO Signaling Impairs Growth in Patient-Derived Organoids

To validate the efficacy of combined PI3K α / δ -SUMO inhibition in advanced human model systems, we performed drug testing in 5 genetically and phenotypically characterized epithelial-like and mesenchymal-like PDOs with different activity of pathways associated with the mesenchymal subtype (Figure 5A and B). We tested their response toward FOLFIRINOX (folinic acid, fluorouracil, irinotecan, and oxaliplatin) (Figure 5C) and the PI3K α / δ - and SUMO-inhibition (pictilisib/subasumstat) combination treatment (Figure 5D). Of note, PDOs associated with mesenchymal transcriptomic features



displayed poor response in the SOC treatment but an improved response in the pictilisib/subasumstat combination treatment compared with epithelial-like PDOs (Figure 5C and D). By GSEA we identified significant enrichments of SUMOylation signatures in responder PDOs associated with mesenchymal transcriptomic features (Figure 5E).

Next, we used in situ resistance assays¹⁹ to assess viability after long-term treatment with monotherapy or combination therapy over a 5-week period. Outgrowth was defined on a confluence threshold of >50%, which was considered indicative of therapy failure. Cells treated with monotherapy exhibited outgrowth after 3 to 4 weeks, respectively (Figure 5F). In contrast, PI3K α/δ -SUMO combination therapy resulted in a pronounced loss of confluence, with >90% of cultures deemed nonviable by week 4 to 5 (Figure 5F).

In summary, the PI3K α/δ -SUMO-targeted combination therapy demonstrated efficacy in PDOs and in long-term assays.

Combined PI3K α/δ and SUMO Targeting Acts by Licensing the Antitumor Immune Response

We next investigated the PI3K α/δ -SUMO combination therapy in MiaPaCa-2 xenografts to translate our findings into an in vivo model. We observed a reduced tumor

volume in combination-treated xenografts compared with monotherapy (Supplementary Figure 5).

Subasumstat treatment induced multifaceted immune effects.^{17,37,38} Gene ontology biological process GSEA indicates up-regulated major histocompatibility complex-I and antigen processing and presentation upon combination treatment in MiaPaCa-2 (Figure 6A and B). Therefore, to investigate whether efficacy of combined PI3K α/δ -SUMO was different in an immune-competent model and whether PI3K α/δ -SUMO targeting could be associated with an antitumor response, we generated syngeneic orthotopic tumor grafts (Figure 6C). Here PI3K α/δ -SUMO treatment in a dose-escalation schedule exhibited significant effects on tumor growth compared with control treatments (Figure 6D). To investigate the effects of combined PI3K α/δ -SUMO treatment on tumor and immune dynamics, cyclic immunofluorescence (cycIF) was performed using the T-cell markers cluster of differentiation (CD) 3, CD4, CD8, and programmed cell death protein 1. This analysis revealed an increased infiltration of CD3⁺ T cells (Figure 6E). Because we did not observe significant differences in CD4⁺ or CD8⁺ T-cell infiltration, immune histochemical analysis of CD3⁺ T-cell infiltration was additionally performed, which confirmed the cycIF findings (Figure 6F).

Next, to investigate the complete landscape of therapy-induced reprogramming of the tumor microenvironment (TME), we analyzed tumor samples from all groups by

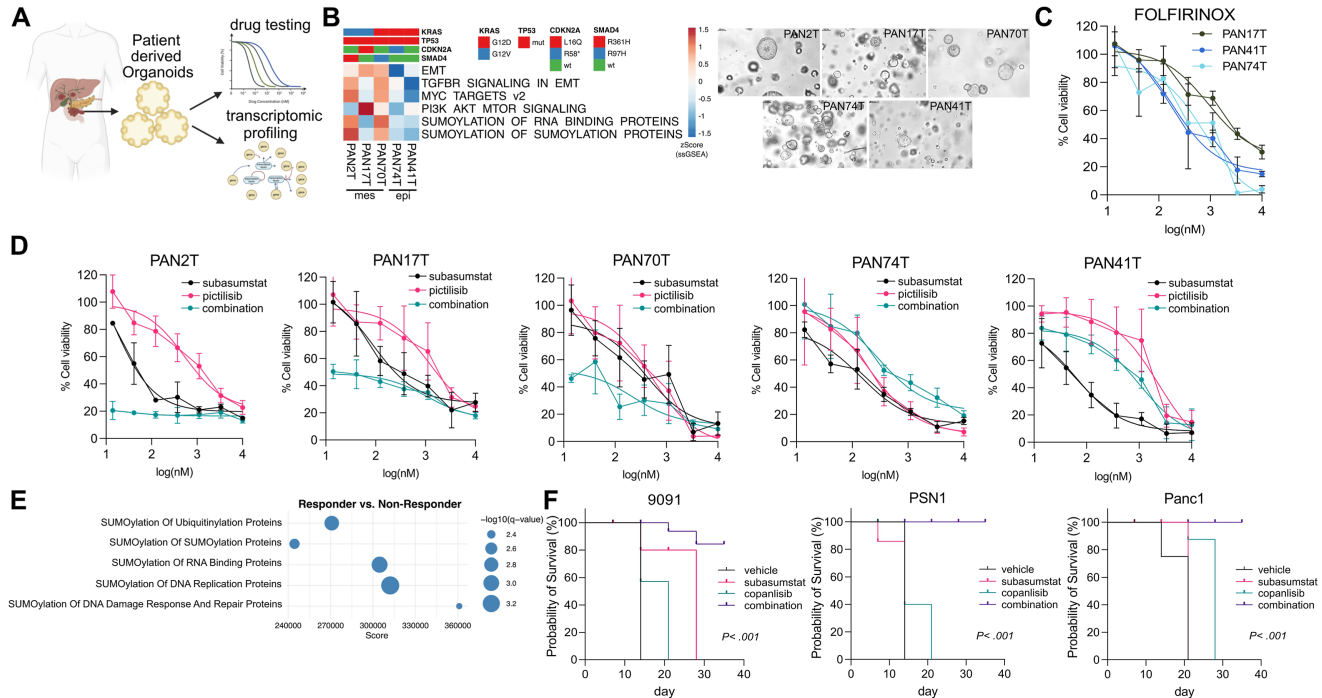


Figure 5. PDOs and in situ resistant assays reveal reduced tumor cell growth upon PI3K α/δ and SUMO inhibition. (A) PDOs from 5 patients with PDAC were isolated and used for drug testing and transcriptomic profiling (schematic overview). (B) Left: Mutation status of *KRAS*, *CDKN2A*, *TP53*, and *SMAD4*, and GSEA of indicated PDOs. PAN2T, PAN17T, and PAN70T display mesenchymal-like features (mes); PAN41T and PAN74T display epithelial-like features (epi). Right: Representative phase-contrast images (similar magnification) of PDOs. EMT, epithelial-mesenchymal transition. (C) Cell viability, measured by adenosine triphosphate quantification (CellTiter-Glo) 96 hours after treatment with indicated concentrations of FOLFIRINOX (folinic acid, fluorouracil, irinotecan, and oxaliplatin) mes and epi PDOs ($n = 3$). (Original magnification, 20 \times objective.) (D) Cell viability of PDOs supplemented for 96 hours with subasumstat (10 nmol/L), pictilisib (indicated concentration), or the combination of both measured by adenosine triphosphate quantification (CellTiter-Glo) ($n = 3$). The range bars designate standard deviation. (E) GSEA (Reactome) of transcriptome data depicts increased SUMOylation signatures in mes-PDOs (responder), compared with nonresponding epi-PDOs. (F) In situ resistance assay in mesenchymal murine PDAC cell line 9091PPT and the 2 basal-like human PDAC cell lines PSN1 and Panc1. Log-rank P value is indicated.

snRNAseq (Figure 6G and Supplementary Figure 6A and B). Here, we observed increased expression of cycling and cytotoxic T cells, indicating T-cell activation, although surface CD8 detection may be reduced posttranscriptionally (Figure 6G and H and Supplementary Figure 6C). We found that PI3K α/δ -SUMOi combination treatment significantly induced transcriptional activation of *Xcl1* and *Il18r1* in T cells, suggesting enhanced effector function (Figure 6I). In support, cyclIF revealed a significant increase in CD3⁺CD8⁺CCL5⁺ (chemokine ligand 5) and CD3⁺CD8⁺Ki67⁺ cells, compatible with elevated cytotoxic activity and T-cell proliferation (Figure 6J). These findings point to a PI3K α/δ -SUMOi combination-induced amplification of T-cell phenotypes associated with antitumor immunity.

Macrophage profiling revealed a shift from immunosuppressive M2-like macrophages to antigen-presenting tumor-associated macrophages (Figure 6K and L and Supplementary Figure 6D), compatible with a TME with enhanced antitumor immunity.³⁹ Additionally, cyclIF showed up-regulation of chemokine ligand 5, a chemokine known to recruit effector T cells, natural killer cells, dendritic cells, and monocytes into the TME (Figure 6M).⁴⁰ In

line with our cell culture-based data, we observed an augmented induction of interferon- α/γ and apoptosis pathways in tumor cells treated with the combination therapy in vivo (Supplementary Figure 6E).

Preliminary shallow analysis of toxicity regarding hematologic, liver, or kidney effects revealed no signals for PI3K α/δ -SUMOi combination therapy in the investigated mouse cohorts (Supplementary Figure 7).

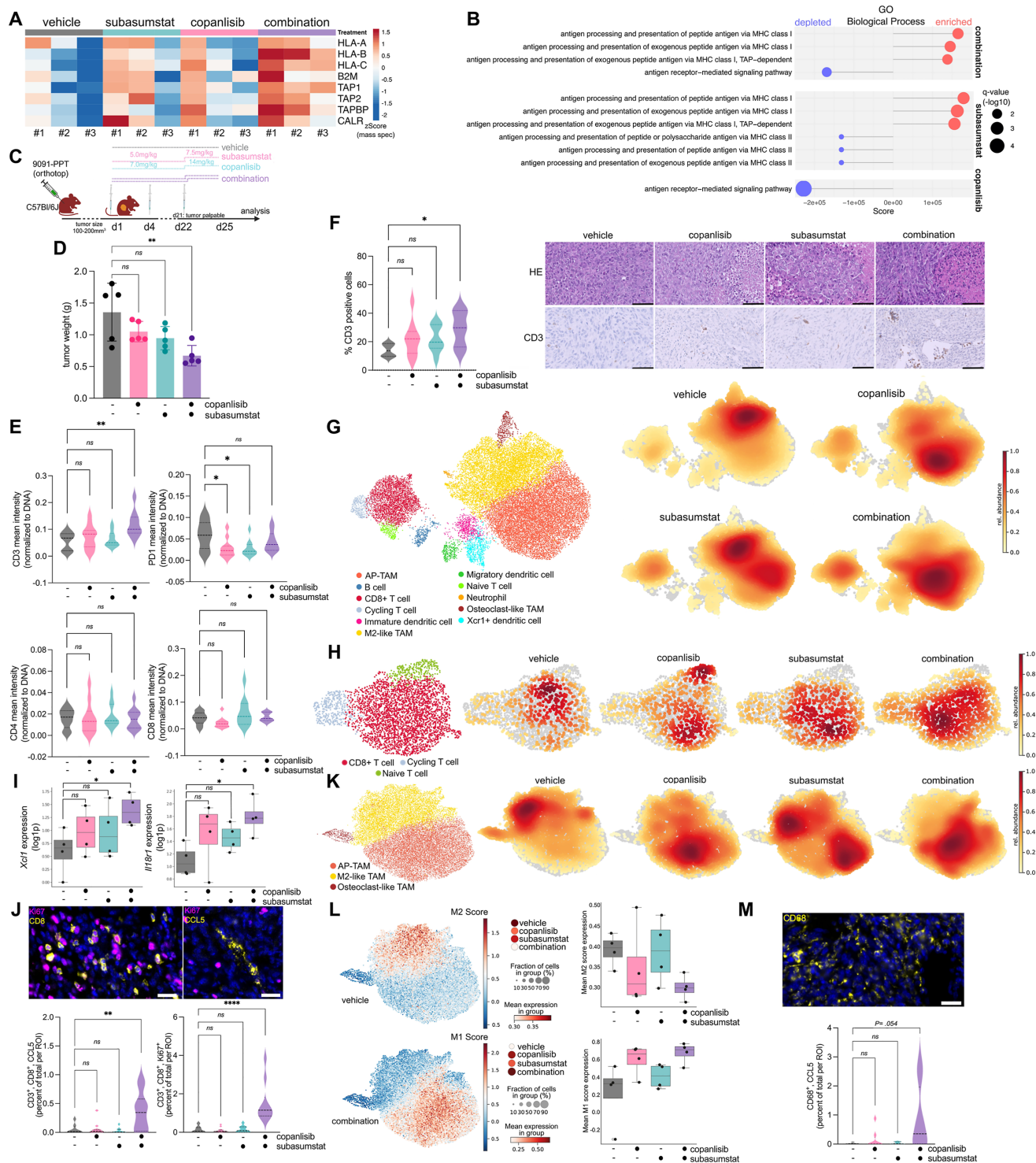
Together, these findings indicate that the combination therapy of SUMOi and PI3K α/δ modulates the TME to favor immune-mediated tumor-cell killing, predominantly involving cytotoxic T cells and antigen-presenting macrophages.

Discussion

The analysis of genome-wide PI3Ki-CRISPR resistance screens²⁷ and our genome-wide SUMOi-CRISPR and drug screens led to the identification of PI3K α/δ -SUMO targeting as a novel treatment strategy for PDAC. Our study reveals that mesenchymal/basal-like PDACs exhibit a mutual co-dependence on PI3K signaling and the SUMOylation pathway. By targeting both pathways, we achieved

consistent efficacy across multiple basal-like/mesenchymal models, including human and murine PDAC cell lines, PDOs, and mouse models, including an immune-proficient orthotopic model. Furthermore, our study underscores the importance of precise PI3K inhibitor application, because only PI3K α / δ -inhibitors synergize with SUMOylation inhibitors.

Direct targeting PI3Ks is a treatment strategy in PDAC worth considering.⁸ Our data confirm the connection between the PI3K pathway and basal-like/mesenchymal PDACs previously reported.⁴¹ Importantly, PI3K α is an important positive effector of oncogenic KRAS.⁴² The interconnection of these 2 oncogenic signaling nodes is also evident in PDAC tumorigenesis, where PI3K α , but not



PI3K β , is an essential mediator of oncogenic KRAS signaling. Furthermore, oncogenic PI3K α is crucial for maintenance and metastatic progression of PDAC.^{5,6,41,43,44} The observation that survival of PDAC cells genetically lacking KRAS is largely dependent on PI3K signaling²⁶ additionally emphasizes the pertinency of the PI3K pathway as a therapeutic target. In contrast to PI3K α , the role of other class I PI3Ks in PDAC remains complex and is less well understood.

Immunohistochemistry demonstrated the expression of PI3K γ in most of the investigated human PDAC cases, and knockout of the *PI3K γ* gene delayed tumor development in murine PDAC models, involving nonautonomous mechanisms.^{45–47} Furthermore, PDAC cells with mutated KRAS^{G12R}, which cannot interact with PI3K α , overexpress and depend on PI3K γ to induce micropinocytosis, a pathway that fuels the cancer cell's metabolic demands.⁴⁸ Protein abundance of PI3K δ is up-regulated in tumor-enriched PDAC samples.⁴⁹ We demonstrate that the synergy of the SUMO and the PI3K pathway inhibition depend on specifically blocking PI3K α and PI3K δ signaling. Thus, rational and specific inhibitor selection is needed to fully exploit PI3K inhibition in a specific context as shown here for the combination with SUMO targeting.

Recent studies by us and others have shown that the SUMOylation machinery is a putatively relevant therapeutic target in PDAC, and a highly potent and specific clinical

grade SUMO E1 inhibitor has been evaluated in the clinic.^{16,17,36} Concurrent with the activity of the PI3K pathway in basal-like PDACs, we observed increased expression of the core SUMOylation machinery in this subtype. The observed global/group protein SUMOylation upon PI3K inhibition appears consistent with cellular stress responses seen under conditions such as DNA damage or heat shock, where similar widespread SUMOylation shifts were identified.⁵⁰ This phenotype may reflect an adaptive or compensatory signaling mechanism engaged by cells to mitigate the disruption of homeostasis caused by PI3K pathway blockade. Our findings thus support the growing view that group SUMOylation plays a role in orchestrating broad stress-response programs, potentially as a protective means to buffer therapeutic stress.⁵¹

Importantly, inhibition of both the SUMO and the PI3K pathways resulted in activation of the other pathway, possibly as a mechanism to cope with various stresses, creating a therapeutically exploitable vulnerability and synthetic lethality. As shown previously, activation of SUMOylation confers a selective advantage against various stresses, contributing to cellular resilience against oncogenic, hypoxic, therapeutic, or oxidative stress.⁵² Combined PI3K and SUMO inhibition induced multimodal effects and therapeutic synergism, with disruption of cell survival signaling and an RCD pattern reflecting features of oxidative stress-associated cell death.

Figure 6. Enhanced efficacy of combined subasumstat and copanlisib treatment in immunocompetent mice. (A) Analysis of mass spectrometry data from MiaPaCa-2 cells treated with subasumstat (200 nmol/L), copanlisib (1000 nmol/L), combination, or dimethyl sulfoxide as vehicle control ($n = 3$, each condition), reveals a significant induction of major histocompatibility complex (MHC)-I-associated proteins expression upon combination treatment. B2M, β_2 microglobulin; CALR, calreticulin; HLA, human leukocyte antigen; TAP, transporter associated with antigen processing; TAPBP, TAP binding protein. (B) GSEA (gene ontology [GO]/biological process) indicates up-regulated MHC-I and antigen processing and presentation upon combination treatment in MiaPaCa-2. (C) Experimental setup to investigate the combination treatment in orthotopic PDAC tumors (D–M). Mesenchymal 9091PPT cells were orthotopically transplanted. Mice were treated with vehicle, subasumstat, copanlisib, or the combination with the indicated schedule. (D) Tumor burden was measured over time and shows significantly decreased volume in response to combination therapy ($n = 5$ mice, each cohort). $^{**}P < .01$ by analysis of variance (ANOVA) with Tukey's post hoc test; ns, not significant. (E) Quantification of indicated markers normalized to DNA (4',6-diamidino-2-phenylindole) show significantly increased CD3⁺ T-cell infiltration upon combination treatment, without significant change in CD4⁺, CD8⁺ and programmed cell death protein 1 (PD1⁺) cells. Dark dashed lines inside the violin plot indicate the median, light dashed lines indicate the interquartile range. P value determined by analysis of variance (ANOVA) with Tukey's post hoc test (bottom). (F) Representative images of histologic hematoxylin-eosin (HE) stains and immune histochemical analysis for CD3 expression of tissue sections of tumors from orthotopically transplanted mice. Scale bars, 50 μ mol/L (right). CD3 quantification in 5 mice ($n = 5$ high-power fields each). P value determined by ANOVA with Tukey's post hoc test (left). (G) snRNAseq of tumors from orthotopically transplanted mice treated with vehicle, subasumstat, copanlisib, or the combination. Uniform Manifold Approximation and Projection (UMAP) colored according to cell types (left). Visualization of the cell density within each cohort (embedding density estimation). (H) UMAP colored according to T-cell phenotype (left). Visualization of the cell density within each condition (embedding density estimation). (I) Mean expression of *Xcl1* and *Il18r1* in T-cell cluster per pseudobulk expression. P values are based on pseudobulk differential expression genes. (J) Representative images of tissue sections of tumors from orthotopically transplanted mice upon treatment, labeled with 4',6-diamidino-2-phenylindole (DAPI), Ki67, CD8, or chemokine ligand 5 (CCL5). Scale bars, 200 μ m–20 μ m (top). P value determined by ANOVA with Tukey's post hoc test (bottom). (K) UMAP colored according to macrophage phenotype (left). Visualization of the cell density within each condition, using embedding density estimation. (L) M2 score (top) M1 score (bottom) expression in the macrophage cluster upon no, monotreatment, or combination treatment. Left: UMAP plots for vehicle and combination treatment. Center: M2/M1 scores of all treatment groups. Right: Individual M1/M2 scores of the mean of each tumor. Box and whisker plot: The boxes indicate the 25th percentile (bottom border), median (center line), and 75th percentile (top border), the whiskers show the maximum and minimum ranges, and the circles indicate outliers. (M) Representative image of tissue sections of tumors from orthotopically transplanted mice upon treatment, labeled with DAPI and CD68, Scale bars, 200 μ m–20 μ m (top). Bottom: Quantification of CCL5 in CD68⁺ cells. ROI, region of interest. P value determined by ANOVA with Tukey's post hoc test.

Despite the withdrawal of approval for the PI3K α / δ -inhibitor copanlisib for relapsed indolent non-Hodgkin lymphoma after the Study of Copanlisib in Combination With Standard Immunochemotherapy in Relapsed Indolent Non-Hodgkin's Lymphoma (iNHL) (CHRONOS-4) phase 3 trial,⁵³ copanlisib demonstrated some clinical activity in PIK3CA-mutated cancer in the National Cancer Institute Molecular Analysis for Therapy Choice (NCI-'MATCH) Eastern Cooperative Oncology Group–American College of Radiology Imaging Network trial with a manageable toxicity profile,⁵⁴ pointing to the clinical potential of PI3K α / δ inhibitors when applied as a principle.

PI3K α / δ i-SUMOi combination therapy enhanced recruitment of CD3⁺ T cells in vivo in immunocompetent mice. After combination therapy, our snRNAseq analysis revealed robust expression of both CD4 and CD8 transcripts in tumor-infiltrating T cells, despite the absence of corresponding protein expression in some cases. This discrepancy suggests that the negative phenotype seen in cycIF and immune histochemical analysis may stem from transcriptionally active but protein-low or protein-suppressed cells, rather than representing a true expansion of double-negative T cells (DNTs). Although PI3K α / δ i-SUMOi-induced DNTs were associated with antitumor effects and changes in the TME in our in vivo model, other DNTs can promote cancer progression through immunosuppressive actions that support tumor growth and evade immune responses.⁵⁵ The anticancer properties of the DNTs could be induced by induction of immunogenic cell death,⁵⁶ and we show that RCD is activated in response to PI3K α / δ i-SUMOi combination therapy in in vitro studies. SUMO inhibition in vivo activated various immune cell subsets and reprogrammed the tumor immune microenvironment to induce an antitumor adaptive response.^{17,57} We here found that PI3K α / δ i-SUMOi combination treatment was specifically associated with a molecular switch from protumorigenic M2-like macrophages to antitumorigenic antigen-presenting macrophages. Together our data thus indicate a multimodal reprogramming of the TME toward a less tumor-permissive state upon PI3K α / δ i-SUMOi combination treatment. Furthermore, SUMOi generated an up-regulation of major histocompatibility complex I expression.³⁷

These established immune-modulatory effects of SUMO pathway inhibition might thus be amplified and beneficial when targeting PDAC with more effective rationale, molecularly targeted strategies such as combined PI3K α / δ -SUMO inhibition. This mode of action of subasumstat also favors the combination with PI3Kis, given their broad impact on both intrinsic tumor survival pathways and the immune landscape.^{8,58} PI3K α / δ i has been shown to modulate immune suppression within the TME, which may enhance the efficacy of immunotherapy-based approaches⁵⁹ that have been insufficiently effective in PDAC.⁶⁰ In this context, it is important that subasumstat generated a feed-forward loop by simultaneous activation of cytotoxic T cells and induction of the antigen-presenting machinery in PDAC and other tumor entities.^{17,37}

Conclusion

In summary, we here reveal the mutual codependency between the SUMOylation machinery and the PI3K pathway that warrants further development toward clinical application. In addition to synthetic lethal effects induced on tumor cells, the PI3K α / δ i-SUMOi combination therapy induced affected immune cell subsets and resulted in the complex reprogramming of the TME to an antitumorigenic state in vivo. Our findings could serve as a novel path toward already available but heretofore unsuccessful immunotherapy strategies for PDAC.

Supplementary Material

Note: To access the supplementary material accompanying this article, visit the online version of *Gastroenterology* at www.gastrojournal.org, and at <https://doi.org/10.1053/j.gastro.2025.08.018>.

References

1. Buckley CW, O'Reilly EM. Next-generation therapies for pancreatic cancer. *Expert Rev Gastroenterol Hepatol* 2024;18:55–72.
2. Halbrook CJ, Lyssiotis CA, Pasca di Magliano M, et al. Pancreatic cancer: advances and challenges. *Cell* 2023;186:1729–1754.
3. Singhal A, Li BT, O'Reilly EM. Targeting KRAS in cancer. *Nat Med* 2024;30:969–983.
4. Dilly J, Hoffman MT, Abbassi L, et al. Mechanisms of resistance to oncogenic KRAS inhibition in pancreatic cancer. *Cancer Discov* 2024;14:2135–2161.
5. Schonhuber N, Seidler B, Schuck K, et al. A next-generation dual-recombinase system for time- and host-specific targeting of pancreatic cancer. *Nat Med* 2014;20:1340–1347.
6. Eser S, Reiff N, Messer M, et al. Selective requirement of PI3K/PDK1 signaling for Kras oncogene-driven pancreatic cell plasticity and cancer. *Cancer Cell* 2013;23:406–420.
7. Li H, Wen X, Ren Y, et al. Targeting PI3K family with small-molecule inhibitors in cancer therapy: current clinical status and future directions. *Mol Cancer* 2024;23:164.
8. Conway JR, Herrmann D, Evans TJ, et al. Combating pancreatic cancer with PI3K pathway inhibitors in the era of personalised medicine. *Gut* 2019;68:742–758.
9. He Y, Sun MM, Zhang GG, et al. Targeting PI3K/Akt signal transduction for cancer therapy. *Signal Transduct Target Ther* 2021;6:425.
10. Andre F, Ciruelos E, Rubovszky G, et al. Alpelisib for PIK3CA-mutated, hormone receptor-positive advanced breast cancer. *N Engl J Med* 2019;380:1929–1940.
11. Mateo J, Ganji G, Lemech C, et al. A first-time-in-human study of GSK2636771, a phosphoinositide 3 kinase beta-selective inhibitor, in patients with advanced solid tumors. *Clin Cancer Res* 2017;23:5981–5992.

12. Hong DS, Postow M, Chmielowski B, et al. Egane-lisib, a first-in-class PI3Kgamma Inhibitor, in patients with advanced solid tumors: results of the phase 1/1b MARIO-1 Trial. *Clin Cancer Res* 2023; 29:2210–2219.
13. Borazanci E, Pishvaian MJ, Nemunaitis J, et al. A phase Ib study of single-agent idelalisib followed by idelalisib in combination with chemotherapy in patients with meta-static pancreatic ductal adenocarcinoma. *Oncologist* 2020;25:e1604–e1613.
14. Yue EW, Li YL, Douty B, et al. INCB050465 (parsaclisib), a novel next-generation inhibitor of phosphoinositide 3-kinase delta (PI3Kdelta). *ACS Med Chem Lett* 2019; 10:1554–1560.
15. Seeler JS, Dejean A. SUMO and the robustness of cancer. *Nat Rev Cancer* 2017;17:184–197.
16. Biederstadt A, Hassan Z, Schneeweis C, et al. SUMO pathway inhibition targets an aggressive pancreatic cancer subtype. *Gut* 2020;69:1472–1482.
17. Kumar S, Schoonderwoerd MJA, Kroonen JS, et al. Targeting pancreatic cancer by TAK-981: a SUMOylation inhibitor that activates the immune system and blocks cancer cell cycle progression in a preclinical model. *Gut* 2022;71:2266–2283.
18. Tapia Contreras C, Falke JD, et al. KRAS(G) (12C)-inhibitor-based combination therapies for pancreatic cancer: insights from drug screening. *Mol Oncol* 2025; 19:295–310.
19. Sealover NE, Theard PT, Hughes JM, et al. In situ modeling of acquired resistance to RTK/RAS-pathway-targeted therapies. *iScience* 2024;27:108711.
20. Wu DM, Zhang T, Liu YB, et al. The PAX6-ZEB2 axis promotes metastasis and cisplatin resistance in non-small cell lung cancer through PI3K/AKT signaling. *Cell Death Dis* 2019;10:349.
21. Rittler D, Baranyi M, Molnar E, et al. The antitumor effect of lipophilic bisphosphonate BPH1222 in melanoma models: the role of the PI3K/Akt pathway and the small G protein Rheb. *Int J Mol Sci* 2019;20:4917.
22. Chen Y, Wang T, Du J, et al. The critical role of PTEN/PI3K/AKT signaling pathway in shikonin-induced apoptosis and proliferation inhibition of chronic myeloid leukemia. *Cell Physiol Biochem* 2018;47:981–993.
23. Singh H, Xiu J, Kapner KS, et al. Clinical and genomic features of classical and basal transcriptional subtypes in pancreatic cancer. *Clin Cancer Res* 2024; 30:4932–4942.
24. Mueller S, Engleitner T, Maresch R, et al. Evolutionary routes and KRAS dosage define pancreatic cancer phenotypes. *Nature* 2018;554:62–68.
25. Zhou X, An J, Kurilov R, et al. Persister cell phenotypes contribute to poor patient outcomes after neoadjuvant chemotherapy in PDAC. *Nat Cancer* 2023;4:1362–1381.
26. Muzumdar MD, Chen PY, Dorans KJ, et al. Survival of pancreatic cancer cells lacking KRAS function. *Nat Commun* 2017;8:1090.
27. Milton CK, Self AJ, Clarke PA, et al. A genome-scale CRISPR screen identifies the ERBB and UBA2 signaling networks as key determinants of response to PI3K inhibition in pancreatic cancer. *Mol Cancer Ther* 2020; 19:1423–1435.
28. Kunz K, Piller T, Muller S. SUMO-specific proteases and isopeptidases of the SENP family at a glance. *J Cell Sci* 2018;131.
29. Langston SP, Grossman S, England D, et al. Discovery of TAK-981, a first-in-class inhibitor of SUMO-activating enzyme for the treatment of cancer. *J Med Chem* 2021; 64:2501–2520.
30. Folkes AJ, Ahmadi K, Alderton WK, et al. The identification of 2-(1H-indazol-4-yl)-6-(4-methanesulfonyl-piperazin-1-ylmethyl)-4-morpholin-4-yl-thieno[3,2-d]pyrimidine (GDC-0941) as a potent, selective, orally bioavailable inhibitor of class I PI3 kinase for the treatment of cancer. *J Med Chem* 2008;51:5522–5532.
31. Liu N, Rowley BR, Bull CO, et al. BAY 80-6946 is a highly selective intravenous PI3K inhibitor with potent p110alpha and p110delta activities in tumor cell lines and xenograft models. *Mol Cancer Ther* 2013; 12:2319–2330.
32. Matasar MJ, Capra M, Ozcan M, et al. Copanlisib plus rituximab versus placebo plus rituximab in patients with relapsed indolent non-Hodgkin lymphoma (CHRONOS-3): a double-blind, randomised, placebo-controlled, phase 3 trial. *Lancet Oncol* 2021; 22:678–689.
33. Morschhauser F, Machiels JP, Salles G, et al. On-target pharmacodynamic activity of the PI3K inhibitor copanlisib in paired biopsies from patients with malignant lymphoma and advanced solid tumors. *Mol Cancer Ther* 2020;19:468–478.
34. Yang Q, Modi P, Newcomb T, et al. Idelalisib: first-in-class PI3K delta inhibitor for the treatment of chronic lymphocytic leukemia, small lymphocytic leukemia, and follicular lymphoma. *Clin Cancer Res* 2015; 21:1537–1542.
35. Schild C, Wirth M, Reichert M, et al. PI3K signaling maintains c-myc expression to regulate transcription of E2F1 in pancreatic cancer cells. *Mol Carcinog* 2009; 48:1149–1158.
36. Schneeweis C, Hassan Z, Schick M, et al. The SUMO pathway in pancreatic cancer: insights and inhibition. *Br J Cancer* 2021;124:531–538.
37. Demel UM, Boger M, Yousefian S, et al. Activated SUMOylation restricts MHC class I antigen presentation to confer immune evasion in cancer. *J Clin Invest* 2022; 132:e152383.
38. Lightcap ES, Yu P, Grossman S, et al. A small-molecule SUMOylation inhibitor activates antitumor immune responses and potentiates immune therapies in preclinical models. *Sci Transl Med* 2021;13:eaba7791.
39. Rannikko JH, Hollmen M. Clinical landscape of macrophage-reprogramming cancer immunotherapies. *Br J Cancer* 2024;131:627–640.
40. Hu WT, Li M, Ma PJ, et al. A silence catalyst: CCL5-mediated intercellular communication in cancer. *Arch Toxicol* 2025;99:2699–2712.
41. Thibault B, Ramos-Delgado F, Pons-Tostivint E, et al. Pancreatic cancer intrinsic PI3Kalpha activity

- accelerates metastasis and rewires macrophage component. *EMBO Mol Med* 2021;13:e13502.
42. Gupta S, Ramjaun AR, Haiko P, et al. Binding of ras to phosphoinositide 3-kinase p110alpha is required for ras-driven tumorigenesis in mice. *Cell* 2007;129:957–968.
 43. Baer R, Cintas C, Dufresne M, et al. Pancreatic cell plasticity and cancer initiation induced by oncogenic Kras is completely dependent on wild-type PI 3-kinase p110alpha. *Genes Dev* 2014;28:2621–2635.
 44. Wu CY, Carpenter ES, Takeuchi KK, et al. PI3K regulation of RAC1 is required for KRAS-induced pancreatic tumorigenesis in mice. *Gastroenterology* 2014;147:1405–1416.e7.
 45. Edling CE, Selvaggi F, Buus R, et al. Key role of phosphoinositide 3-kinase class IB in pancreatic cancer. *Clin Cancer Res* 2010;16:4928–4937.
 46. Torres C, Mancinelli G, Cordoba-Chacon J, et al. p110gamma deficiency protects against pancreatic carcinogenesis yet predisposes to diet-induced hepatotoxicity. *Proc Natl Acad Sci U S A* 2019;116:14724–14733.
 47. Kaneda MM, Cappello P, Nguyen AV, et al. Macrophage PI3Kgamma drives pancreatic ductal adenocarcinoma progression. *Cancer Discov* 2016;6:870–885.
 48. Hobbs GA, Baker NMOL/L, Miermont AM, et al. Atypical KRAS(G12R) mutant is impaired in PI3K signaling and macropinocytosis in pancreatic cancer. *Cancer Discov* 2020;10:104–123.
 49. Cintas C, Douche T, Dantes Z, et al. Phosphoproteomics identifies PI3K inhibitor-selective adaptive responses in pancreatic cancer cell therapy and resistance. *Mol Cancer Ther* 2021;20:2433–2445.
 50. Psakhye I, Jentsch S. Protein group modification and synergy in the SUMO pathway as exemplified in DNA repair. *Cell* 2012;151:807–820.
 51. Enserink JM. Sumo and the cellular stress response. *Cell Div* 2015;10:4.
 52. Sheng Z, Zhu J, Deng YN, et al. SUMOylation modification-mediated cell death. *Open Biol* 2021;11:210050.
 53. Zinzani PL, Wang H, Feng J, et al. CHRONOS-4: phase 3 study of copanlisib plus rituximab-based immunotherapy in relapsed indolent B-cell lymphoma. *Blood Adv* 2024;8:4866–4876.
 54. Damodaran S, Zhao F, Deming DA, et al. Phase II study of copanlisib in patients with tumors with PIK3CA mutations: results from the NCI-MATCH ECOG-ACRIN Trial (EAY131) Subprotocol Z1F. *J Clin Oncol* 2022;40:1552–1561.
 55. Velikkakam T, Gollob KJ, Dutra WO. Double-negative T cells: setting the stage for disease control or progression. *Immunology* 2022;165:371–385.
 56. Ahmed A, Tait SWG. Targeting immunogenic cell death in cancer. *Mol Oncol* 2020;14:2994–3006.
 57. Erdem S, Lee HJ, Shankara Narayanan JSN, et al. Inhibition of SUMOylation induces adaptive antitumor immunity against pancreatic cancer through multiple effects on the tumor microenviro nmol/Lent. *Mol Cancer Ther* 2024;23:1597–1612.
 58. Sivaram N, McLaughlin PA, Han HV, et al. Tumor-intrinsic PIK3CA represses tumor immunogenicity in a model of pancreatic cancer. *J Clin Invest* 2019;129:3264–3276.
 59. Carnevalli LS, Sinclair C, Taylor MA, et al. PI3Kalpha/delta inhibition promotes anti-tumor immunity through direct enhancement of effector CD8(+) T-cell activity. *J Immunother Cancer* 2018;6:158.
 60. Brahmer JR, Tykodi SS, Chow LQ, et al. Safety and activity of anti-PD-L1 antibody in patients with advanced cancer. *N Engl J Med* 2012;366:2455–2465.

Received February 19, 2025. Accepted August 12, 2025.

Correspondence

Address correspondence to: Günter Schneider, MD, Department of Surgery, University Medical Center Göttingen, Robert-Koch-Str. 40, 37075 Göttingen, Germany. e-mail: gunter.schneider@med.uni-goettingen.de; or Ulrich Keller, MD, Department of Hematology, Oncology and Cancer Immunology, Campus Benjamin Franklin, Charité - Universitätsmedizin Berlin, Hindenburgdamm 30, 12203 Berlin, Germany. e-mail: ulrich.keller@charite.de; or Matthias Wirth, PhD, Department of Surgery, University Medical Center Göttingen, Robert-Koch-Str. 40, 37075 Göttingen, Germany, and Department of Hematology, Oncology and Cancer Immunology, Campus Benjamin Franklin, Charité - Universitätsmedizin Berlin, Hindenburgdamm 30, 12203 Berlin, Germany. e-mail: matthias.wirth@med.uni-goettingen.de.

Acknowledgments

The authors thank Judith-Achler Galitzki, Konstandina Isaakidis, Gerhild Fiolka, and Jennifer Appelhans for their excellent technical assistance and express their gratitude to the Sartorius Corporate Research Department for the support of this research. Illustrations were created with [BioRender.com](https://www.bio-render.com). Part of results shown are based on data generated by The Cancer Genome Atlas Research Network (<https://www.cancer.gov/tcga>). The authors thank the fluorescence-activated cell sorter core facility of the University Medical Center Göttingen (DFG project number 63915960).

CRedit Authorship Contributions

Hazal Köse, MSc (Conceptualization: Supporting; Data curation: Equal; Formal analysis: Equal; Funding acquisition: Supporting; Investigation: Equal; Methodology: Lead; Validation: Lead; Visualization: Equal; Writing – original draft: Supporting)

Christian Schneeweis, PhD (Data curation: Equal; Investigation: Equal; Methodology: Supporting; Validation: Equal)

Philipp Putze, MSc (Formal analysis: Equal; Methodology: Equal)

Constanza Tapia Contreras, PhD (Data curation: Supporting; Formal analysis: Supporting; Investigation: Equal)

Laura Ferreira, MSc (Data curation: Supporting; Formal analysis: Supporting; Investigation: Supporting; Validation: Supporting)

Leonie Witte, PhD (Data curation: Supporting; Formal analysis: Supporting; Investigation: Supporting; Validation: Supporting)

Ilaria Deidda, MSc (Data curation: Supporting; Formal analysis: Supporting; Investigation: Supporting; Validation: Supporting)

Frederik Herzberg, MD (Formal analysis: Supporting; Methodology: Supporting)

Sophie Ebert, MSc (Investigation: Supporting; Validation: Supporting)

Juraj Jakubik, PhD (Formal analysis: Supporting; Methodology: Supporting)

Leoni Moldaner, MSc (Formal analysis: Supporting; Methodology: Supporting)

Jovan Todorovic, MD (Formal analysis: Supporting; Methodology: Supporting)

Isabelle Träger, MD (Investigation: Supporting; Validation: Supporting)

Chuanbing Zang, PhD (Investigation: Supporting; Validation: Supporting)

Uta M. Demel, MD (Validation: Supporting), Elisabeth Hessmann, MD (Resources: Equal)

Marieluise Kirchner, PhD (Formal analysis: Supporting; Investigation: Supporting; Methodology: Equal; Resources: Equal)

Simone Rhein, PhD (Formal analysis: Equal; Methodology: Equal)

Jens Hoffmann, PhD (Resources: Equal)

Zuzana Tatarova, PhD (Formal analysis: Supporting; Methodology: Equal; Resources: Equal)

Michael Ghadimi, MD (Resources: Equal)

Dieter Saur, MD (Methodology: Supporting; Resources: Supporting)

Kai Kappert, MD (Investigation: Supporting; Methodology: Supporting; Resources: Supporting)

Philipp Mertins, PhD (Methodology: Equal; Resources: Supporting)

Günter Schneider, MD (Conceptualization: Equal; Funding acquisition: Equal; Resources: Equal; Supervision: Equal; Writing – original draft: Equal)

Ulrich Keller, MD (Conceptualization: Equal; Funding acquisition: Equal; Project administration: Equal; Supervision: Equal; Writing – original draft: Equal)

Matthias Wirth, PhD (Conceptualization: Equal; Data curation: Equal; Formal analysis: Equal; Funding acquisition: Equal; Investigation: Equal; Project administration: Equal; Resources: Supporting; Supervision: Equal; Visualization: Lead; Writing – original draft: Equal)

Conflicts of interest

These authors disclose the following: Ulrich Keller received reimbursement for advisory board function, speaker honorarium, and travel support from Takeda for content unrelated to this manuscript. Hazal Köse, Ulrich Keller, Günter Schneider, and Matthias Wirth have filed a patent application related to aspects of this work (application number EP25189303.8, pending). The remaining authors disclose no conflicts.

Funding

This work was supported by funding from Deutsche Forschungsgemeinschaft (WI 6148/1-1 project number 529255113 to Matthias Wirth, KE 222/10-1 project number 494535244, KE 222/11-1 project number 58460329, and

German Research Foundation Excellence Strategy - EXC 3118/1 - project number 533770413 to Ulrich Keller, and CRU5002 to Günter Schneider and Elisabeth Hessmann), German Cancer Aid (70115444 to Matthias Wirth and 700111944, 70114724, and 70116097 to Ulrich Keller), Hector-Stiftung (M2408 to Matthias Wirth), Wilhelm-Sander-Stiftung (2017.048.2 to Ulrich Keller, Günter Schneider, and Matthias Wirth), SPARK-BIH (to Hazal Köse, Ulrich Keller, and Matthias Wirth), and Stiftung Charité (Ulrich Keller) and The German Cancer Consortium (Zuzana Tatarova).

Data Availability

All data generated in this study provided within the article and its supplementary data files are available via online repositories or upon request. RNA sequencing and single nuclei RNA sequencing data are deposited at European Nucleotide Archive, accession number ENA ID: PRJEB83901; proteomics data are available via PRIDE ID: PXD059116. [Supplementary Table 1](#) CRISPR beta scores. [Supplementary Table 2](#) drug screening data. All other raw data are available upon request from the corresponding authors.

Supplemental information

Targeting Mutual Dependence of Phosphatidylinositol-3-Kinase α/δ and Small Ubiquitin-Like Modifier Signaling in Pancreatic Cancer

Hazal Köse, Christian Schneeweis, Philipp Putze, Constanza Tapia Contreras, Laura Ferreira, Leonie Witte, Ilaria Deidda, Frederik Herzberg, Sophie Ebert, Juraj Jakubik, Leoni Moldaner, Jovan Todorovic, Isabelle Träger, Chuanbing Zang, Uta M. Demel, Elisabeth Hessmann, Marieluise Kirchner, Simone Rhein, Jens Hoffmann, Zuzana Tatarova, Michael Ghadimi, Dieter Saur, Kai Kappert, Philipp Mertins, Günter Schneider, Ulrich Keller, and Matthias Wirth

Supplementary Material and Methods:

Global Proteome and Phosphoproteome Profiling using TMT-based Mass Spectrometry.

Cell pellets were resuspended in lysis buffer (1% Sodium deoxycholate, 100mM Tris-HCl pH 8, 150mM NaCl, 1mM EDTA, 40mM chloroacetamide, 10mM dithiothreitol, phosphatase inhibitor cocktail 2 and 3 (Sigma)), heated for 10 minutes at 95°C, cooled down and treated with Benzonase® (Merck, 50 units) for 30 min at 37°C. Endopeptidase LysC (Wako) and sequence-grade trypsin (Promega) were added to 200 µg protein extract (enzyme-to-protein ratio of 1:50), followed by an incubation over night at 37°C. A reference mix sample with equal peptide amount from all samples was prepared and processed in parallel. Samples were acidified with formic acid (1% final concentration), desalted with Sep-Pak C18 cc Cartridges (Waters), resuspended in 50 mM HEPES and labeled with 16-plex tandem mass tag reagents (TMTpro, Fisher Scientific) following the vendors instructions. TMT channel assignment was randomized between two plexes, where reference was placed to the same channel (channel 16) in both plexes. Samples and references were combined, fractionated by high-pH reversed phase off-line chromatography (1290 Infinity, Agilent) and pooled into 30 fractions. 10% of each fraction was taken out for global proteome measurements. The remaining 90% were further pooled onto 15 fractions and applied to IMAC based phosphopeptide enrichment using Fe(III)-IMAC cartridges and the AssayMAP Bravo Platform (Agilent Technologies).

For LC-MS/MS measurements, peptides were reconstituted in 3% acetonitrile with 0.1% formic acid and separated on a reversed-phase column (20 cm fritless silica microcolumns (inner diameter of 75 µm, packed with ReproSil-Pur C18-AQ 1.9 µm resin (Dr. Maisch GmbH)), using a 98-min gradient of increasing Buffer B (90% ACN, 0.1% FA) concentration (from 2% to 60%) with a 250 nl/min flow rate on a High-Performance Liquid Chromatography (HPLC) system (Thermo Fisher Scientific) and analyzed on an Exploris 480 instrument (Thermo Fisher Scientific). The mass spectrometer was operated in data-dependent acquisition mode using 60K resolution, 375–1500 m/z scan range, maximum injection time of 50 ms and 300 % AGC target value. MS2 scans were obtained at 45K resolution with an 0.4 m/z isolation window, 100 % AGC target value and a maximum injection time of 86 ms. Cycle time was set to 1 s. Dynamic exclusion was set to 20 s and only precursor with a charge state between 2-6 were selected for fragmentation. For analysis of phosphopeptide enriched samples the parameters were the same, with the exception of MS2 maximum injection time that was set to 120 ms.

RAW data were analyzed with MaxQuant software package (v 1.6.10.43) using the Uniprot human databases (UP000005640_2022_03) and default protein contaminants. Reporter ion MS2 for TMT16 was selected (internal and N-terminal) and TMT batch specific corrections factors were specified. Minimum reporter precursor intensity fraction was set to 0.5. The search included variable modifications of methionine oxidation, N-terminal acetylation, deamidation (NQ), phosphorylation (STY) and fixed modification of carbamidomethyl cysteine. The FDR (false discovery rate) was set to 1% for peptide and protein identifications.

The resulting text files were used for data analyses. Reverse hits, potential contaminants and proteins only identified by site were excluded. Protein groups and phosphosite tables were further filtered for 100 % valid value. Corrected reporter ion intensities were log2 transformed and normalized by subtraction of the internal reference channel contained in each TMT plex. The resulting TMT ratios were normalized via median z-score within each sample. Differences in

protein and phosphosite abundance between experimental groups were calculated using Student's T-Test. Signals passing the significance cut-off of FDR 5%.

Note on Large Language Model (LLM) use. This manuscript was generated by human researchers (author list), but parts of the manuscript have been corrected and edited by a Large Language Model (LLM) such as ChatGPT. The LLM was used to assist with the formatting, organization, and clarity of the text, but did not contribute to the conceptualization, design, or interpretation of the experiments.

Ethics, Consent to Participate and to Publish declarations. All animal experiments were performed by EPO (Experimental Pharmacology and Oncology, Berlin-Buch) and were approved by the local responsible authorities and performed in accordance with the German Animal Protection law. The primary human PDAC models were established/analyzed in accordance with the declaration of Helsinki. The study was approved by the local ethics committee of the University Medical Center Göttingen (UMG) (vote 11/5/17). Written informed consent from the patients for research use was obtained prior to the investigation. Both sequencing data and expression profiles / count tables are not provided in the manuscript to prevent identification if any individuals. Therefore, consent to publish is not applicable.

Single cell RNA sequencing Meta-analysis. We collected raw scRNAseq data from a publicly available PDAC dataset (GEO: GSE205049) ¹ and analyzed immune cell populations and phenotype using a common analysis pipeline. The gene expression matrix and metadata were imported into R (version 4.4.2) using Seurat (version 5.1.0). Cells with fewer than 100 detected genes, and more than 25% mitochondrial gene content were filtered out. Data were normalized using log-normalization, scaled, and subjected to PCA for dimensionality reduction. To address batch effects, Harmony (version 1.2.3) was applied. Cell clustering was performed using the Louvain algorithm (resolution=0.5), and UMAP was used for visualization. Double-negative (DN) T cells were identified by low expression of CD4, CD8 and NK markers, but positive CD3E expression. Code available upon request.

Patient-derived organoids. Excised tumor tissue was minced into small fragments using a scalpel and transferred to a 15 mL conical tube containing Human Digestion Medium. This medium consisted of Advanced DMEM/F-12 (#12634028, Gibco), 10 mM HEPES (#15630080, Gibco), 1× GlutaMAX (#35050061, Gibco), 0.1% BSA (#A9576, Sigma-Aldrich), 10% R-spondin1-conditioned medium (R-spondin1-expressing HEK293T cells), 50% Wnt-3a-conditioned medium (HEK293-WNT3A cells), 1× B27 (#17504001, Thermo Fisher), 10 mM Nicotinamide (#N0636, Sigma-Aldrich), 1.25 mM N-acetylcysteine (#A9165, Sigma-Aldrich), 100 µg/mL Primocin (#ant-pm-2, Invivogen), 100 ng/mL mNoggin (#250-38, Peprotech), 50 ng/mL hEGF (#PHG0313, Invitrogen), 100 ng/mL hFGF10 (#100-26, Peprotech), 10 nM hGastrin I (#3006, Tocris), and 500 nM A83-01 (#2939, Tocris). Medium was supplemented with 5 mg/mL Collagenase Type XI (#C9407, Sigma-Aldrich), 10 µg/mL DNase I (#D5025, Sigma-Aldrich), and 10.5 µM Y-27632 (#Y0503, Sigma-Aldrich). Digestion was performed at 37°C for 15 minutes on a rotator set to 300 rpm. Digested tissue fragments were allowed to settle, and supernatant was collected as first fraction. Fresh digestion medium was added to undigested tissue fragments for a second round of digestion, and resulting supernatant was combined with the first fraction. Combined fractions were centrifuged at 500 g for 5 minutes at 4°C, and the pellet was retained for further processing. If necessary, red blood cells were lysed by incubating the sample with ACK lysis buffer (#A10492-01, Gibco) for 3 minutes at room temperature. Following centrifugation at 500 g for 5 minutes at 4°C, the pellet was resuspended in Matrigel Growth Factor Reduced Basement Membrane Matrix (#356231, Corning), and 50 µL Matrigel domes were plated into pre-warmed 24-well plates. Plates

were incubated at 37°C for 30 minutes to allow Matrigel solidification, after which 500 µL of Human Complete Feeding Medium supplemented with 10.5 µM Y-27632 was added to each well. The plates were incubated at 37°C in a 5% CO₂ atmosphere.

For propagation, patient-derived organoids (PDOs) were cultured in a medium containing Advanced DMEM/F-12 (#12634028, Gibco), 10 mM HEPES (#15630080, Gibco), 1× GlutaMAX (#35050061, Gibco), 0.1% BSA (#A9576, Sigma-Aldrich), 10% R-spondin1-conditioned medium, 1× B27 (#17504001, Thermo Fisher), 10 mM Nicotinamide (#N0636, Sigma-Aldrich), 1.25 mM N-acetylcysteine (#A9165, Sigma-Aldrich), 100 µg/mL Primocin (#ant-pm-2, Invivogen), 100 ng/mL mNoggin (#250-38, Peprotech), 100 ng/mL hFGF10 (#100-26, Peprotech), 10 nM hGastrin I (#3006, Tocris), and 500 nM A83-01 (#2939, Tocris).

For organoid passaging, the Matrigel was mechanically disrupted by pipetting, and the suspension was collected in a 15 mL conical tube kept on ice. Sample was centrifuged at 500 g for 5 minutes at 4°C, and the pellet was resuspended in Express Enzyme (#12605028, Gibco) supplemented with 10 µg/mL DNase I (#D5025, Sigma-Aldrich) and 10.5 µM Y-27632 (#Y0503, Sigma-Aldrich). After incubation at 37°C for 15 minutes, the reaction was stopped by adding 5 mL of ice-cold wash medium (Advanced DMEM/F-12 supplemented with 10 mM HEPES, 1× GlutaMAX, and 0.1% BSA). The pellet was then resuspended in Cultrex Reduced Growth Factor Basement Membrane Extract (#3536-005-02, R&D Systems) and plated as 50 µL domes in pre-warmed 24-well plates. Plates were incubated for 1 hour at 37°C for Cultrex solidification, after which 500 µL of Human Complete Feeding Medium supplemented with 10.5 µM Y-27632 was added. Organoids were cultured at 37°C in a humidified incubator with 5% CO₂.

Cell culture and treatment, Chemicals, Viral Infection. MiaPaCa-2 (CVCL_0428) and Panc-1 (CVCL_0480) were cultured in Dulbecco's Modified Eagle's Medium (Thermo Fisher Scientific #41965062) supplemented with 10% Fetal Bovine Serum (Thermo Fisher Scientific #10270106). BxPc3 (CVCL_0186), PSN1 (CVCL_1644), AsPc1 (CVCL_0152) and DanG (CVCL_0243) were cultured in Roswell Park Memorial Institute 1640 Medium (Thermo Fisher Scientific #21875091) supplemented with 10% Fetal Bovine Serum (Thermo Fisher Scientific #10270106). 9091PPT (kindly provided by D. Saur) and 53631PPT murine PDACs cell lines were cultured in DMEM (Thermo Fisher Scientific #41965062). Cells were cultured in a humidified incubator at 37°C with 5% CO₂. Cells were regularly tested for Mycoplasma contamination by PCR and confirmed to be negative. Cell identity was analyzed by short tandem repeat (STR) profiling.

Generation of copanlisib-resistant cells. MiaPaCa-2 cells were continuously cultured for six months. The adaptation process involved supplementing the culture medium with increasing concentrations of copanlisib. Treatment commenced at a sub-lethal concentration of 10nM and was gradually escalated every two weeks reaching a final concentration of 1000nM. Cells were routinely passaged every 3-4 days. The successful development of copanlisib-resistant cells was evidenced by the increased cell viability and reduced apoptosis under copanlisib treatment. For comparison parental cells were kept in culture in parallel for the same period of time.

Chemicals. Subasumstat was either purchased from MedChemExpress or provided by Millennium Pharmaceuticals, Inc., a wholly owned subsidiary of Takeda Pharmaceutical Company Limited. Subasumstat doses and treatment durations are indicated in the figure legends. Pictilisib (RG7321) was purchased from Selleckchem. Copanlisib (HY-15346), zVAD-fmk (HY-16658B) and necrostatin-1 (HY-15760) were purchased from MedChemExpress, Parsaclisib (HY-109068), Eganelisib (HY-100716), GSK2636771 (HY-15245), Idelalisib (HY-13026). Alpelisib was purchased from TargetMol (T1921).

Viral infection. For the generation of lentiviral particles, HEK293T cells were co-transfected with the indicated lentiviral plasmids and viral packaging plasmids (Lipofectamine 2000, Invitrogen

#11668027). Virus supernatants were collected 48h after transfection and used to transduce the indicated cell line in the presence of 1ug/ml polybrene (Sigma-Aldrich, #TR-1003-G).

Cyclic Immunofluorescence. To prepare slides for cyclic immunofluorescence (cyclIF) staining, tissue sections were deparaffinized by baking at 65°C for 30 min a laboratory oven. Subsequently, slides were immersed in xylene and then rehydrated in a graded series of ethanol to distilled water (100%, 95%, 70%). To retrieve epitopes masked during tissue fixation, slides were subjected to heat and pH-mediated antigen retrieval: Slides were immersed in pH 6 citrate buffer (Antigen Retrieval Citra Plus, BiogeneX HK080-9K), heated in a pressure cooker and then transferred to warm Tris/EDTA buffer (Target Retrieval Solution, Dako S2368). Endogenous peroxidases were blocked using 3% hydrogen peroxide (H₂O₂, Sigma-Aldrich H1009) for 10 minutes with illumination and initial fluorescence bleaching was performed to reduce background signal before the first cycle. From now, washing of slides in 1x PBS with agitation was performed 3 times with 2-10 minutes each between further steps.

Subsequent iterative cyclIF rounds consisted of staining, imaging and quenching of fluorophores. Fluorophore-conjugated anti-mouse antibodies used in cyclIF are: CD3ε (Cell Signaling Technology; CST, E4T1B, 56611), CD4 (CST, D7D2Z, 93960), CD8α (CST, D4W27, 98941), PD1 (CST, D7D5W, 61237), Ki67 (CST, D3B5, 12075), CC3 (CST, D3E9, 97774S), CD68 (CST, E3O7V, 17846). Antibodies were diluted in blocking buffer (10% Normal Goat Serum, GIBCO #16210), 1% Bovine Serum Albumin, Sigma-Aldrich A9647; in 1x PBS) and incubated on the slides for 2 hours at room temperature in a humidified chamber protected from light. Cover glass was mounted using mounting medium (SlowFade™ Gold Antifade Mountant with DAPI, Invitrogen S36938) and images acquired with an automated slide scanner (Zeiss AxioScan Z1, Carl Zeiss Germany). Cover glass was removed by gentle agitation of slides in 1x PBS and fluorophores bleached twice with freshly prepared quenching solution (3% H₂O₂, 20 mM Sodium Hydroxide in 1x PBS) for 25 minutes each whilst being illuminated.

DNA content measured by DAPI staining and expression of each marker was quantified from images by signal coverage using Fiji (NIH Image to ImageJ). Staining of each single marker was manually threshold-ed to a binary black/white scale excluding background signal.

Genome-wide CRISPR/Cas9 knockout library screen. The human Brunello library (Addgene, #73178) was used to identify genes for synthetic lethal interactions with subasumstat in PDAC cells. First, stable Cas9-expressing cell lines were established by lentiviral transduction (Addgene, #181981). The expression of Cas9 was confirmed by western blotting and the function was validated by electroporation with specific guide RNAs and target knockout analysis. The final dose of subasumstat used was the GI30 dose (30% Growth Inhibition). Cas9 expressing cells were transduced with the lentiviral libraries and selected with Puromycin (Gibco™, #A1113803, final concentration 1ug/ml) for 5 days. Cells were harvested for day0 condition, and the rest was then split into control (vehicle, DMSO) and treatment groups (120nM subasumstat). Cells were passaged every 3-4 days for 2 weeks and drug treatment was refreshed each time. On day 14, cells were harvested, and genomic DNA was extracted using the DNeasy Blood and Tissue kit (Qiagen, #69504) according to the manufacturer's instructions.

Flow cytometry. Apoptosis assay. For detection of apoptotic cell death, cells were stained with AnnexinV/PI by flow cytometry. Briefly, 1x10⁶ cells were centrifuged at 300g for 5min, resuspended in 300uL 1X Annexin V binding buffer (BD Pharmingen, #8008652), added 4uL APC Annexin V (BioLegend #640941) and 10ug/mL PI (Sigma, #P4864) and incubated for 15min at 4°C in the dark. Cells were analyzed by flow cytometry using a CytoFLEX S Flow Cytometer (Beckman Coulter). Annexin V staining was quantified as early apoptotic (Annexin V+, PI-) and apoptotic-dead cells (Annexin V+, PI+). Analysis was performed using FlowJo™ v10.6.0 software.

Cell cycle assay. 5×10^5 were collected and washed with PBS and fixed with 70% ethanol and stored at 4°C overnight. Cells were resuspended in PBS containing 0,25% Triton X-100 and incubated on ice for 15 minutes. Pellets were washed with PBS containing 0,5% BSA and resuspended finally with PBS containing 10 µg/ml of RNase A and 20 µg/ml of PI, incubated at room temperature for 30 minutes in the dark then analyzed by flow cytometry. Analysis was performed using FlowJo™ v10.6.0 software.

Western Blot. Cells were seeded at a density of 2×10^6 in 10 cm dishes. The following day, dishes were washed with PBS and medium replaced with medium plus corresponding treatment. At indicated timepoints, cells were harvested in RIPA buffer and fractioned on SDS-PAGE gels. Protein lysates were transferred to PVD-FL membranes (Immobilon-Merck) and incubated with specific primary antibodies at 4°C overnight. For ECL measurements, membranes were incubated for 1h at room temperature with HRP-conjugated secondary antibodies (Cell Signaling Technologies #7076S and #7074P) and HRP-substrate (Merck Millipore Immobilon Western #24191B4) was used. Membranes were developed with the OdysseyM imager (LiCor Biosciences). A list of antibodies used can be found in **STable3**. All the quantification of the blots was analyzed by EmpiriaStudio3.1.

In vivo drug efficacy analysis in mice and Immunohistochemistry. All animal experiments were performed by EPO (Experimental Pharmacology and Oncology, Berlin-Buch) and were approved by the local responsible authorities and performed in accordance with the German Animal Protection law. Subcutaneous MiaPaCa-2 xenograft experiments were performed in *NMRI nu/nu* mice. Tumor growth was monitored daily by measurement with a caliper. Once the tumor volume reached 0.2 cm³, mice were randomized into the different groups and treated with vehicle, subasumstat, copanlisib, or the combination for 18 days. For the orthotopic pancreatic tumor model, cancer cells were transplanted into the pancreas of syngeneic immunocompetent *C57Bl/6J* mice. When tumor volume reached 0.1 cm³, mice were randomized into the different treatment cohorts. Animals were sacrificed when individual mouse reached the human endpoint or at completion of treatment.

Library preparation, Next-Generation Sequencing and MaGECK analysis. The PCR was set up according to manufacturer's protocol. One PCR reaction (100 µL) contained up to 10 µg of gDNA, 50 µL NEBNext High-Fidelity 2X MasterMix (NEB, #M0541S) and 1 µL of each primer (P7 with unique sequencing-barcodes and P5 with staggers). AMPure XP purification beads (Beckman Coulter #A63881) were used according to manufacturer's instructions. All samples were sent to Novogene (Cambridge, UK) where they were sequenced on a NovaSeq Illumina machine. Sequencing analysis was conducted using the MaGECK pipeline ².

RNA isolation. MiaPaCa-2 cells were seeded at day 0 onto 6-well dishes at a density of 5×10^5 cells/well. On day 1, cells were treated for 6 or 24 hours. Cells were lysed and RNA isolated with the RNeasy Isolation kit (Qiagen, #74104).

GSEA and ssGSEA. Gene Set Enrichment Analysis (GSEA) was performed using the GenePattern platform from the Broad Institute under standard settings. Single-sample GSEA (ssGSEA) was conducted using GenePattern with the sample normalization method set to log.rank ³. Additionally, GSEA analysis was carried out using the GeneTrail web tool ⁴, and the resulting data were visualized as dot plots generated in R.

Colony formation assay. Cells were seeded onto 6-well or 24-well plates, grown for 24h, and then treated with indicated compounds for 96 hours. Wells were washed with PBS, fixed and stained with Crystal violet. Plates were either scanned and cell growth was assessed by readout

with the OdysseyM imager (LiCor Biosciences) or first solubilized and optical density was measured at 590nm. Density of vehicle-treated cells was arbitrarily set to 100% and dose-response was calculated as relative viability.

Single-cell library preparation

Three 50 µm FFPE sections per sample were dissociated following the 10x Genomics protocol for FFPE tissue sections (CG000632_RevD), using the gentleMACS Octo Dissociator workflow. Library preparation was performed using the Fixed RNA Profiling protocol (CG000527_RevF, 10x Genomics). For each sample, 550,000 cells were used for probe and barcode hybridization, which was carried out for 22 hours at 42°C. After hybridization, samples were pooled, and 210,000 cells were loaded into a single GEM well of a Chip Q. Sample index PCR was performed with 10 cycles.

Sequencing and alignment

The library was sequenced on a NovaSeq X Plus 25B flow cell (Illumina) with 150 bp paired-end reads. Reads were demultiplexed with bcl2fastq v4.2.7 (Illumina). FASTQ files were processed with Cell Ranger v9.0.1 (10x Genomics) using the multi pipeline with the mouse reference (refdata-gex-GRCm39-2024-A) and the Chromium Mouse Transcriptome Probe Set v1.1.1.

Preprocessing of GEM Flex scRNA-seq data

Ambient RNA was removed using scAR⁵ on the raw feature barcode matrix with default parameters. Further analysis was performed using scanpy v1.10.3⁶. Calculation of quality metrics and filtering of low-quality cells based on median absolute deviations (MAD) was performed in adherence to single-cell best practices⁷. Samples were integrated using scVI⁸ on the intersection of highly variable genes per sample, with the following parameters: n_hidden=256, n_latent=12, n_layers=3, and gene_likelihood='zinb'. Dimensionality reduction was performed using Uniform Manifold Approximation and Projection (UMAP), with the number of neighbors set to the number of cells divided by 1,000 (rounded to the nearest integer). Finally, cells were grouped based on leiden clustering and marker genes were derived with the scanpy rank_genes() function using the Wilcoxon test. The marker genes were then used to annotate the clusters.

Downstream analysis GEM Flex scRNA-seq data

Gene set scores were calculated using the scanpy score_genes() function. ((either here or list in supplementary: For the M1 score, the following genes were used: Cd86, H2-Ab1, Tlr4, Fcgr1, Itgax, Il1b, Tnf, Cxcl9, Nos2, Stat1. For the M2 score, Mrc1, Arg1, Chil3, Stab1, Tgfb1, Il10, Mmp12, Clec10a, Stat3, Klf4.)) Pseudobulk profiles were generated to perform differential gene expression analysis between treatment groups. For each sample, cells were randomly shuffled and evenly split into two groups, forming two pseudobulk replicates. The raw counts of each group were summed to generate the pseudobulk profiles. Lowly expressed genes were removed by filtering for genes with at least 50 counts in 70% of pseudoreplicates. Subsequent analyses were performed following the standard DESeq2 workflow⁹. The decoupler package¹⁰ was utilized to compute pathway enrichment scores across cells. Gene Set Enrichment Analysis (GSEA) was conducted using gseapy employing the signal-to-noise ratio as the ranking metric ¹¹.

STable 3a Western Blot Antibodies:

Target	Company	Article number
SUMO1	Abcam	ab133352
SUMO2-3	Abcam	ab81371
panAKT	Cell Signaling Technology	#9272
phosphoAKT (Ser479)	Cell Signaling Technology	#9271

phosphoAKT(Thr308)	Cell Signaling Technology	#9275
UBLE1A/SAE1	Cell Signaling Technology	#13585
UBA2	Cell Signaling Technology	#8688
UBE2I/Ubc9	Cell Signaling Technology	#4786
P110 α	Cell Signaling Technology	#4249
P110 δ	Cell Signaling Technology	#34050
β -actin	Sigma-Aldrich	#A1978
vinculin	Cell Signaling Technology	#4650

Table 3b Flow Cytometry/IF Antibodies:

Epitope	Reactivity	Fluorochrome	Company	Article number
AnnexinV	Human	APC	Biolegend	#640941
DAPI	all	-	Biolegend	#422801
Cleaved caspase-3	Human-mouse	Alexa 488	Cell Signaling Technology	#9603
Anti-CD3	Human	PE	Biolegend	#344805
Anti-CD3	Human	APC	Biolegend	#344811
Anti-CD14	Human	APC	Biolegend	#325607
Anti-CD56	Human	PE	Biolegend	#362507
Anti-CD16	Human	PE	Biolegend	#302007

Table 4 CRISPR/Cas9 sgRNA sequences:

sgRNA target	sgRNA sequence
PIK3CA ex2_fw	taatacgactcactataGGTTCACCTGATGATGGTTCGgttttagagctagaaatagc
PIK3CA ex2_rv	taatacgactcactataGGCTTTAGAATGCCTCCGTGgttttagagctagaaatagc
PIK3CD ex3_fw	taatacgactcactataGGTTGGCATTGCGGGACACAgtttagagctagaaatagc
PIK3CD ex3_rv	taatacgactcactataGGTGAGCTTTTGTACCCGCgttttagagctagaaatagc

Supplementary References

1. Yousuf S, Qiu M, Voith von Voithenberg L, et al. Spatially Resolved Multi-Omics Single-Cell Analyses Inform Mechanisms of Immune Dysfunction in Pancreatic Cancer. *Gastroenterology* 2023;165:891-908 e14.
2. Li W, Koster J, Xu H, et al. Quality control, modeling, and visualization of CRISPR screens with MAGeCK-VISPR. *Genome Biol* 2015;16:281.
3. Barbie DA, Tamayo P, Boehm JS, et al. Systematic RNA interference reveals that oncogenic KRAS-driven cancers require TBK1. *Nature* 2009;462:108-12.
4. Backes C, Keller A, Kuentzer J, et al. GeneTrail--advanced gene set enrichment analysis. *Nucleic Acids Res* 2007;35:W186-92.
5. Sheng C, Lopes R, Li G, et al. Probabilistic machine learning ensures accurate ambient denoising in droplet-based single-cell omics. *bioRxiv* 2022:2022.01.14.476312.
6. Wolf FA, Angerer P, Theis FJ. SCANPY: large-scale single-cell gene expression data analysis. *Genome Biol* 2018;19:15.
7. Heumos L, Schaar AC, Lance C, et al. Best practices for single-cell analysis across modalities. *Nat Rev Genet* 2023;24:550-572.

8. Lopez R, Regier J, Cole MB, et al. Deep generative modeling for single-cell transcriptomics. *Nat Methods* 2018;15:1053-1058.
9. Love MI, Huber W, Anders S. Moderated estimation of fold change and dispersion for RNA-seq data with DESeq2. *Genome Biol* 2014;15:550.
10. Badia IMP, Velez Santiago J, Braunger J, et al. decoupleR: ensemble of computational methods to infer biological activities from omics data. *Bioinform Adv* 2022;2:vbac016.
11. Fang Z, Liu X, Peltz G. GSEAPy: a comprehensive package for performing gene set enrichment analysis in Python. *Bioinformatics* 2023;39.

Supplemental Figure Legends

SFig.1: Both SUMOylation and PI3K pathways are PDAC vulnerabilities.

A. Top: OncoPrint diagram of mutational frequencies and types of alterations of PDAC driver gene and *PI3K* genes across independent PAAD datasets: Biankin et al. (Nature, 2012), Bailey et al. (Nature, 2016), TCGA Firehose Legacy, TCGA GDC, TCGA Pan-Cancer Atlas, Witkiewicz et al. (Nat Commun, 2015), and Cao et al. (Cell, 2021). Bottom, left: Expression of mRNA in pancreatic epithelial cells with and without expression of mutant Kras^{G12D} (Data derived from GSE154543). Bottom, middle: Expression of mRNA in normal pancreas and PDAC samples from human patients (Data derived from Badea et al., 2008). Bottom, right: Protein expression in human normal tissue (N) and PDAC (T) samples (CPTAC data derived from Cao et al., 2021).

B. MSigDb (Hallmark) ssGSEA analysis of ICGC PDAC patient data (Bailey et al. (Nature, 2016) indicates an overrepresentation of PI3K/AKT/MTOR and MYC gene sets in the squamous subtype (blue) compared to other subtypes (red).

C. Heat map depicting the results of a pharmacological screen conducted in *KRAS* knockout cells, confirming an increased PI3K dependency of *KRAS* deficient cells. Data derived from Muzumdar *et al.* (Nat Commun, 2015)²⁴.

D. Landscape plots depicting the synergistic area of concentrations of RMC-6236 (*KRAS* inhibitor) and GDC-0941 (pictilisib) combination treatment (Bliss synergy score). Viability was measured by ATP quantification using by CellTiterGlo® 72h after treatment with indicated concentrations in depicted cell lines.

E. Quantification of immunoblots from Figs. 1E, F. Top: Relative SUMO1, SUMO2/3, SAE1 and UBA2 expression was determined by normalization to loading controls. MiaPaCa-2 cells were treated with 1000nM pictilisib in for the indicated time points (0, 6, 12, 24, 48, 72h). Bottom: Relative SUMO1, SUMO2/3, SAE1, UBA2 and UBE2I protein expression levels in MiaPaCa-2 control cells (parental) or in copanlisib resistant cells, generated by increasing concentrations of copanlisib over a period of 6 months, resulting in the resistant cell lines R-500nM and R-1000nM. Protein bands were normalized to the corresponding loading controls.

F. Immunoblot analysis of SUMO1 and SUMO2/3 upon indicated treatment (left). Quantified relative expression of SUMO1 and SUMO2-3 (right). P-values were determined by ANOVA **P* < .05, ****P* < .001.

G. Relative protein expression levels determined by mass-spec of indicated Sentrin/SUMO-specific proteases (SENPs) after 6h (top) or 24h (bottom) of copanlisib treatment (1000nM) in MiaPaCa-2 cells.

P-values were determined by ANOVA

H. Immunoblot analysis of indicated PI3K downstream targets upon copanlisib (1000nM for 6 and 24hours) and vehicle (DMSO) treatment in MiaPaCa-2 cells.

I. GSEA (MSigDb – Reactome) of transcriptome data from PDOs, derived from chemotherapy treated PDAC patients compared to PDOs, derived from non-treated (naïve) PDAC patients, display significantly enriched SUMOylation gene sets Zhou et al. (Nature Cancer, 2023)²³.

J. Heatmap showing the expression pattern (mRNA) of indicated SUMO core machinery components in SOC treated PDAC with different (indicated) mutations in the *KRAS* gene. Mean expression of the entire SUMO core machinery was compared in treatment groups versus treatment naïve PDOs. P-value was determined by Student's t-test * $P < .05$.

SFig.2: The PI3K pathway cooperates with SUMOylation in PDAC.

Landscape plots depicting the synergistic area of concentrations of copanlisib and subasumstat combination treatment in PDAC cells. Cells were treated with single and combination treatments using a 4 × 6 matrix for 96h. Cell confluency was assessed with clonogenic assay quantification by readout with the Odyssey M imaging system (LiCor Biosciences). Data depicted are mean values from n=3 independent experiments (ZIP synergy score is depicted as mean with corresponding P values).

SFig.3: Insights into the mode of action of the copanlisib and subasumstat combination.

A. Landscape plots depicting the synergistic area of concentrations of PI3K isoform specific inhibitors eganelisib, idelalisib, alpelisb, GSK2636771 or parsaciclib (indicated on the plots) and subasumstat combination treatment with indicated concentrations in MiaPaCa-2 cells. Cells were treated with single and combination treatments using a 4 × 6 matrix for 96h. Cell confluency was assessed with clonogenic assay quantification by readout with the Odyssey M imaging system (LiCor Biosciences). Data depicted are mean values from n=3 independent experiments (ZIP synergy score).

B. Immunoblot analysis of indicated CRISPR/Cas9 mediated p110 isoform MiaPaCa-2 knockout cells (two different clones, each), probed with SUMO1, SUMO2/3 and beta-actin as loading control.

C. Immunoblot analysis of SUMO2/3, cleaved PARP, pAKT (Ser473), AKT, MCL1 and BCL-xL in MiaPaCa-2 cells supplemented with subasumstat (200nM), pictilisib (1000nM) or the combination of both. Alpha-Tubulin served as loading control.

SFig.4: Effects of combination treatment on cell death and cell cycle.

A. Representative images of cleaved caspase 3 (green) and DAPI (blue) upon combination treatment in MiaPaCa-2 cells for the indicated timepoints (subasumstat 200nM, copanlisib 1000nM or combination). Scale bars, 100µm (top). Quantification of imaging results with MiaPaCa-2 cells equipped with a cleaved-caspase reporter system upon indicated treatment (subasumstat 200nM, copanlisib 1000nM or combination) (bottom).

B. Flow cytometry analysis of cell cycle upon single or combination treatment for 72h in PSN1 and MiaPaCa-2 cells (subasumstat 200nM, pictilisib 1000nM or combination). The percentage of cells in each phase of the cell cycle is shown. Data are mean \pm SD; n=3. P-value of one-way ANOVA with Tukey's post hoc test ****< .0001, ***< .001, **< .01.

SFig.5: Disease progression in xenograft model upon combined treatment.

Outline of experimental setup for the investigation of the *in vivo* effects of combined subasumstat and copanlisib treatment. The human MiaPaCa-2 cells were used to generate murine xenograft model. Mice were treated with vehicle, subasumstat, copanlisib and the combination (left). Tumor volume was measured over time (n=4 mice in each group). Data are mean \pm SD; n=4. P-value determined by two-way ANOVA with Tukey's post hoc test (right).

SFig.6: Single cell RNA Sequencing from orthotopically transplanted mice treated with SUMOi, PI3Ki or combination of both.

A. Uniform manifold approximation and projection (UMAP) all cells detected in the 4 treatment groups: vehicle (n=4), subasumstat (n=4), copanlisib (n=4), combination (n=4) are annotated by cell type.

B. Mean expression of mRNA of cell type specific markers to dissect tumor and stroma cell populations derived from all 4 treatment groups.

C. Mean expression of mRNA of T cell specific markers to dissect tumor and stroma cell populations derived from all 4 treatment groups.

D. Mean expression of mRNA of macrophage specific markers to dissect tumor and stroma cell populations derived from all 4 treatment groups.

E. Gene set enrichment analysis of the tumor cell population using the Hallmark set of the Molecular Signature Database in indicated treatment groups, each compared to vehicle control. Only significant pathways (Nominal P-value < .05) are displayed with corresponding normalized enrichment scores.

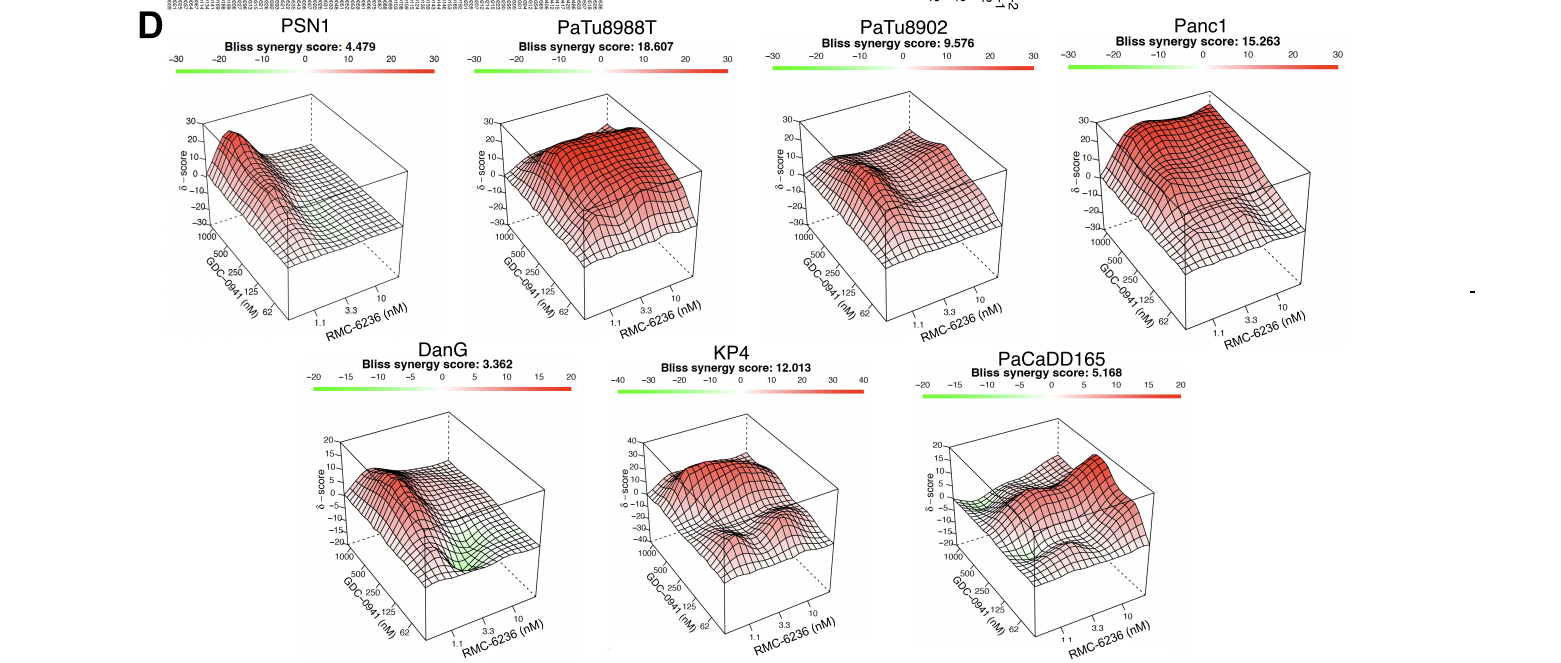
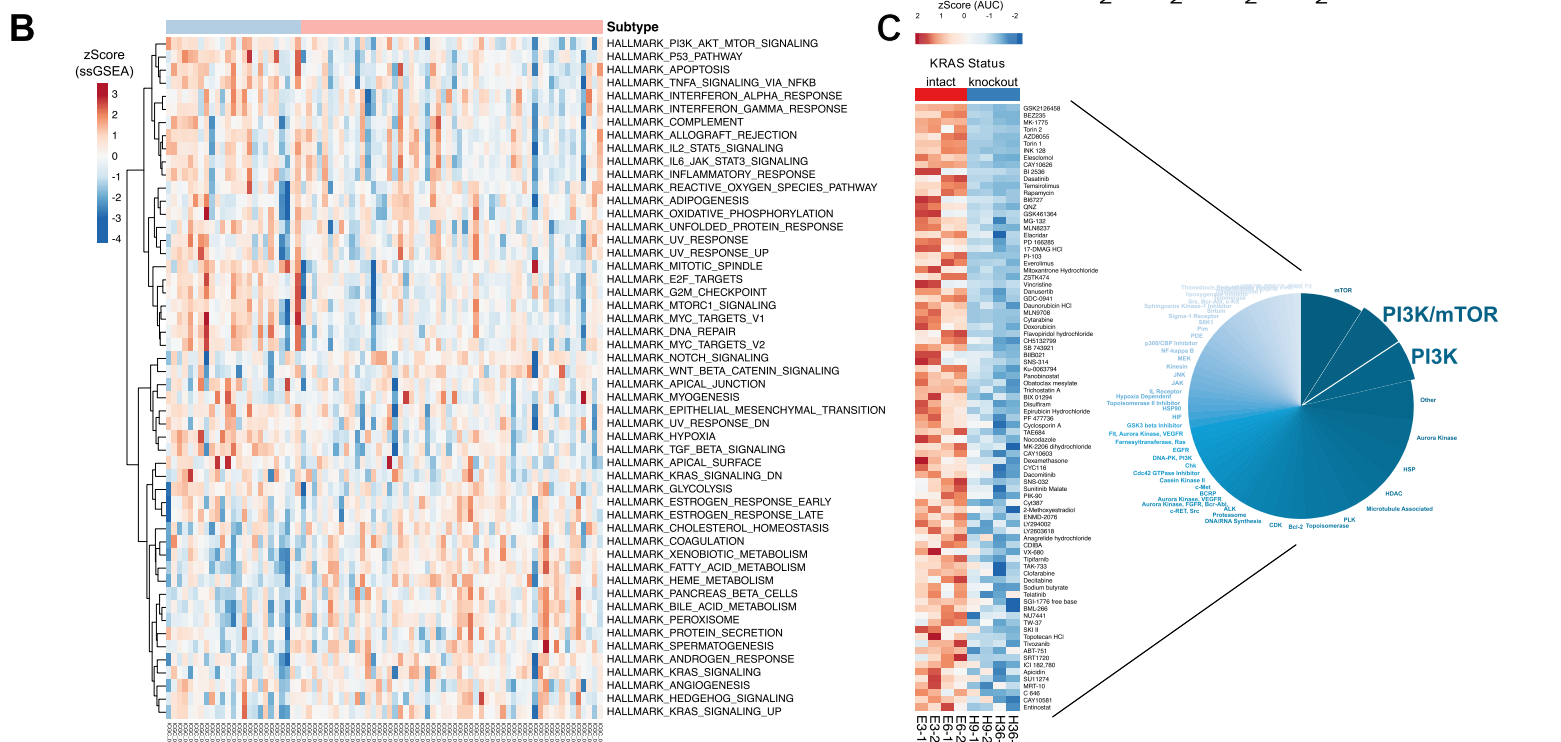
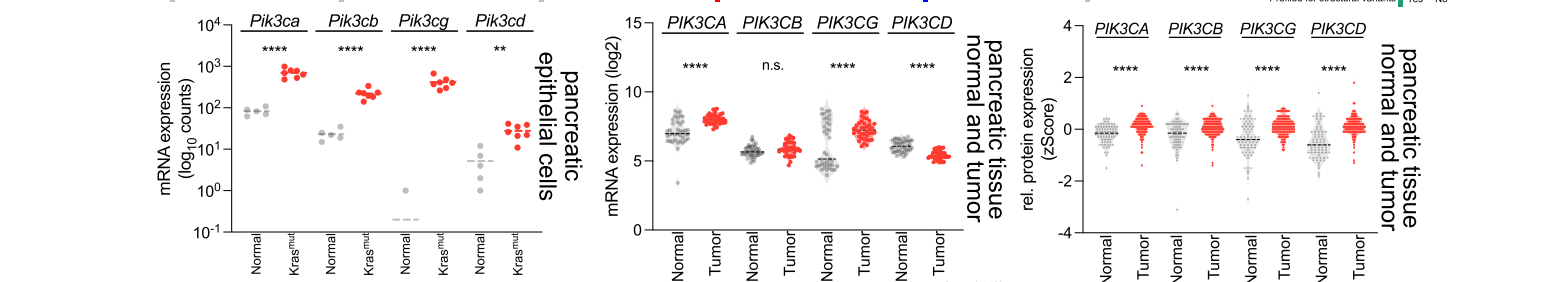
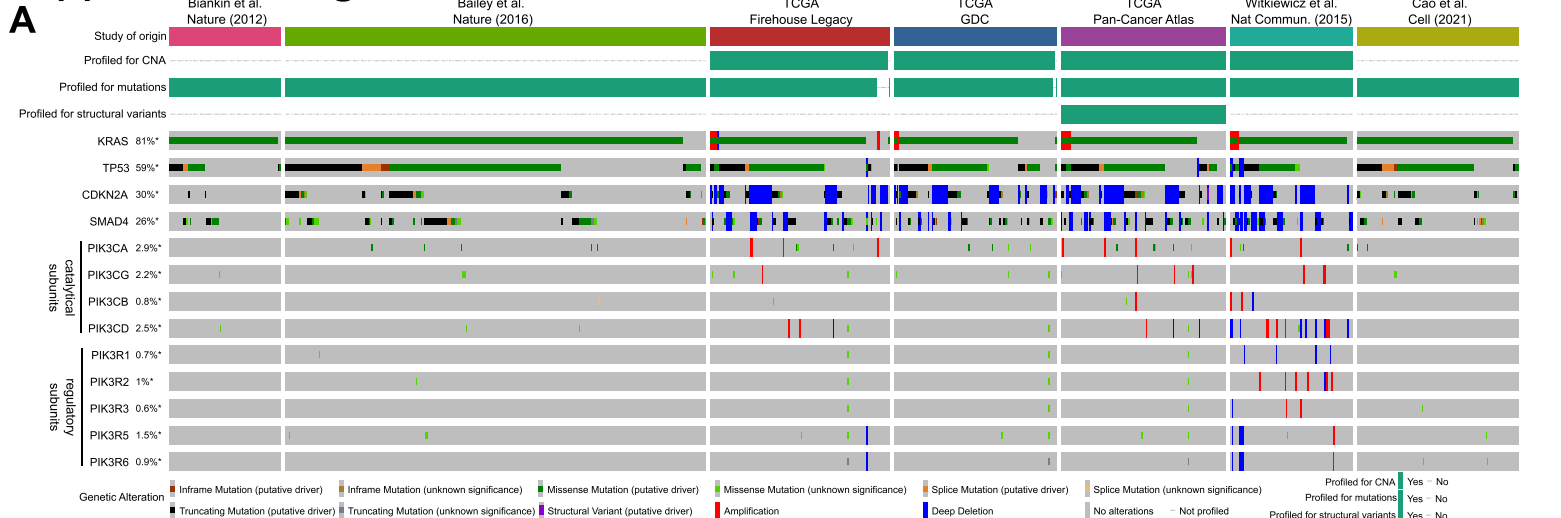
SFig.7: Combination of subasumstat and copanlisib *in vivo* does not induce signs of toxicity or intolerability.

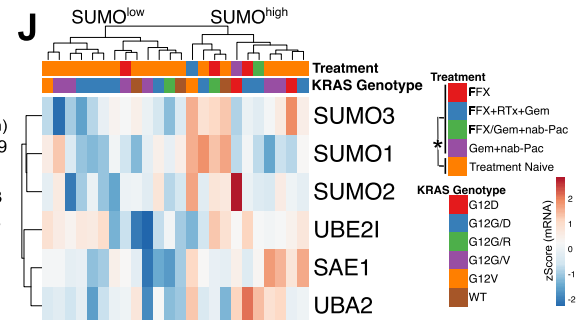
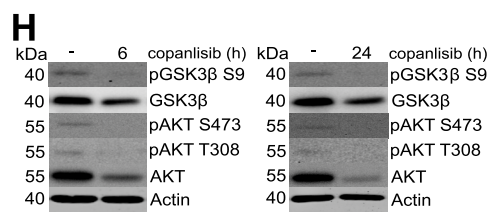
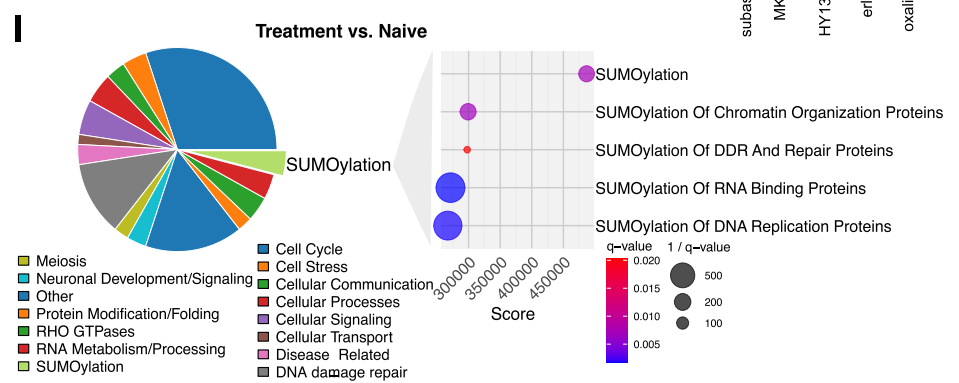
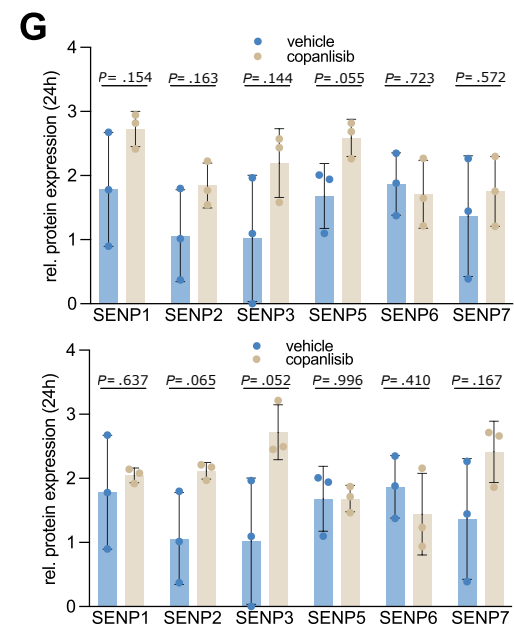
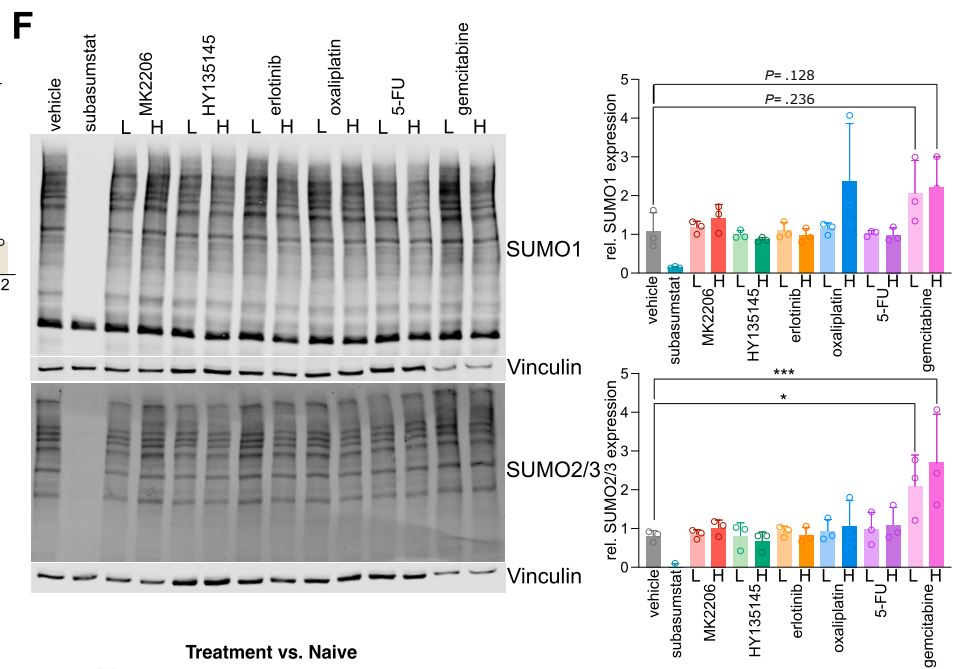
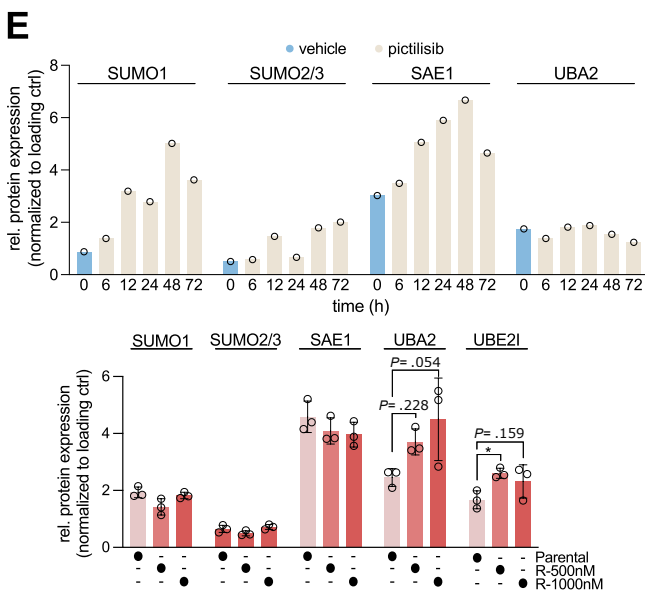
A. Body weight of *C57BL6/J* mice treated with the indicated regimens. Comparisons have been done at the endpoint. Significance determined with one-way ANOVA with Tukey's post hoc test * < .05.

B. Complete blood count from the *C57BL6/J* mice treated with the indicated regimens reveals normal counts (LYM: Lymphocytes, MON: Monocytes, GRA: Granulocytes, EOS: Eosinophils, RBC: Red Blood Cell, HGB: Hemoglobin, HCT: Hematocrit, MCV: Mean Corpuscular Volume, MCH: Mean Corpuscular Hemoglobin, MCHC: Mean Corpuscular Hemoglobin Concentration, RDW: Red Cell Distribution Width, PLT: Platelets, MPV: Mean Platelet Volume). Significance determined with one-way ANOVA with Tukey's post hoc test.

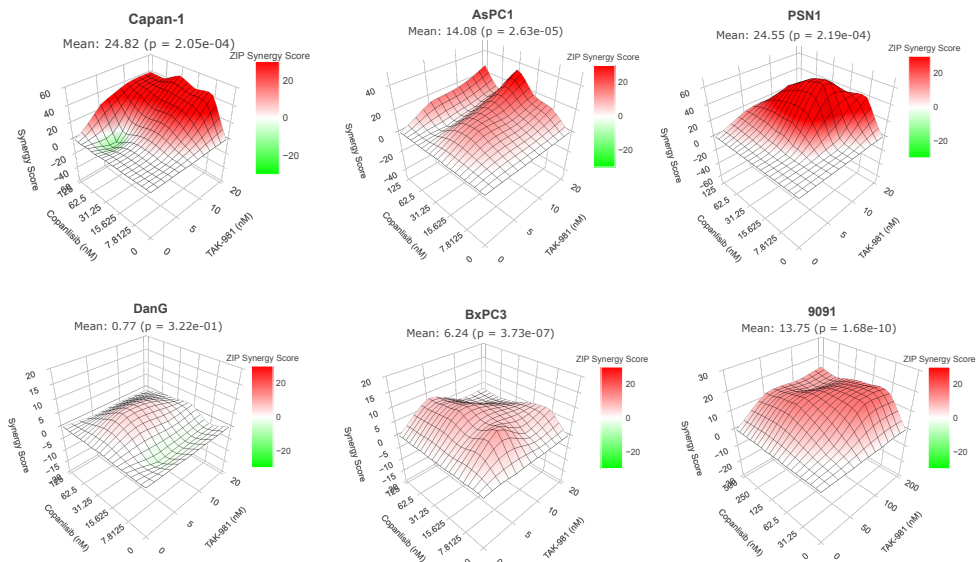
C. Blood serum and liver enzyme analysis from the *C57BL6/J* mice treated with the indicated regimens does not show any sign of toxicity (LDH: Lactate Dehydrogenase, ALP: Alkaline Phosphatase, GPT: Glutamine Pyruvate Transaminase, ALT: Alanine Aminotransferase, GOT: Glutamate Oxaloacetate Transaminase, AST: Aspartate Aminotransferase, Calcium, Inorganic phosphate, Albumin, Urea, total protein, Bilirubin). Significance determined with one-way ANOVA with Tukey's post hoc test.

Supplemental Figure 1

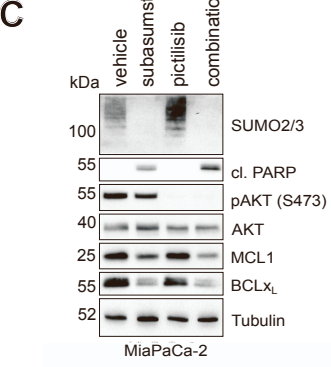
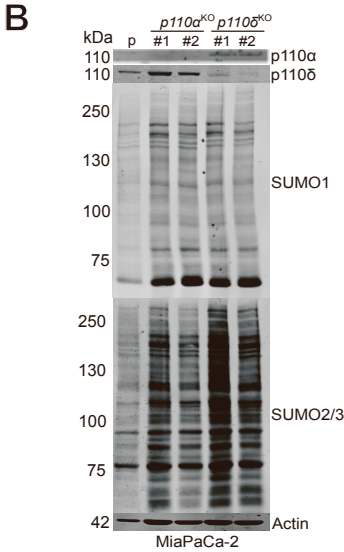
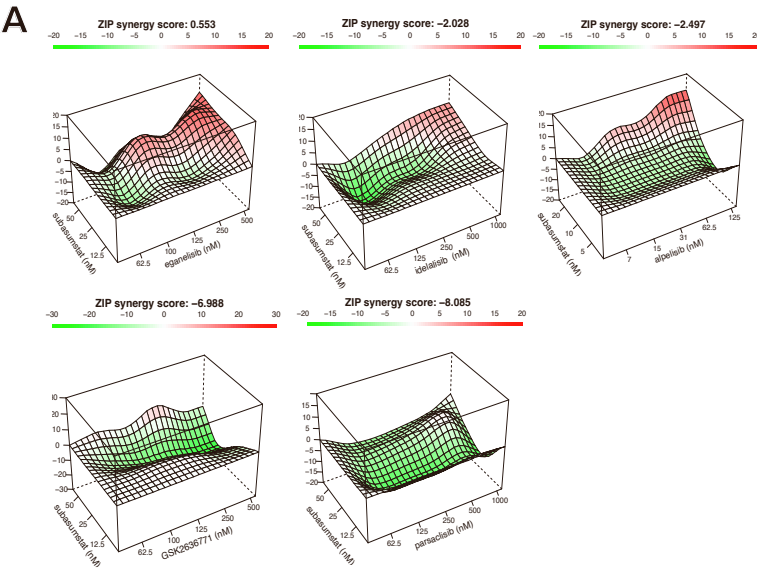




Supplemental Figure 2

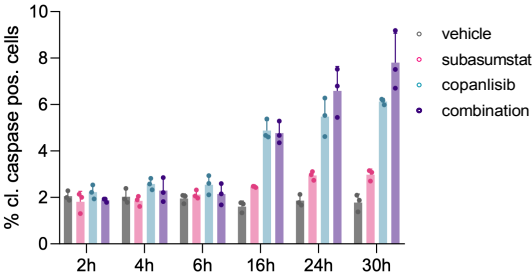
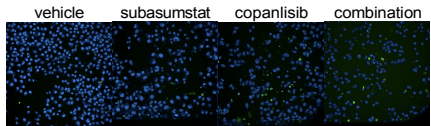


Supplemental Figure 3

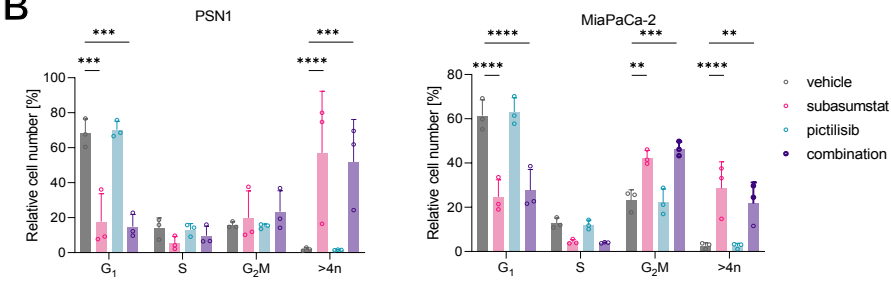


Supplemental Figure 4

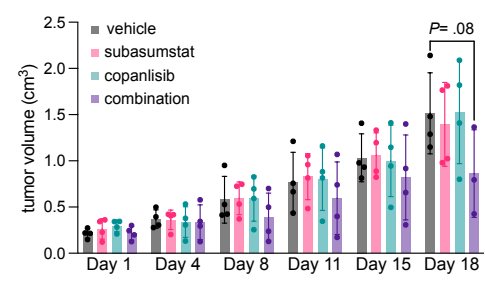
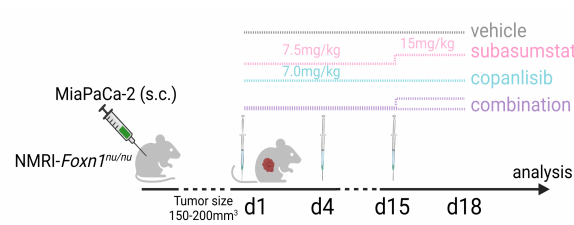
A



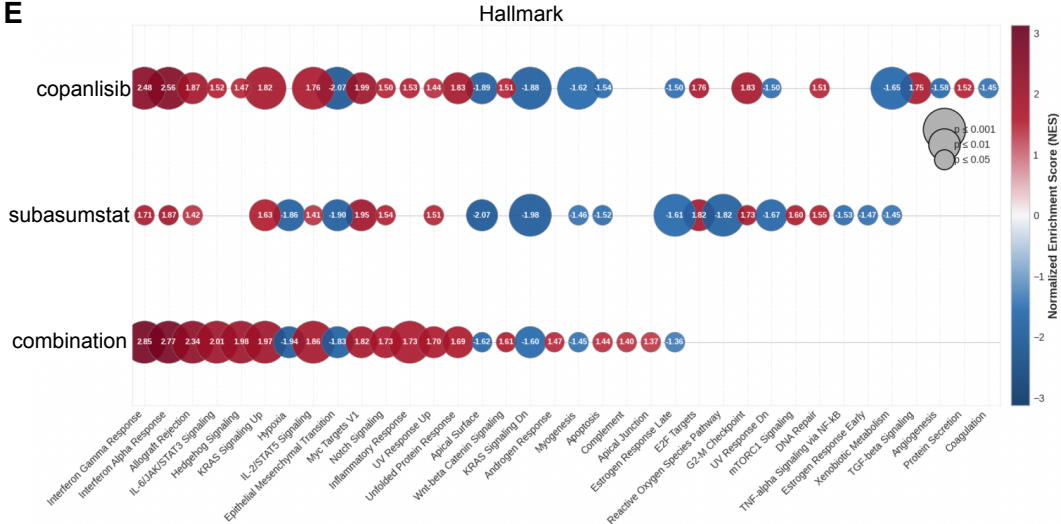
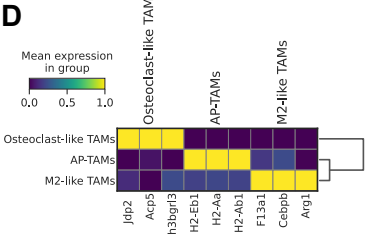
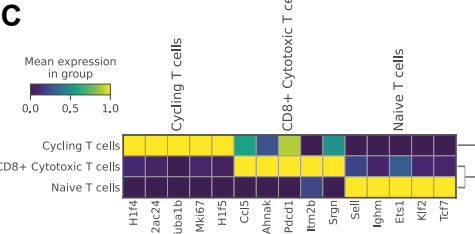
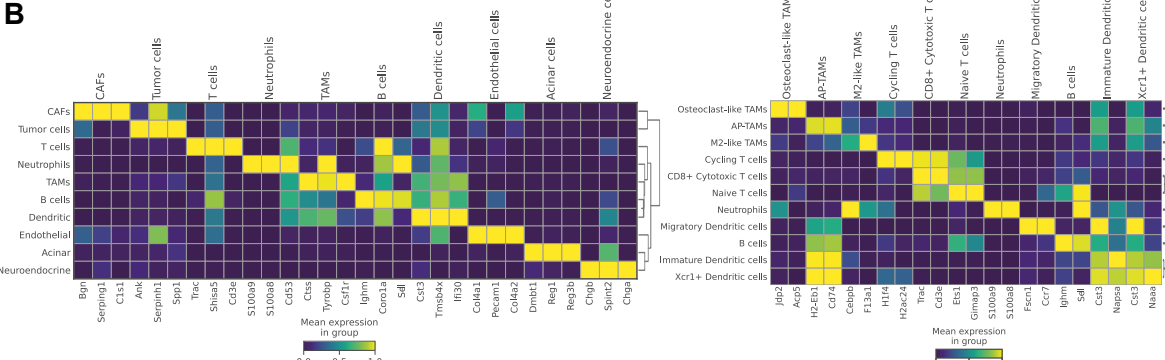
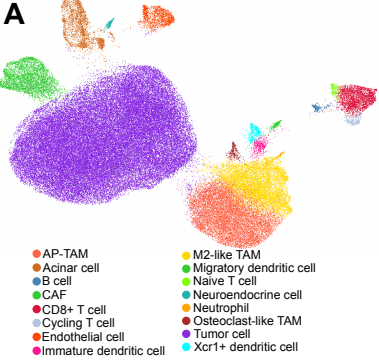
B



Supplemental Figure 5

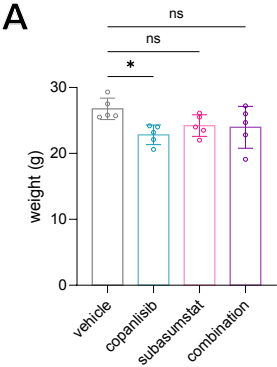


Supplementary Figure 6

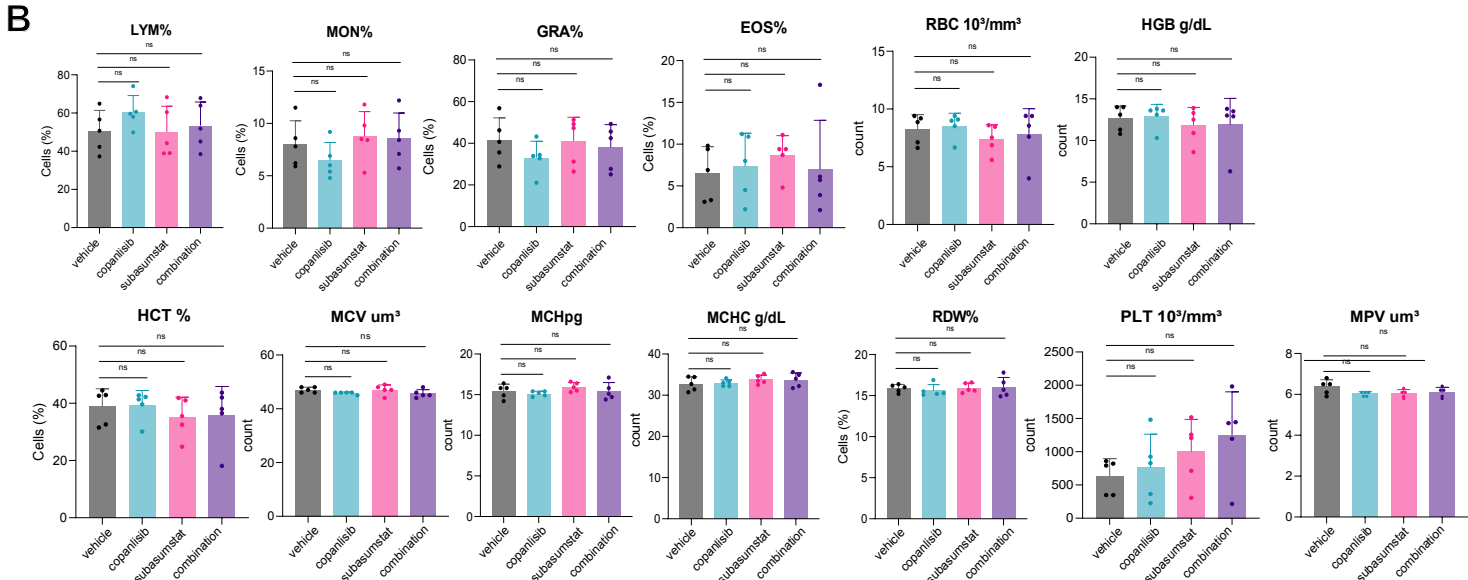


Supplemental Figure 7

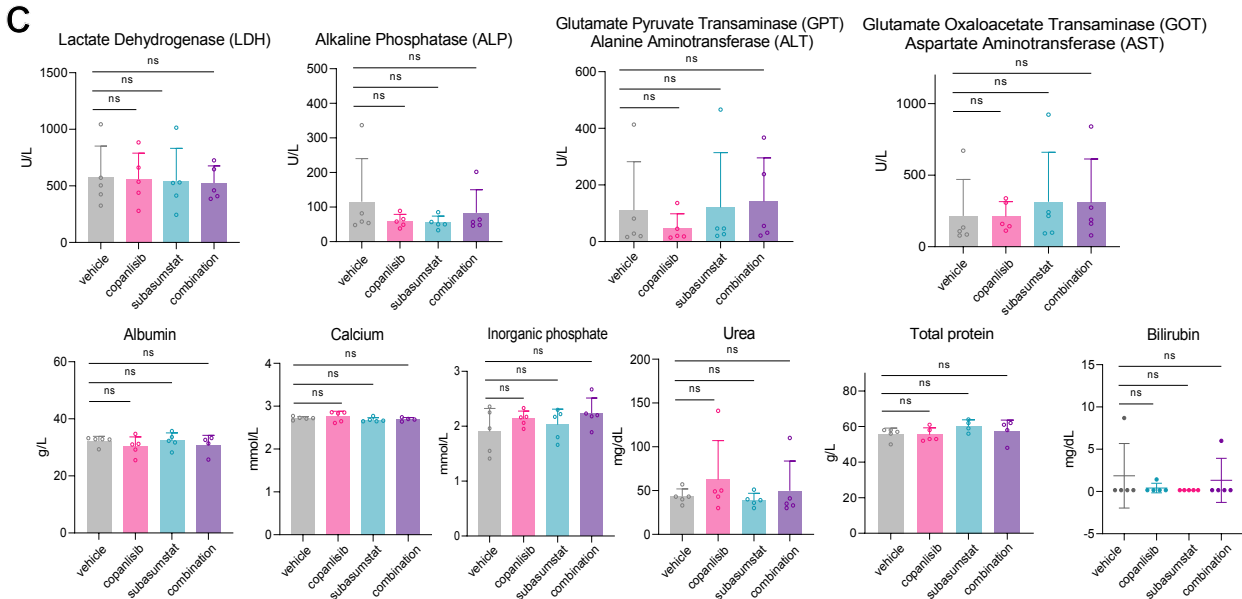
A



B



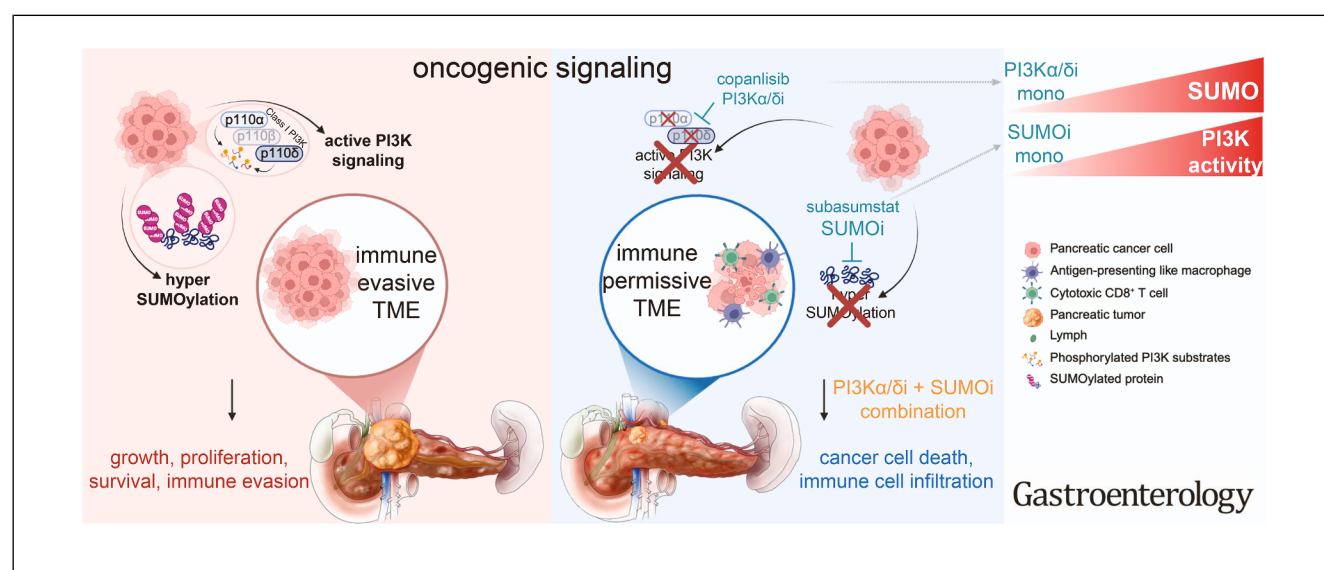
C



Targeting Mutual Dependence of Phosphatidylinositol-3-Kinase α/δ and Small Ubiquitin-Like Modifier Signaling in Pancreatic Cancer

Hazal Köse,^{1,2} Christian Schneeweis,³ Philipp Putze,³ Constanza Tapia Contreras,⁴ Laura Ferreira,^{1,2} Leonie Witte,⁴ Ilaria Deidda,⁴ Frederik Herzberg,^{1,2} Sophie Ebert,⁴ Juraj Jakubik,^{5,6} Leoni Moldaner,^{5,6} Jovan Todorovic,⁷ Isabelle Träger,^{1,2} Chuanbing Zang,^{1,2} Uta M. Demel,^{1,2} Elisabeth Hessmann,^{8,9,10} Marieluise Kirchner,^{11,12} Simone Rhein,¹³ Jens Hoffmann,¹³ Zuzana Tatarova,^{5,6,14} Michael Ghadimi,⁴ Dieter Saur,^{3,15} Kai Kappert,¹⁶ Philipp Mertins,^{11,12} **Günter Schneider,**^{3,4,9,10,§} **Ulrich Keller,**^{1,2,17,§} and **Matthias Wirth**^{1,2,4,18,§}

¹Department of Hematology, Oncology and Cancer Immunology, Charité - Universitätsmedizin Berlin, corporate member of Freie Universität Berlin and Humboldt-Universität zu Berlin, Berlin, Germany; ²Max-Delbrück-Center for Molecular Medicine, Berlin, Germany; ³Institute for Translational Cancer Research and Experimental Cancer Therapy, Technical University Munich, Munich, Germany; ⁴Department of General, Visceral and Pediatric Surgery, University Medical Center Göttingen, Göttingen, Germany; ⁵Institute for Tumor Biology and Experimental Therapy, German Center for Translational Cancer Research (DKTK), Partner Site Frankfurt/Mainz, Georg-Speyer-Haus, Frankfurt, Germany; ⁶German Cancer Research Center (DKFZ), Heidelberg, Germany; ⁷Institute of Pathology, University Medical Center Göttingen, Göttingen, Germany; ⁸Department of Gastroenterology, Gastrointestinal Oncology and Endocrinology, University Medical Center Göttingen, Göttingen, Germany; ⁹CCC-N (Comprehensive Cancer Center Lower Saxony), Göttingen, Germany; ¹⁰Clinical Research Unit 5002, KFO5002, University Medical Center Göttingen, Göttingen, Germany; ¹¹Max Delbrück Center for Molecular Medicine, Berlin, Germany; ¹²Core Unit Proteomics, Berlin Institute of Health at Charité - Universitätsmedizin Berlin, Berlin, Germany; ¹³EPO, Experimental Pharmacology and Oncology Berlin-Buch GmbH, Berlin, Germany; ¹⁴Frankfurt Cancer Institute, Frankfurt, Germany; ¹⁵German Center for Translational Cancer Research (DKTK), Partner Site Munich, Munich, Germany; ¹⁶Institute of Diagnostic Laboratory Medicine, Clinical Chemistry and Pathobiochemistry, Charité - Universitätsmedizin Berlin, corporate member of Freie Universität Berlin and Humboldt-Universität zu Berlin, Berlin, Germany; ¹⁷Cluster of Excellence ImmunoPreCept, Berlin, Germany; and ¹⁸German Center for Translational Cancer Research (DKTK), Partner Site Berlin, Berlin, Germany



BACKGROUND & AIMS: Pancreatic ductal adenocarcinoma (PDAC) is a highly aggressive and lethal cancer, with a 5-year survival rate of <13%. Despite advances in diagnostics and treatments, the standard of care for PDAC remains inadequate, and most patients develop resistance to therapy. Targeted approaches, such as Kirsten rat sarcoma (KRAS) inhibition,

have shown promise in preclinical models, although clinical application remains challenged by the rapid development of resistance. The phosphatidylinositol-3-kinase (PI3K) signaling pathway is critical for PDAC development and maintenance, yet pharmacologic targeting has failed to yield significant clinical benefits. **METHODS:** To investigate the relationship

between the PI3K and small ubiquitin-like modifier (SUMO) pathways in PDAC, we used a comprehensive approach that included unbiased genome-wide clustered regularly interspaced short palindromic repeats/clustered regularly interspaced short palindromic repeats-associated protein 9 resistance screens, pharmacologic screens, transcriptomics, proteomics, and phosphoproteomics experiments. Genetic knockout models were applied to validate our findings. A novel molecularly targeted combination therapy was tested in pre-clinical mouse models. **RESULTS:** Using genetic and pharmacologic screenings, we discovered a mutual and targetable codependence between the PI3K and the SUMO pathways. Simultaneous inhibition of PIK3 α and PIK3 δ , combined with SUMO-activating E1 targeting, triggered synthetic lethality and cell death. In syngeneic orthotopic immune-competent PDAC models, this combination therapy reduced tumor growth and promoted immune cell infiltration and activity. **CONCLUSIONS:** Our study introduces a novel rational combination therapy in PDAC. Dual targeting of PI3K α/δ and SUMO signaling bears potential for clinical translation.

Keywords: Pancreatic Cancer; PI3K; SUMOylation; Regulated Cell Death; Combination Therapy.

Pancreatic ductal adenocarcinoma (PDAC) is one of the most aggressive and deadliest cancers, with a 5-year survival rate of just 13%. Despite its increasing incidence, including in younger patients, treatment options for PDAC remain limited and nonsatisfying.¹ PDAC is defined by a distinct genetic landscape, with frequent mutations in *KRAS*, *TP53*, *CDKN2A*, and *SMAD4*.² Activating *KRAS* mutations, present in 90% of cases, position the Kirsten rat sarcoma virus (*KRAS*)/mitogen-activated protein kinase signaling pathway as a central driver of tumor progression and a critical therapeutic target. Consequently, the recently developed *ras* sarcoma (RAS) inhibitors, including mutant-selective and pan-RAS inhibitors, have demonstrated promising early signs of clinical efficacy in PDAC.³ However, genetic and adaptive resistance to RAS inhibition remains challenging,³ underscoring the need of additional molecular targeted treatment strategies.

The phosphatidylinositol-3-kinase-(PI3K)-protein kinase B (AKT)-mechanistic target of rapamycin pathway has recently been implicated in resistance to RAS inhibitors.⁴ Furthermore, the finding that oncogenic PI3K-signaling can compensate *KRAS*-dependency to initiate and drive carcinogenesis and tumor progression in murine PDAC models^{5,6} highlights the PI3K pathway's significance as a therapeutic target. PI3K family kinases include 3 classes. Class Ia (p110 α /PIK3CA, p110 β /PIK3CB, and p110 δ /PIK3CD) and class Ib (p110 γ /PIK3CG) catalytic subunits are particularly relevant in clinical settings, with inhibitors targeting these isoforms available.⁷ PIK3CA mutations are the most common alterations within class I PI3Ks and may predict sensitivity to PI3K inhibition in preclinical PDAC models.⁷⁻⁹ Moreover, several isoform-specific PI3K inhibitors have been evaluated in clinical trials for solid tumors, including PDAC. Alpelisib (BYL-719), a PI3K α inhibitor (NCT02155088,

WHAT YOU NEED TO KNOW

BACKGROUND AND CONTEXT

Resistance to therapeutic interventions for pancreatic ductal adenocarcinoma remains challenging. Phosphatidylinositol-3-kinase signaling is critical for pancreatic ductal adenocarcinoma maintenance and progression, but pharmacologic targeting has failed to yield significant clinical benefits.

NEW FINDINGS

Simultaneous inhibition of phosphatidylinositol-3-kinase α/δ , combined with small ubiquitin-like modifier-activating E1 targeting, triggered synthetic lethality. In syngeneic immune-competent pancreatic ductal adenocarcinoma models, this combination therapy reduced tumor growth and promoted immune cell infiltration.

LIMITATIONS

Combining phosphatidylinositol-3-kinase α/δ and small ubiquitin-like modifier inhibitors triggered an immune-assisted anti-tumor response, marked by an unexpected immunophenotype, a phenomenon that requires further investigation in future studies.

CLINICAL RESEARCH RELEVANCE

The dual targeting of phosphatidylinositol-3-kinase α/δ and small ubiquitin-like modifier shows efficacy, manageable toxicity in mice and potential for clinical translation in pancreatic ductal adenocarcinoma, a cancer with significant unmet medical needs.

BASIC RESEARCH RELEVANCE

Blockade of the phosphatidylinositol-3-kinase pathway leads to the adaptive activation of the small ubiquitin-like modifier (SUMO)ylation machinery and vice versa. Only the combined inhibition of both phosphatidylinositol-3-kinase α and δ with a clinical-grade E1 small ubiquitin-like modifier inhibitor induced synergistic cell death in vitro and demonstrated synergy in an immunocompetent in vivo model. Our work highlights the unexpected requirement of phosphatidylinositol-3-kinase α and δ in the small ubiquitin-like modifier-ylation-associated stress response.

§ Authors share co-senior authorship.

Abbreviations used in this paper: AKT, protein kinase B; Cas, clustered regularly interspaced short palindromic repeats-associated; CD, cluster of differentiation; CRISPR, clustered regularly interspaced short palindromic repeats; cyclIF, cyclic immunofluorescence; GSEA, gene set enrichment analysis; *KRAS*, Kirsten rat sarcoma viral oncogene homologue; MYC, myelocytomatosis oncogene; PDAC, pancreatic ductal adenocarcinoma; PDO, patient-derived organoid; PI3K, phosphatidylinositol-3-kinase; PI3Ki, phosphatidylinositol-3-kinase inhibitor; RAS, rat sarcoma; RCD, regulated cell death; RNAseq, RNA sequencing; SAE1, small ubiquitin-like modified-activating enzyme subunit 1; snRNA, single nuclei RNA; SOC, standard of care; SUMO, small ubiquitin-like modifier; SUMOi, small ubiquitin-like modifier E1 inhibitor; TME, tumor microenvironment.

© 2025 The Author(s). Published by Elsevier Inc. on behalf of the AGA Institute. This is an open access article under the CC BY license (<http://creativecommons.org/licenses/by/4.0/>).

0016-5085

<https://doi.org/10.1053/j.gastro.2025.08.018>

NCT02437318), has demonstrated tolerability in PDAC patients and efficacy in *PIK3CA*-mutated breast cancer.¹⁰ GSK2636771, a PI3K β inhibitor, is currently under investigation (NCT04439188) in patients with *PTEN* loss.¹¹ Eganalisib (IPI549), targeting PI3K γ (NCT02637531), has shown immune-modulation and antitumor activity when combined with nivolumab in solid tumors.¹² In contrast, idelalisib (CAL-101) and piasclisib (INCB050465), both targeting PI3K δ (NCT02468557, NCT02559492), have exhibited limited efficacy in solid tumors.^{13,14} These findings highlight the clinical potential of isoform-specific PI3K inhibitors; however, their role and targeting spectrum in the treatment of PDAC has yet to be established.

The small ubiquitin-like modifier (SUMO)ylation signaling pathway is a cellular process in which SUMOs are attached to target proteins, altering their function, stability, or localization. SUMOylation plays a crucial role in regulating processes such as transcription, DNA repair, the cell cycle, and stress responses.¹⁵ Pharmacologic targeting of the SUMO pathway has shown efficacy in PDAC and other malignancies in preclinical models.^{16,17}

To harness the therapeutic potential of PI3K-pathway inhibition in PDAC, we investigated pathway co-dependencies to inform translational strategies. We observed that blockade of the PI3K pathway leads to the adaptive activation of the SUMOylation machinery and furthermore observed a vice versa process. Only the combined inhibition of both PI3K α and PI3K δ with a clinical-grade SUMO-inhibitor induced synergistic cell death in vitro and demonstrated synergy in an immunocompetent in vivo model. Our work highlights the unexpected requirement of PI3K α and PI3K δ in the SUMO-associated stress response and unveils a novel combination therapy approach with the potential for clinical applicability.

Methods

Pharmacologic Screen

The drug library consisting of ≥ 99 inhibitors targeting various relevant cancer pathways in PDAC was purchased from Selleckchem. Subastumstat was kindly gifted by Takeda. Copanlisib (cat no HY-15346R) and pictilisib (cat no HY-50094) were purchased from MedChemExpress LLC. The drug screen was conducted in MiaPaCa-2, PSN-1, and 53631PPT cells, as recently described.¹⁸ After 72 hours of treatment, viability was measured. Plates were incubated at room temperature for 30 minutes. 25 μ L of CellTiter-Glo (Promega) was added to each well, incubated for 15 minutes, and luminescence was measured (FLUOstar-OPTIMA-microplate-reader, BMG-Labtech). Area under the curve and half-maximal growth inhibitory concentration values were calculated with RStudio (Posit Software) using a GRmetrics script.

Western Blot

Cells were treated with various conditions and harvested at different time points, and their protein lysates were analyzed by Western blot using specific primary antibodies and horseradish peroxidase-conjugated secondary antibodies.

The blots were developed using the OdysseyM imager (LI-COR Biotech), and the data were analyzed using EmpiriaStudio software (LI-COR Biotech).

Growth Curves by Cell-Live Imaging

Cells were seeded onto 96-well plates (5×10^3 cells/well), grown for 24 hours, and then treated with the indicated compounds. Confluency was determined by monitoring cells in real time with a confluency image mask, which was filtered for each cell line specifically. Cell confluency was quantified by 2024A version of the Incucyte software.

CRISPR/Cas9-based Gene Editing

Depletion of PI3K α a fragment from exon-2 and depletion of PI3K δ from exon-3 was mediated by clustered regularly interspaced short palindromic repeat (CRISPR)/clustered regularly interspaced short palindromic repeat associated protein 9 (Cas9). Then, 150,000 cells were transfected with 500 ng of single-guide (sg)RNA and 1 μ g of Cas9 protein (PNA-Bio) with a Neon-Transfection-System (Thermo Fisher/Invitrogen). A list of single-guide RNA sequences is available in the [Supplementary Material and Methods](#). Cleavage efficacy was tested 72 hours after transfection with Terra PCR Direct Card Kit (Takara Bio). Single cells were generated by serial dilution. Clones were screened for efficient gene editing, and selected clones were analyzed for protein expression by immunoblotting.

In Situ Resistance Assay

Cells were seeded onto a 96-well plate at a density of 250 cells/well on day 0. On day 1, treatment was added. Medium was changed and drugs refreshed weekly. Each week, cell confluency was analyzed using Incucyte (Live-Cell Imager, Sartorius). Wells reaching $>50\%$ confluency were scored as resistant. Data were plotted as a Kaplan-Meier plot.¹⁹

Toxicity Analysis in Mice

Serum samples of mice were isolated by postmortem cardiac puncture centrifuged at 2000g for 10 minutes. The concentrations of lactate dehydrogenase activity, albumin, calcium, urea, total protein, bilirubin, alanine aminotransferase, aspartate aminotransferase, alkaline phosphate, and inorganic phosphate were analyzed by photometry on a Roche cobas analyzer (Roche Diagnostics, Rotkreuz, Switzerland).

Detailed information on single-nuclei (sn)RNA sequencing (seq), RNAseq, processing, and analysis of gene expression data; CRISPR/Cas9-knockout screen; cell culture and treatment, chemicals, viral infection, and colony formation assay; cyclic immunofluorescence; in vivo drug efficacy analysis in mice and immunohistochemistry; patient-derived organoids; global and phosphoproteomics; and flow cytometry is available in the [Supplementary Material](#).

Statistics

Statistical analyses were performed using GraphPad Prism (GraphPad Software). *P* values $< .05$ were considered significant. All *P* values and tests are indicated in the figure legends.

Results

The SUMOylation Pathway Is Activated by PI3K Inhibition

PI3K-signaling is considerably involved in therapy resistance in multiple tumor entities.^{20–22} In PDAC, catalytic class-I PI3-kinase expression is increased (Supplementary Figure 1A). Both basal-like and mesenchymal subtypes, which overlap and are known to be more resistant to chemotherapy,²³ exhibit elevated PI3K/AKT-pathway activity, although mutations are rarely found (Figure 1A and B²⁴ and Supplementary Figure 1A and B). Mining data of patient-derived organoids (PDOs) isolated from treatment-naïve patients and patients after standard-of-care (SOC) chemotherapy²⁵ revealed a significant enrichment of the PI3K/AKT-signaling signatures in SOC-treated PDAC patients (Figure 1C). Furthermore, KRAS-knockout PDAC cells exhibited activated PI3K-dependent mitogen-activated protein kinase signaling and were sensitive to PI3K inhibition (Supplementary Figure 1C).²⁶ The combination of KRAS-inhibition by RMC-6236, a multiselective RAS^{on} inhibitor, and PI3K inhibition by pictilisib (a PIK3 α/δ inhibitor) acted synergistic in selected PDAC cell lines (Supplementary Figure 1D). Together, these data highlight the critical role of PI3K-dependent rewiring of oncogenic networks in cells with perturbed KRAS. Therefore, specifically in the context of PDAC, PI3K signaling plays a crucial role in adaptation to therapy and in treatment resistance.

To gain a deeper understanding of PI3K-controlled molecular networks, we analyzed a CRISPR^{knockout}-based PI3K-inhibitor (pictilisib) resistance screen²⁷ and identified SUMOylation-related pathways as synthetic lethal (Figure 1D). To causally test the relationship between PI3K-inhibition and changes in SUMOylation, we investigated the course of global protein SUMOylation upon PI3K inhibition with the formerly United States Food and Drug Administration-approved PIK3 α/δ inhibitor copanlisib. Indeed, over time, PI3K inhibition induced protein SUMOylation (Figure 1E and Supplementary Figure 1E), pointing to a role of SUMO in cells with inactivated PI3K signaling.

To extend our findings, we generated PI3K-inhibitor (copanlisib)-resistant PDAC cells (PI3K-R) and identified the induction of the SUMO-pathway core components SUMO1, SUMO2, SUMO3, and SUMO-activating enzyme subunit 1 (SAE1), ubiquitin-like modifier activating enzyme 2 (UBA2), and UBE2I (Figure 1F and Supplementary Figure 1E). We also examined the SUMOylation status after application of several selected SOC or targeted compounds. We observed induction of SUMOylation in some treatments, but not a general SUMO induction (Supplementary Figure 1F).

We next evaluated SUMOylation induction in PI3K inhibitor-treated MiaPaCa-2 by proteomics and phosphoproteomics (Figure 1G). Here, we found a significant induction of SUMO1 after 6 hours and SUMO2 after 24 hours (Figure 1H) upon PI3K inhibition. Additionally, various SUMOylation-related signatures were induced already after 6 hours, with some sustained after 24 hours (Figure 1I),

indicating early changes of protein SUMOylation in PI3K-inhibited cells. Sentrin/SUMO-specific proteases, which contribute to the maturation and homeostasis of SUMOylated proteins,²⁸ also showed a tendency toward induction after PI3K inhibition, with the SUMO2/3-specific deSUMOylase sentrin/SUMO-specific protease 3 being induced in particular (Supplementary Figure 1G). Phosphoproteomics and immunoblotting confirmed efficacy of PI3K inhibitor treatment as indicated by reduced phosphorylation of downstream targets (Figure 1J and Supplementary Figure 1H).

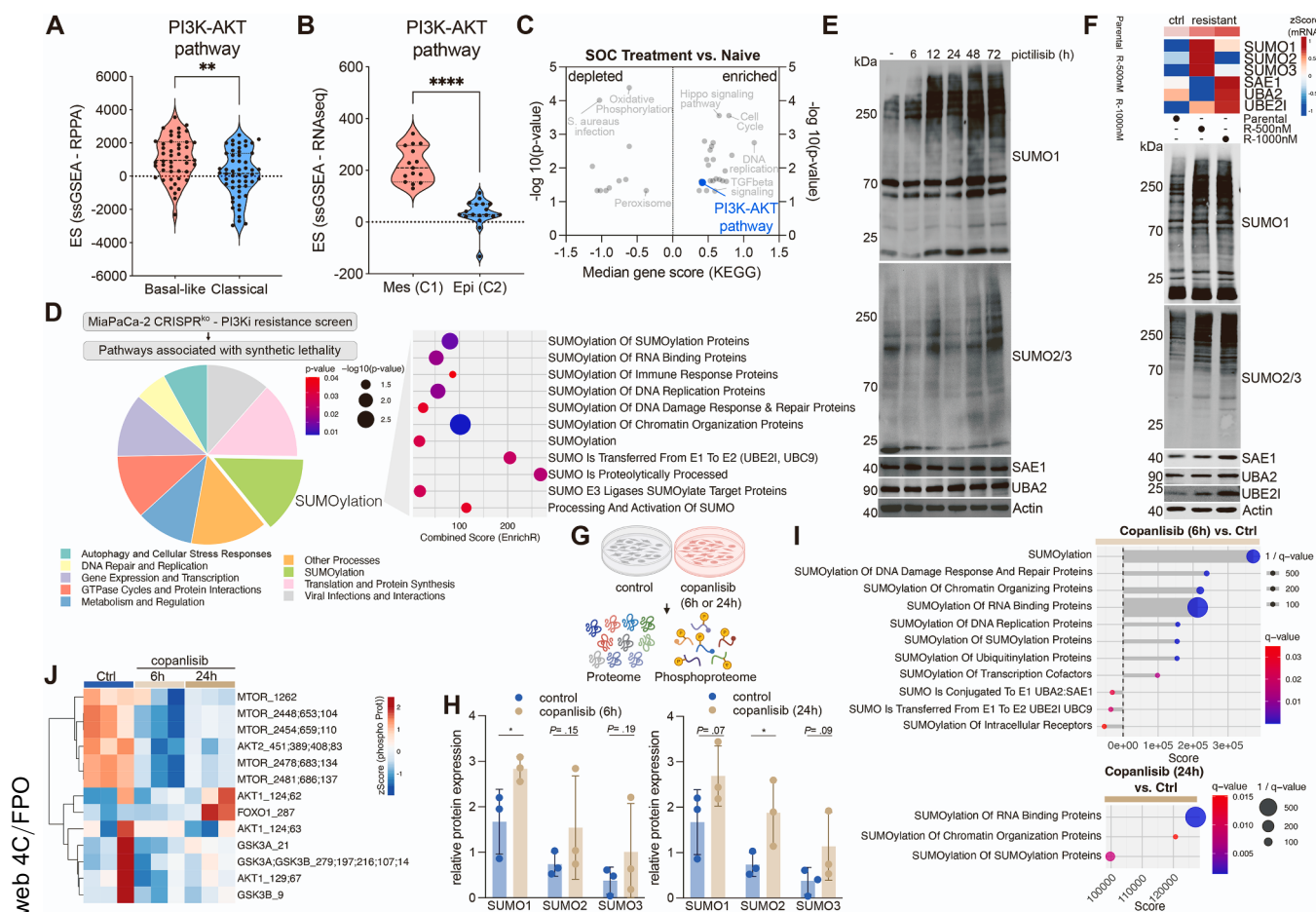
Together, these data show the induction of SUMOylation upon blockade of the PI3K pathway. Considering the synthetic lethal relation detected in the CRISPR screen (Figure 1D), the activation of SUMOylation pointed toward a functional relevance for PDAC cell survival.

SUMOylation Inhibition Induces PI3K Dependence

Observing the activation of SUMOylation in response to PI3K inhibition and in patients receiving SOC (Supplementary Figure 1I and J), we next sought to identify global PDAC dependencies in the context of SUMO pathway targeting. To this end we applied the highly specific clinical-grade SUMO E1 inhibitor (SUMOi) subasumstat²⁹ in a genome-wide CRISPR-knockout resistance screening in MiaPaCa-2 and PSN1 (Figure 2A). Indeed, we revealed that loss of genes associated with the PI3K/AKT pathway exhibited significant synthetic lethality in the context of SUMO blockade (Figure 2B and Supplementary Table 1). Complementary to the forward-directed genetic screen, we performed a subasumstat-anchored pharmacologic screen in human (MiaPaCa-2 and PSN1) and murine 53631PPT PDAC cell lines (Supplementary Table 2). Again, we identified a synthetic lethal relation between the SUMO and PI3K pathways (Figure 2C), which could be validated by multidose treatment with subasumstat (Figure 2D). In sum, these findings pointed toward a potential codependence of the 2 pathways in PDAC.

Pictilisib and copanlisib both exhibit equipotent inhibition of PIK3 α and PIK3 δ and less potent inhibition of PIK3 β and PIK3 γ isoforms.^{30,31} Owing to the ample (pre)clinical data, including some efficacy as well as toxicity and tolerability from clinical studies in lymphoma³² and other cancer entities,³³ we focused further studies on the formerly Food and Drug Administration-approved compound copanlisib. Combined treatment with copanlisib and subasumstat proved a targetable codependence between both pathways (Figure 2E and F). The synergistic effects of combined PI3K/SUMO targeting were confirmed in an expanded panel of PDAC cell lines (Supplementary Figure 2).

Taken together, these data indicate that SUMOylation inhibition provoked a cellular dependency on PI3K signaling. PI3K signaling thus represents a convergent node and specific vulnerability in PDAC cells lacking a functional SUMOylation machinery, and vice versa.



Simultaneous Inhibition of PIK3 α/δ and SUMO Is Required to Induce Synthetic Lethality

Our data indicate that inhibition of PIK3 α and PIK3 δ effectively induced susceptibility to SUMOylation inhibition, a crucial finding for clinical translation. To further

corroborate the dependency on specific PI3K isoforms and to provide robust data vital for clinical translation, we directly tested various PI3K inhibitors with known specificities for individual PI3K isoforms: alpelisib (PI3K α),¹⁰ GSK2636771 (PI3K β),¹¹ eganelisib (PI3K γ),¹² idelalisib

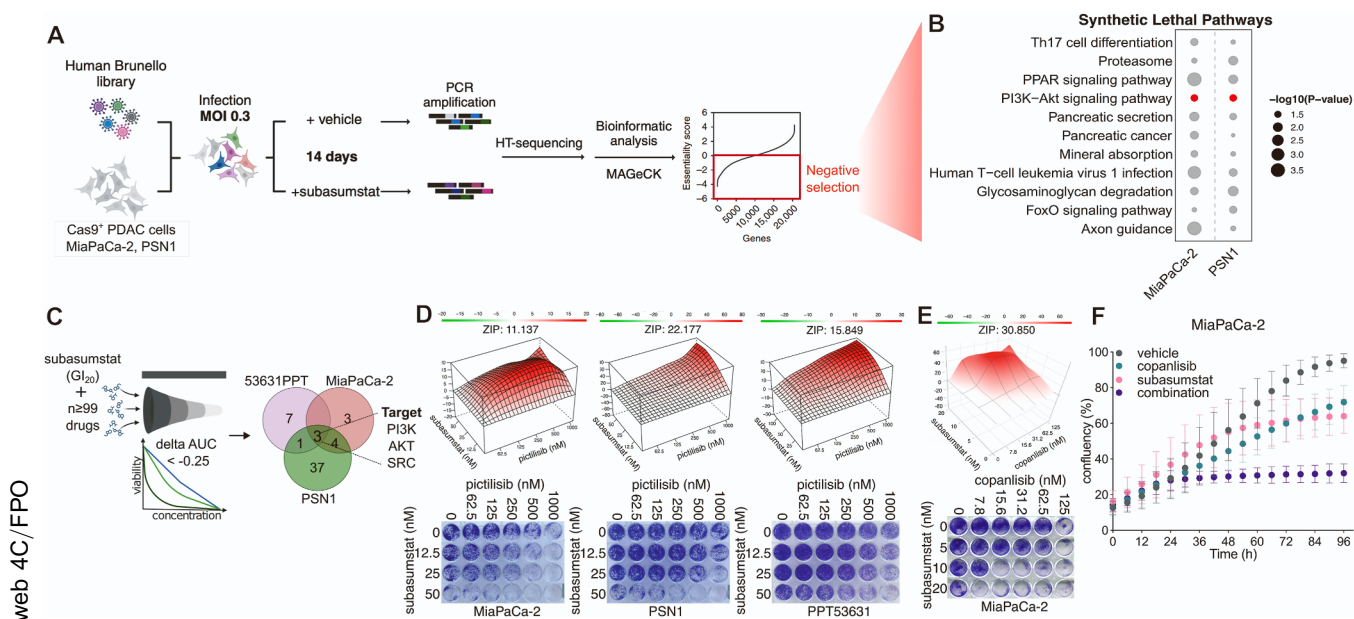


Figure 2. Synthetic lethal interaction between SUMO and PI3K pathways. (A) Schematic overview of the genome-wide CRISPR/Cas9 knockout subasumstat-resistance screen strategy conducted in MiaPaCa-2 and PSN1. HT, high throughput; MAGeCK, Model-based Analysis of Genome-wide CRISPR/Cas9 Knockout; MOI, multiplicity of infection; PCR, polymerase chain reaction. (B) Kyoto Encyclopedia of Genes and Genomes (KEGG) pathway analysis of negatively selected genes from CRISPR^{knockout} screens in the MiaPaCa-2 and PSN1 exposes the PI3K-Akt pathway as a common synthetic lethal pathway. PPAR, peroxisome proliferator-activated receptors; Th17, T helper 17. (C) Illustration/results of the subasumstat-anchored pharmacologic screen setup of subasumstat 20% growth inhibitory concentration (GI₂₀) and multidose treatment of n ≥ 99 compounds indicating in 3 indicated cell lines. AUC, area under the curve. (D) *Top*: Landscape plots depicting the synergistic area of concentrations of subasumstat and the PI3K inhibitor (pictilisib) in the 3 PDAC indicated cell lines. Synergy score was determined by SynergyFinder using the Zero Interaction Potency (ZIP) method. *Bottom*: Representative colony-growth images after treatment with subasumstat and pictilisib. (E) *Top*: Landscape plot depicting the synergistic area of concentrations of subasumstat and copanlisib in MiaPaCa-2. *Bottom*: Representative colony-growth image after treatment with subasumstat and copanlisib. (F) Proliferation of MiaPaCa-2 supplemented with subasumstat, copanlisib, or the combination of both. Cell confluency data were obtained by live cell imaging (n = 3). The range bars designate standard deviation.

(PI3K δ),³⁴ and parsacalisib (PI3K δ),¹⁴ all in combination with subasumstat. None of the isoform-specific PI3K inhibitors displayed synergism with subasumstat (Figure 3A and B, Supplementary Figure 3A). To substantiate these findings, we performed genetic knockouts of PIK3 α or PI3K δ isoforms by CRISPR/Cas9 (Figure 3C and Supplementary Figure 3B). Single knockout of the PIK3 α or PI3K δ isoforms did not exhibit synergism under subasumstat treatment. However, treating PI3K α knockout cells with a PI3K δ -specific inhibitor displayed synthetic lethality with the SUMO inhibitor subasumstat (Figure 3D and E). Confirming our previous data on SUMO pathway activation upon pharmacological PI3K-targeting (Figure 1) and supporting the codependence of the 2 pathways and in particular the specific PI3K isoforms, the SUMO state was increased in p110 δ /PI3K δ and p110 α /PI3K α knockout cells (Figure 3F, and Supplementary Figure 3B). In parental cells, the induction of a polySUMOylation high state upon PIK3 α / δ inhibition was blocked upon combination with subasumstat (Supplementary Figure 3C).

Together, these results show that highly specific PI3K α / δ inhibition or loss of PI3K α / δ induced profound activation of protein SUMOylation and created a targetable vulnerability. Consequently, inhibition of specifically PI3K α / δ is required

and sufficient for optimal synergy with SUMO-targeting by subasumstat.

Combined PI3K α / δ -SUMO Inhibition Induces Regulated Cell Death in Pancreatic Ductal Adenocarcinoma

To identify relevant pathways responsible for the fate of PDAC cells upon dual PI3K and SUMO inhibition, we examined the transcriptome and (phospho-)proteome upon monotreatment and combination treatment with copanlisib and subasumstat (Figure 4A). Single-sample gene set enrichment analysis (GSEA) revealed distinct patterns in the transcriptome (Figure 4B) and proteome (Figure 4C). PI3K signaling was significantly reduced and myelocytomatosis oncogene (MYC) signatures were depleted in both copanlisib monotherapy and combination with subasumstat, consistent with earlier observations.^{35,36} By analyzing hallmark signatures of the molecular signature database (MSigDb) enriched in the transcriptome and the proteome in the combination treatment, we identified 6 overlapping signatures, including metabolic, heme metabolism, and apoptosis signatures (Figure 4D). Therefore, we analyzed the expression of proteins related to apoptosis

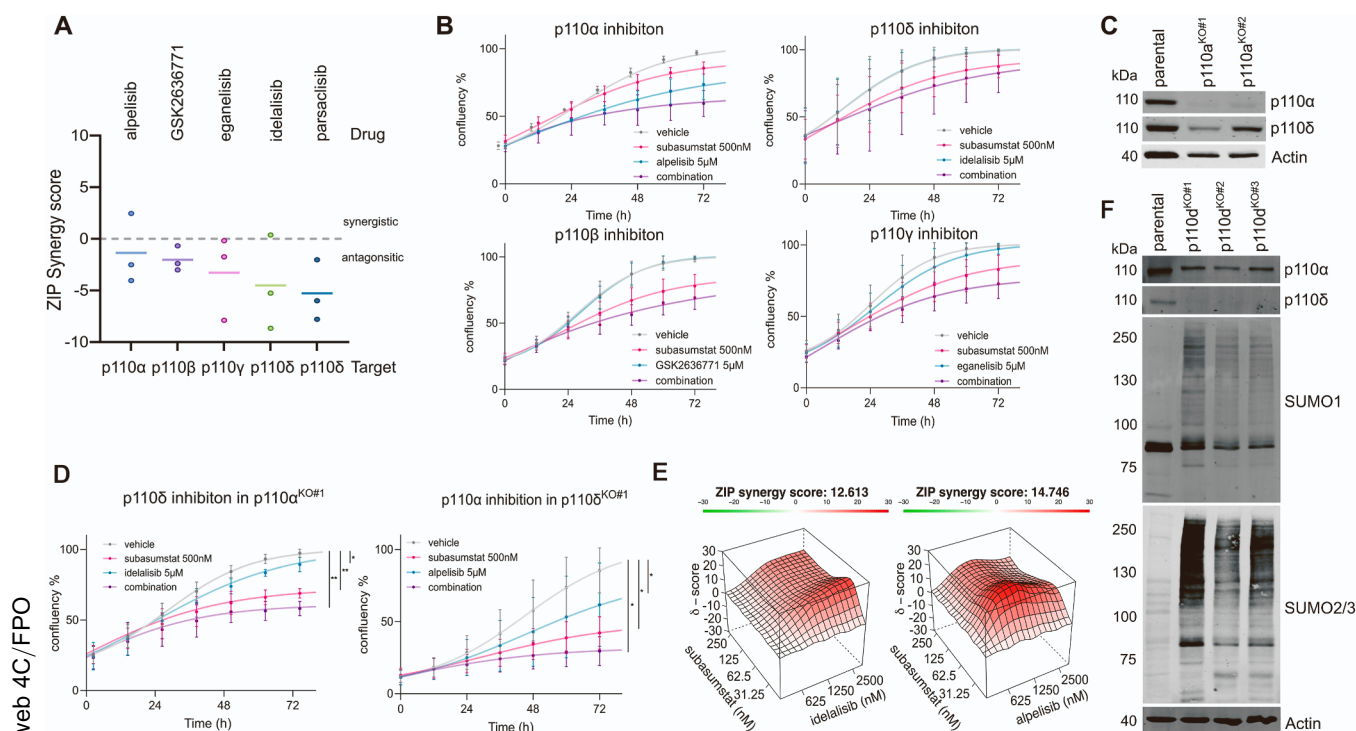


Figure 3. Double targeting of PI3K α /PI3K δ and SUMOylation induces synthetic interaction. (A) Zero Interaction Potency (ZIP) synergy scores upon combination of subasumstat and indicated PI3K inhibitors in MiaPaCa-2. Cells were treated with single and combination treatments using a 4 \times 5 matrix. Cell confluency was assessed after 96 hours, and clonogenic assay quantification was imaged. Synergy score was determined by SynergyFinder using the ZIP method (n = 3). (B) Proliferation of MiaPaCa-2 supplemented with 500 nmol/L subasumstat, 5 μ mol/L of indicated PI3K-specific inhibitors, or the combination of both. Cell confluency data were obtained by live cell imaging (12-hour intervals over 72 hours; n = 3). The range bars designate standard deviation. (C) Immunoblot analysis of p110 α / δ expression in MiaPaCa-2 harboring a CRISPR/Cas9-mediated PI3K α -de(p)letion. (D) Proliferation of p110 α -depleted MiaPaCa-2 supplemented with 500 nmol/L subasumstat, 5 μ mol/L idelalisib, or the combination (left), and p110 δ -depleted MiaPaCa-2 supplemented with 500 nmol/L subasumstat, 5 μ mol/L alpelisib, or the combination (right). Cell confluency data were obtained by live cell imaging (12-hour intervals over 72 hours; n = 3). **P < .01 by analysis of variance. The range bars designate standard deviation. (E) Landscape plots depict the synergistic area of concentrations of idelalisib and subasumstat combination treatment in p110 α -de(p)leted MiaPaCa-2 treated for 96 hours (left) and of concentrations of alpelisib and subasumstat combination treatment in p110 δ -depleted MiaPaCa-2 treated for 96 hours (right). Data (n = 3) were obtained by confluency measurement. (F) Immunoblot analysis of indicated proteins in MiaPaCa-2 harboring a CRISPR/Cas9-mediated PI3K δ -de(p)letion.

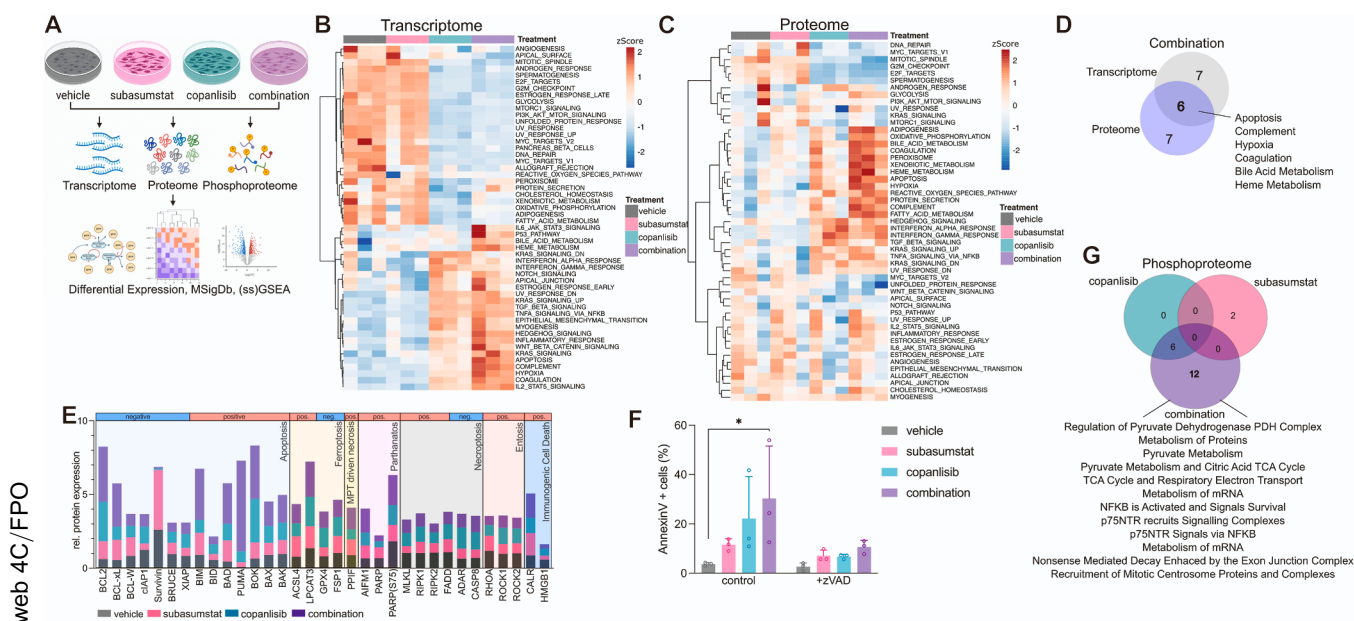
and other regulated cell death (RCD) modes (Figure 4E). Because we observed a trend for the regulation of proteins favoring apoptosis, we stained for cleaved caspase 3 and performed annexin-V/propidium iodide fluorescence-activated cell sorter. We observed an increase of cleaved caspase 3 (Supplementary Figure 4A) and annexin-V-positive cells upon combination treatment, which was blocked by a pan-caspase inhibitor (Figure 4F). However, the sole induction of apoptosis, which was relatively mild compared with the strong synergism observed, does not fully account for the cell-death mode. Analyses of cell-cycle profiles did not provide additional insights into the mode of action of the synergistic effects in the combination treatment (Supplementary Figure 4B). Considering the functional impact of SUMOylation on protein function and stability, we next investigated signatures and signaling pathways regulated at the protein level only. Applying phosphoproteomics, we identified that the SUMO α -PI3K inhibitor (PI3ki) combination specifically altered metabolic pathways, messenger RNA metabolism, and mitotic

regulation (Figure 4G), suggesting that affecting such pathways contribute to the strong synergism.

In summary, these data identified a multimodal induction of RCD by the combined inhibition of the PI3K α / δ and SUMOylation pathways.

Inhibition of PI3K α / δ and SUMO Signaling Impairs Growth in Patient-Derived Organoids

To validate the efficacy of combined PI3K α / δ -SUMO inhibition in advanced human model systems, we performed drug testing in 5 genetically and phenotypically characterized epithelial-like and mesenchymal-like PDOs with different activity of pathways associated with the mesenchymal subtype (Figure 5A and B). We tested their response toward FOLFIRINOX (folinic acid, fluorouracil, irinotecan, and oxaliplatin) (Figure 5C) and the PI3K α / δ - and SUMO-inhibition (pictilisib/subasumstat) combination treatment (Figure 5D). Of note, PDOs associated with mesenchymal transcriptomic features



displayed poor response in the SOC treatment but an improved response in the pictilisib/subasumstat combination treatment compared with epithelial-like PDOs (Figure 5C and D). By GSEA we identified significant enrichments of SUMOylation signatures in responder PDOs associated with mesenchymal transcriptomic features (Figure 5E).

Next, we used in situ resistance assays¹⁹ to assess viability after long-term treatment with monotherapy or combination therapy over a 5-week period. Outgrowth was defined on a confluence threshold of >50%, which was considered indicative of therapy failure. Cells treated with monotherapy exhibited outgrowth after 3 to 4 weeks, respectively (Figure 5F). In contrast, PI3K α/δ -SUMO combination therapy resulted in a pronounced loss of confluence, with >90% of cultures deemed nonviable by week 4 to 5 (Figure 5F).

In summary, the PI3K α/δ -SUMO-targeted combination therapy demonstrated efficacy in PDOs and in long-term assays.

Combined PI3K α/δ and SUMO Targeting Acts by Licensing the Antitumor Immune Response

We next investigated the PI3K α/δ -SUMO combination therapy in MiaPaCa-2 xenografts to translate our findings into an in vivo model. We observed a reduced tumor

volume in combination-treated xenografts compared with monotherapy (Supplementary Figure 5).

Subasumstat treatment induced multifaceted immune effects.^{17,37,38} Gene ontology biological process GSEA indicates up-regulated major histocompatibility complex-I and antigen processing and presentation upon combination treatment in MiaPaCa-2 (Figure 6A and B). Therefore, to investigate whether efficacy of combined PI3K α/δ -SUMO was different in an immune-competent model and whether PI3K α/δ -SUMO targeting could be associated with an antitumor response, we generated syngeneic orthotopic tumor grafts (Figure 6C). Here PI3K α/δ -SUMO treatment in a dose-escalation schedule exhibited significant effects on tumor growth compared with control treatments (Figure 6D). To investigate the effects of combined PI3K α/δ -SUMO treatment on tumor and immune dynamics, cyclic immunofluorescence (cycIF) was performed using the T-cell markers cluster of differentiation (CD) 3, CD4, CD8, and programmed cell death protein 1. This analysis revealed an increased infiltration of CD3⁺ T cells (Figure 6E). Because we did not observe significant differences in CD4⁺ or CD8⁺ T-cell infiltration, immune histochemical analysis of CD3⁺ T-cell infiltration was additionally performed, which confirmed the cycIF findings (Figure 6F).

Next, to investigate the complete landscape of therapy-induced reprogramming of the tumor microenvironment (TME), we analyzed tumor samples from all groups by

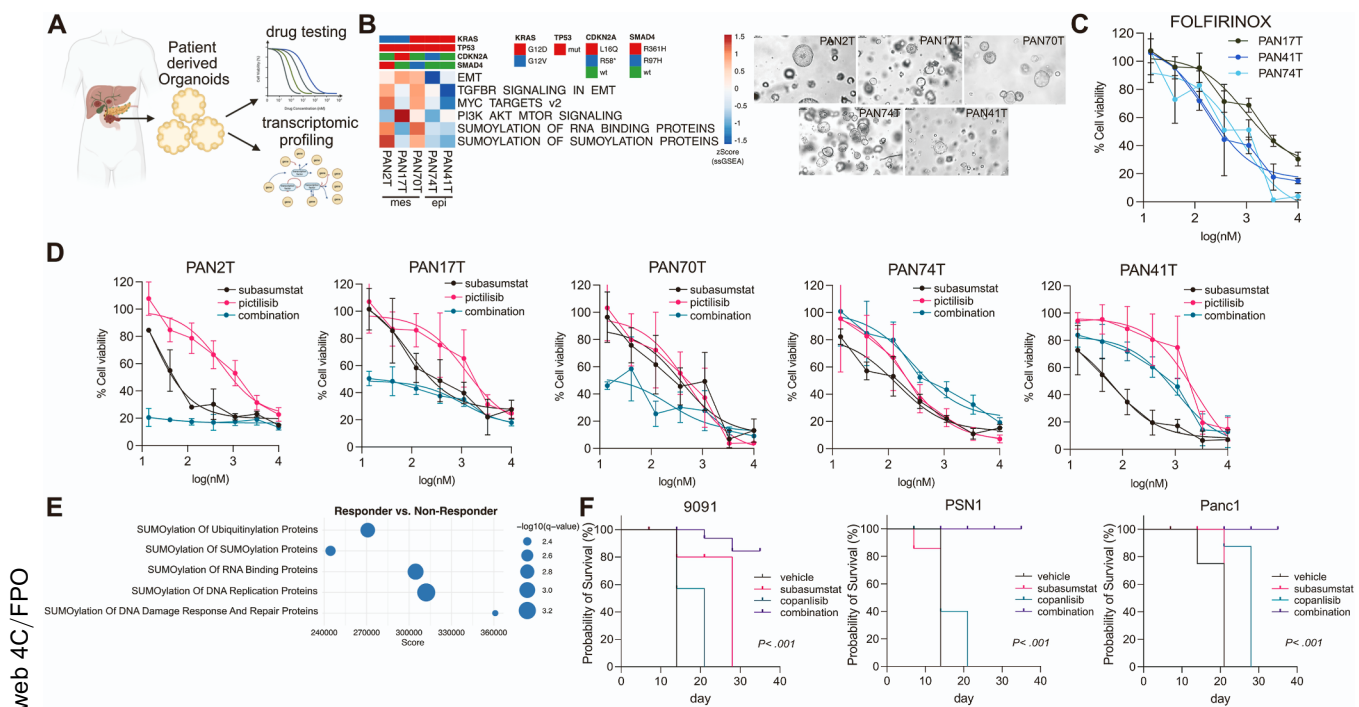


Figure 5. PDOs and in situ resistant assays reveal reduced tumor cell growth upon PI3K α/δ and SUMO inhibition. (A) PDOs from 5 patients with PDAC were isolated and used for drug testing and transcriptomic profiling (schematic overview). (B) Left: Mutation status of *KRAS*, *CDKN2A*, *TP53*, and *SMAD4*, and GSEA of indicated PDOs. PAN2T, PAN17T, and PAN70T display mesenchymal-like features (mes); PAN41T and PAN74T display epithelial-like features (epi). Right: Representative phase-contrast images (similar magnification) of PDOs. EMT, epithelial-mesenchymal transition. (C) Cell viability, measured by adenosine triphosphate quantification (CellTiter-Glo) 96 hours after treatment with indicated concentrations of FOLFIRINOX (folinic acid, fluorouracil, irinotecan, and oxaliplatin) mes and epi PDOs ($n = 3$). (Original magnification, 20 \times objective.) (D) Cell viability of PDOs supplemented for 96 hours with subasumstat (10 nmol/L), pictilisib (indicated concentration), or the combination of both measured by adenosine triphosphate quantification (CellTiter-Glo) ($n = 3$). The range bars designate standard deviation. (E) GSEA (Reactome) of transcriptome data depicts increased SUMOylation signatures in mes-PDOs (responder), compared with nonresponding epi-PDOs. (F) In situ resistance assay in mesenchymal murine PDAC cell line 9091PPT and the 2 basal-like human PDAC cell lines PSN1 and Panc1. Log-rank P value is indicated.

snRNAseq (Figure 6G and Supplementary Figure 6A and B). Here, we observed increased expression of cycling and cytotoxic T cells, indicating T-cell activation, although surface CD8 detection may be reduced posttranscriptionally (Figure 6G and H and Supplementary Figure 6C). We found that PI3K α/δ -SUMOi combination treatment significantly induced transcriptional activation of *Xcl1* and *Il18r1* in T cells, suggesting enhanced effector function (Figure 6I). In support, cyclF revealed a significant increase in CD3⁺CD8⁺CCL5⁺ (chemokine ligand 5) and CD3⁺CD8⁺Ki67⁺ cells, compatible with elevated cytotoxic activity and T-cell proliferation (Figure 6J). These findings point to a PI3K α/δ -SUMOi combination-induced amplification of T-cell phenotypes associated with antitumor immunity.

Macrophage profiling revealed a shift from immunosuppressive M2-like macrophages to antigen-presenting tumor-associated macrophages (Figure 6K and L and Supplementary Figure 6D), compatible with a TME with enhanced antitumor immunity.³⁹ Additionally, cyclF showed up-regulation of chemokine ligand 5, a chemokine known to recruit effector T cells, natural killer cells, dendritic cells, and monocytes into the TME (Figure 6M).⁴⁰ In

line with our cell culture-based data, we observed an augmented induction of interferon- α/γ and apoptosis pathways in tumor cells treated with the combination therapy in vivo (Supplementary Figure 6E).

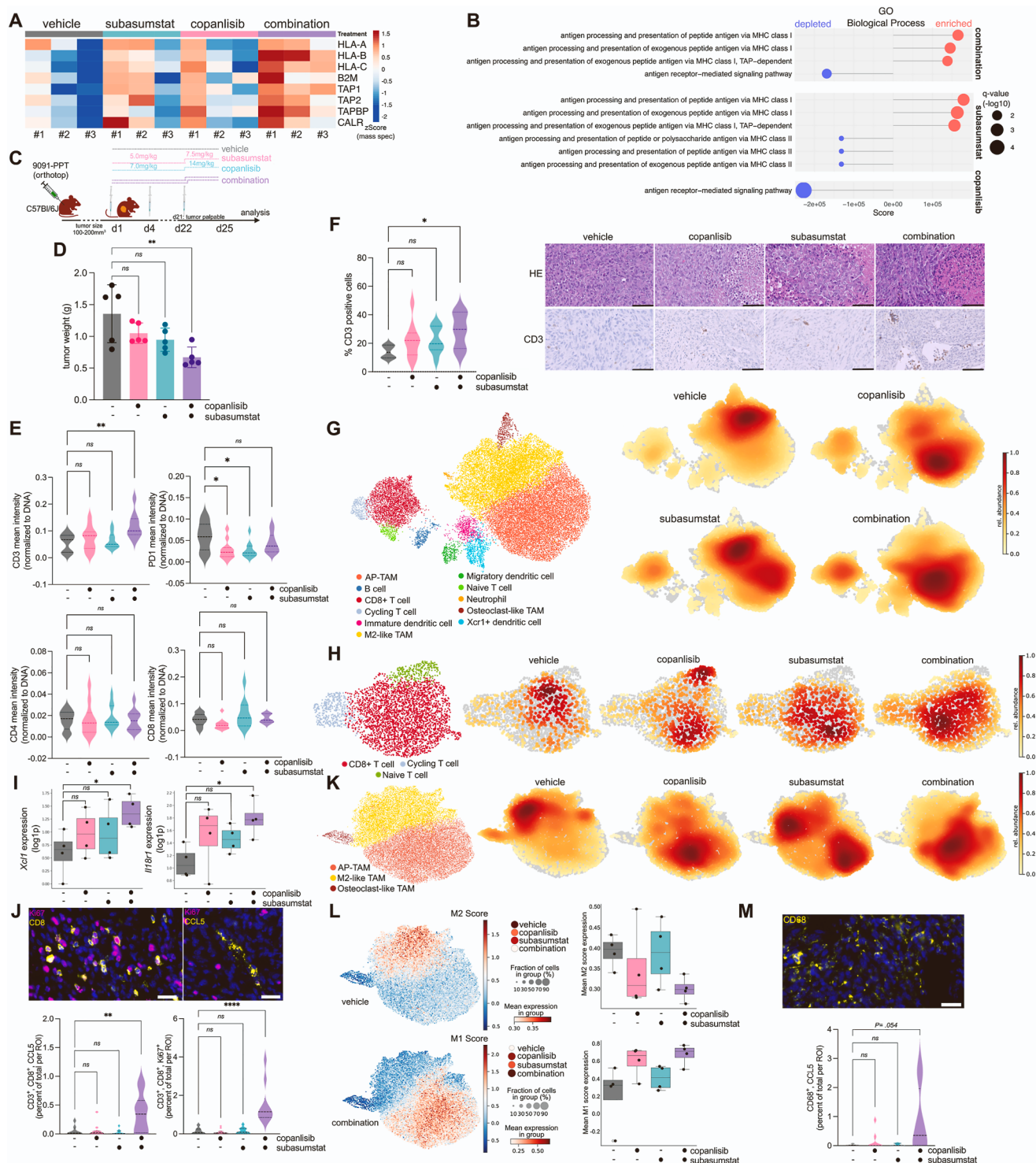
Preliminary shallow analysis of toxicity regarding hematologic, liver, or kidney effects revealed no signals for PI3K α/δ -SUMOi combination therapy in the investigated mouse cohorts (Supplementary Figure 7).

Together, these findings indicate that the combination therapy of SUMOi and PI3K α/δ modulates the TME to favor immune-mediated tumor-cell killing, predominantly involving cytotoxic T cells and antigen-presenting macrophages.

Discussion

The analysis of genome-wide PI3Ki-CRISPR resistance screens²⁷ and our genome-wide SUMOi-CRISPR and drug screens led to the identification of PI3K α/δ -SUMO targeting as a novel treatment strategy for PDAC. Our study reveals that mesenchymal/basal-like PDACs exhibit a mutual co-dependence on PI3K signaling and the SUMOylation pathway. By targeting both pathways, we achieved

Direct targeting PI3Ks is a treatment strategy in PDAC worth considering.⁸ Our data confirm the connection between the PI3K pathway and basal-like/mesenchymal PDACs previously reported.⁴¹ Importantly, PI3K α is an important positive effector of oncogenic KRAS.⁴² The interconnection of these 2 oncogenic signaling nodes is also evident in PDAC tumorigenesis, where PIK3 α , but not



PIK3 β , is an essential mediator of oncogenic KRAS signaling. Furthermore, oncogenic PIK3 α is crucial for maintenance and metastatic progression of PDAC.^{5,6,41,43,44} The observation that survival of PDAC cells genetically lacking KRAS is largely dependent on PI3K signaling²⁶ additionally emphasizes the pertinency of the PI3K pathway as a therapeutic target. In contrast to PI3K α , the role of other class I PI3Ks in PDAC remains complex and is less well understood.

Immunohistochemistry demonstrated the expression of PI3K γ in most of the investigated human PDAC cases, and knockout of the *PI3K γ* gene delayed tumor development in murine PDAC models, involving nonautonomous mechanisms.^{45–47} Furthermore, PDAC cells with mutated KRAS^{G12R}, which cannot interact with PI3K α , overexpress and depend on PI3K γ to induce micropinocytosis, a pathway that fuels the cancer cell's metabolic demands.⁴⁸ Protein abundance of PI3K δ is up-regulated in tumor-enriched PDAC samples.⁴⁹ We demonstrate that the synergy of the SUMO and the PI3K pathway inhibition depend on specifically blocking PIK3 α and PI3K δ signaling. Thus, rational and specific inhibitor selection is needed to fully exploit PI3K inhibition in a specific context as shown here for the combination with SUMO targeting.

Recent studies by us and others have shown that the SUMOylation machinery is a putatively relevant therapeutic target in PDAC, and a highly potent and specific clinical

grade SUMO E1 inhibitor has been evaluated in the clinic.^{16,17,36} Concurrent with the activity of the PI3K pathway in basal-like PDACs, we observed increased expression of the core SUMOylation machinery in this subtype. The observed global/group protein SUMOylation upon PI3K inhibition appears consistent with cellular stress responses seen under conditions such as DNA damage or heat shock, where similar widespread SUMOylation shifts were identified.⁵⁰ This phenotype may reflect an adaptive or compensatory signaling mechanism engaged by cells to mitigate the disruption of homeostasis caused by PI3K pathway blockade. Our findings thus support the growing view that group SUMOylation plays a role in orchestrating broad stress-response programs, potentially as a protective means to buffer therapeutic stress.⁵¹

Importantly, inhibition of both the SUMO and the PI3K pathways resulted in activation of the other pathway, possibly as a mechanism to cope with various stresses, creating a therapeutically exploitable vulnerability and synthetic lethality. As shown previously, activation of SUMOylation confers a selective advantage against various stresses, contributing to cellular resilience against oncogenic, hypoxic, therapeutic, or oxidative stress.⁵² Combined PI3K and SUMO inhibition induced multimodal effects and therapeutic synergism, with disruption of cell survival signaling and an RCD pattern reflecting features of oxidative stress-associated cell death.

Figure 6. Enhanced efficacy of combined subasumstat and copanlisib treatment in immunocompetent mice. (A) Analysis of mass spectrometry data from MiaPaCa-2 cells treated with subasumstat (200 nmol/L), copanlisib (1000 nmol/L), combination, or dimethyl sulfoxide as vehicle control ($n = 3$, each condition), reveals a significant induction of major histocompatibility complex (MHC)-I-associated proteins expression upon combination treatment. B2M, β_2 microglobulin; CALR, calreticulin; HLA, human leukocyte antigen; TAP, transporter associated with antigen processing; TAPBP, TAP binding protein. (B) GSEA (gene ontology [GO]/biological process) indicates up-regulated MHC-I and antigen processing and presentation upon combination treatment in MiaPaCa-2. (C) Experimental setup to investigate the combination treatment in orthotopic PDAC tumors (D–M). Mesenchymal 9091PPT cells were orthotopically transplanted. Mice were treated with vehicle, subasumstat, copanlisib, or the combination with the indicated schedule. (D) Tumor burden was measured over time and shows significantly decreased volume in response to combination therapy ($n = 5$ mice, each cohort). $^{**}P < .01$ by analysis of variance (ANOVA) with Tukey's post hoc test; ns, not significant. (E) Quantification of indicated markers normalized to DNA (4',6-diamidino-2-phenylindole) show significantly increased CD3 $^{+}$ T-cell infiltration upon combination treatment, without significant change in CD4 $^{+}$, CD8 $^{+}$ and programmed cell death protein 1 (PD1 $^{+}$) cells. Dark dashed lines inside the violin plot indicate the median, light dashed lines indicate the interquartile range. P value determined by analysis of variance (ANOVA) with Tukey's post hoc test (bottom). (F) Representative images of histologic hematoxylin-eosin (HE) stains and immune histochemical analysis for CD3 expression of tissue sections of tumors from orthotopically transplanted mice. Scale bars, 50 μ mol/L (right). CD3 quantification in 5 mice ($n = 5$ high-power fields each). P value determined by ANOVA with Tukey's post hoc test (left). (G) snRNAseq of tumors from orthotopically transplanted mice treated with vehicle, subasumstat, copanlisib, or the combination. Uniform Manifold Approximation and Projection (UMAP) colored according to cell types (left). Visualization of the cell density within each cohort (embedding density estimation). (H) UMAP colored according to T-cell phenotype (left). Visualization of the cell density within each condition (embedding density estimation). (I) Mean expression of *Xcl1* and *Il18r1* in T-cell cluster per pseudobulk expression. P values are based on pseudobulk differential expression genes. (J) Representative images of tissue sections of tumors from orthotopically transplanted mice upon treatment, labeled with 4',6-diamidino-2-phenylindole (DAPI), Ki67, CD8, or chemokine ligand 5 (CCL5). Scale bars, 200 μ m–20 μ m (top). P value determined by ANOVA with Tukey's post hoc test (bottom). (K) UMAP colored according to macrophage phenotype (left). Visualization of the cell density within each condition, using embedding density estimation. (L) M2 score (top) M1 score (bottom) expression in the macrophage cluster upon no, monotreatment, or combination treatment. Left: UMAP plots for vehicle and combination treatment. Center: M2/M1 scores of all treatment groups. Right: Individual M1/M2 scores of the mean of each tumor. Box and whisker plot: The boxes indicate the 25th percentile (bottom border), median (center line), and 75th percentile (top border), the whiskers show the maximum and minimum ranges, and the circles indicate outliers. (M) Representative image of tissue sections of tumors from orthotopically transplanted mice upon treatment, labeled with DAPI and CD68, Scale bars, 200 μ m–20 μ m (top). Bottom: Quantification of CCL5 in CD68 $^{+}$ cells. ROI, region of interest. P value determined by ANOVA with Tukey's post hoc test.

Despite the withdrawal of approval for the PI3K α / δ -inhibitor copanlisib for relapsed indolent non-Hodgkin lymphoma after the Study of Copanlisib in Combination With Standard Immunochemotherapy in Relapsed Indolent Non-Hodgkin's Lymphoma (iNHL) (CHRONOS-4) phase 3 trial,⁵³ copanlisib demonstrated some clinical activity in PIK3CA-mutated cancer in the National Cancer Institute Molecular Analysis for Therapy Choice (NCI-'MATCH) Eastern Cooperative Oncology Group–American College of Radiology Imaging Network trial with a manageable toxicity profile,⁵⁴ pointing to the clinical potential of PI3K α / δ inhibitors when applied as a principle.

PI3K α / δ i-SUMOi combination therapy enhanced recruitment of CD3⁺ T cells in vivo in immunocompetent mice. After combination therapy, our snRNAseq analysis revealed robust expression of both CD4 and CD8 transcripts in tumor-infiltrating T cells, despite the absence of corresponding protein expression in some cases. This discrepancy suggests that the negative phenotype seen in cycIF and immune histochemical analysis may stem from transcriptionally active but protein-low or protein-suppressed cells, rather than representing a true expansion of double-negative T cells (DNTs). Although PI3K α / δ i-SUMOi-induced DNTs were associated with antitumor effects and changes in the TME in our in vivo model, other DNTs can promote cancer progression through immunosuppressive actions that support tumor growth and evade immune responses.⁵⁵ The anticancer properties of the DNTs could be induced by induction of immunogenic cell death,⁵⁶ and we show that RCD is activated in response to PI3K α / δ i-SUMOi combination therapy in in vitro studies. SUMO inhibition in vivo activated various immune cell subsets and reprogrammed the tumor immune microenvironment to induce an antitumor adaptive response.^{17,57} We here found that PI3K α / δ i-SUMOi combination treatment was specifically associated with a molecular switch from protumorigenic M2-like macrophages to antitumorigenic antigen-presenting macrophages. Together our data thus indicate a multimodal reprogramming of the TME toward a less tumor-permissive state upon PI3K α / δ i-SUMOi combination treatment. Furthermore, SUMOi generated an up-regulation of major histocompatibility complex I expression.³⁷

These established immune-modulatory effects of SUMO pathway inhibition might thus be amplified and beneficial when targeting PDAC with more effective rationale, molecularly targeted strategies such as combined PI3K α / δ -SUMO inhibition. This mode of action of subasumstat also favors the combination with PI3Kis, given their broad impact on both intrinsic tumor survival pathways and the immune landscape.^{8,58} PI3K α / δ i has been shown to modulate immune suppression within the TME, which may enhance the efficacy of immunotherapy-based approaches⁵⁹ that have been insufficiently effective in PDAC.⁶⁰ In this context, it is important that subasumstat generated a feed-forward loop by simultaneous activation of cytotoxic T cells and induction of the antigen-presenting machinery in PDAC and other tumor entities.^{17,37}

Conclusion

In summary, we here reveal the mutual codependency between the SUMOylation machinery and the PI3K pathway that warrants further development toward clinical application. In addition to synthetic lethal effects induced on tumor cells, the PI3K α / δ i-SUMOi combination therapy induced affected immune cell subsets and resulted in the complex reprogramming of the TME to an antitumorigenic state in vivo. Our findings could serve as a novel path toward already available but heretofore unsuccessful immunotherapy strategies for PDAC.

Supplementary Material

Note: To access the supplementary material accompanying this article, visit the online version of *Gastroenterology* at www.gastrojournal.org, and at <https://doi.org/10.1053/j.gastro.2025.08.018>.

References

1. Buckley CW, O'Reilly EM. Next-generation therapies for pancreatic cancer. *Expert Rev Gastroenterol Hepatol* 2024;18:55–72.
2. Halbrook CJ, Lyssiotis CA, Pasca di Magliano M, et al. Pancreatic cancer: advances and challenges. *Cell* 2023;186:1729–1754.
3. Singhal A, Li BT, O'Reilly EM. Targeting KRAS in cancer. *Nat Med* 2024;30:969–983.
4. Dilly J, Hoffman MT, Abbassi L, et al. Mechanisms of resistance to oncogenic KRAS inhibition in pancreatic cancer. *Cancer Discov* 2024;14:2135–2161.
5. Schonhuber N, Seidler B, Schuck K, et al. A next-generation dual-recombinase system for time- and host-specific targeting of pancreatic cancer. *Nat Med* 2014;20:1340–1347.
6. Eser S, Reiff N, Messer M, et al. Selective requirement of PI3K/PDK1 signaling for Kras oncogene-driven pancreatic cell plasticity and cancer. *Cancer Cell* 2013;23:406–420.
7. Li H, Wen X, Ren Y, et al. Targeting PI3K family with small-molecule inhibitors in cancer therapy: current clinical status and future directions. *Mol Cancer* 2024;23:164.
8. Conway JR, Herrmann D, Evans TJ, et al. Combating pancreatic cancer with PI3K pathway inhibitors in the era of personalised medicine. *Gut* 2019;68:742–758.
9. He Y, Sun MM, Zhang GG, et al. Targeting PI3K/Akt signal transduction for cancer therapy. *Signal Transduct Target Ther* 2021;6:425.
10. Andre F, Ciruelos E, Rubovszky G, et al. Alpelisib for PIK3CA-mutated, hormone receptor-positive advanced breast cancer. *N Engl J Med* 2019;380:1929–1940.
11. Mateo J, Ganji G, Lemech C, et al. A first-time-in-human study of GSK2636771, a phosphoinositide 3 kinase beta-selective inhibitor, in patients with advanced solid tumors. *Clin Cancer Res* 2017;23:5981–5992.

12. Hong DS, Postow M, Chmielowski B, et al. Eganalisib, a first-in-class PI3Kgamma Inhibitor, in patients with advanced solid tumors: results of the phase 1/1b MARIO-1 Trial. *Clin Cancer Res* 2023; 29:2210–2219.
13. Borazanci E, Pishvaian MJ, Nemunaitis J, et al. A phase Ib study of single-agent idelalisib followed by idelalisib in combination with chemotherapy in patients with metastatic pancreatic ductal adenocarcinoma. *Oncologist* 2020;25:e1604–e1613.
14. Yue EW, Li YL, Douty B, et al. INCB050465 (parsaclisib), a novel next-generation inhibitor of phosphoinositide 3-kinase delta (PI3Kdelta). *ACS Med Chem Lett* 2019; 10:1554–1560.
15. Seeler JS, Dejean A. SUMO and the robustness of cancer. *Nat Rev Cancer* 2017;17:184–197.
16. Biederstadt A, Hassan Z, Schneeweis C, et al. SUMO pathway inhibition targets an aggressive pancreatic cancer subtype. *Gut* 2020;69:1472–1482.
17. Kumar S, Schoonderwoerd MJA, Kroonen JS, et al. Targeting pancreatic cancer by TAK-981: a SUMOylation inhibitor that activates the immune system and blocks cancer cell cycle progression in a preclinical model. *Gut* 2022;71:2266–2283.
18. Tapia Contreras C, Falke JD, et al. KRAS(G) (12C)-inhibitor-based combination therapies for pancreatic cancer: insights from drug screening. *Mol Oncol* 2025; 19:295–310.
19. Sealover NE, Theard PT, Hughes JM, et al. In situ modeling of acquired resistance to RTK/RAS-pathway-targeted therapies. *iScience* 2024;27:108711.
20. Wu DM, Zhang T, Liu YB, et al. The PAX6-ZEB2 axis promotes metastasis and cisplatin resistance in non-small cell lung cancer through PI3K/AKT signaling. *Cell Death Dis* 2019;10:349.
21. Rittler D, Baranyi M, Molnar E, et al. The antitumor effect of lipophilic bisphosphonate BPH1222 in melanoma models: the role of the PI3K/Akt pathway and the small G protein Rheb. *Int J Mol Sci* 2019;20:4917.
22. Chen Y, Wang T, Du J, et al. The critical role of PTEN/PI3K/AKT signaling pathway in shikonin-induced apoptosis and proliferation inhibition of chronic myeloid leukemia. *Cell Physiol Biochem* 2018;47:981–993.
23. Singh H, Xiu J, Kapner KS, et al. Clinical and genomic features of classical and basal transcriptional subtypes in pancreatic cancer. *Clin Cancer Res* 2024; 30:4932–4942.
24. Mueller S, Engleitner T, Maresch R, et al. Evolutionary routes and KRAS dosage define pancreatic cancer phenotypes. *Nature* 2018;554:62–68.
25. Zhou X, An J, Kurilov R, et al. Persister cell phenotypes contribute to poor patient outcomes after neoadjuvant chemotherapy in PDAC. *Nat Cancer* 2023;4:1362–1381.
26. Muzumdar MD, Chen PY, Dorans KJ, et al. Survival of pancreatic cancer cells lacking KRAS function. *Nat Commun* 2017;8:1090.
27. Milton CK, Self AJ, Clarke PA, et al. A genome-scale CRISPR screen identifies the ERBB and UBA2 signaling networks as key determinants of response to PI3K inhibition in pancreatic cancer. *Mol Cancer Ther* 2020; 19:1423–1435.
28. Kunz K, Piller T, Muller S. SUMO-specific proteases and isopeptidases of the SENP family at a glance. *J Cell Sci* 2018;131.
29. Langston SP, Grossman S, England D, et al. Discovery of TAK-981, a first-in-class inhibitor of SUMO-activating enzyme for the treatment of cancer. *J Med Chem* 2021; 64:2501–2520.
30. Folkes AJ, Ahmadi K, Alderton WK, et al. The identification of 2-(1H-indazol-4-yl)-6-(4-methanesulfonylpiperazin-1-ylmethyl)-4-morpholin-4-yl-thieno[3,2-d]pyrimidine (GDC-0941) as a potent, selective, orally bioavailable inhibitor of class I PI3 kinase for the treatment of cancer. *J Med Chem* 2008;51:5522–5532.
31. Liu N, Rowley BR, Bull CO, et al. BAY 80-6946 is a highly selective intravenous PI3K inhibitor with potent p110alpha and p110delta activities in tumor cell lines and xenograft models. *Mol Cancer Ther* 2013; 12:2319–2330.
32. Matasar MJ, Capra M, Ozcan M, et al. Copanlisib plus rituximab versus placebo plus rituximab in patients with relapsed indolent non-Hodgkin lymphoma (CHRONOS-3): a double-blind, randomised, placebo-controlled, phase 3 trial. *Lancet Oncol* 2021; 22:678–689.
33. Morschhauser F, Machiels JP, Salles G, et al. On-target pharmacodynamic activity of the PI3K inhibitor copanlisib in paired biopsies from patients with malignant lymphoma and advanced solid tumors. *Mol Cancer Ther* 2020;19:468–478.
34. Yang Q, Modi P, Newcomb T, et al. Idelalisib: first-in-class PI3K delta inhibitor for the treatment of chronic lymphocytic leukemia, small lymphocytic leukemia, and follicular lymphoma. *Clin Cancer Res* 2015; 21:1537–1542.
35. Schild C, Wirth M, Reichert M, et al. PI3K signaling maintains c-myc expression to regulate transcription of E2F1 in pancreatic cancer cells. *Mol Carcinog* 2009; 48:1149–1158.
36. Schneeweis C, Hassan Z, Schick M, et al. The SUMO pathway in pancreatic cancer: insights and inhibition. *Br J Cancer* 2021;124:531–538.
37. Demel UM, Boger M, Yousefian S, et al. Activated SUMOylation restricts MHC class I antigen presentation to confer immune evasion in cancer. *J Clin Invest* 2022; 132:e152383.
38. Lightcap ES, Yu P, Grossman S, et al. A small-molecule SUMOylation inhibitor activates antitumor immune responses and potentiates immune therapies in preclinical models. *Sci Transl Med* 2021;13:eaba7791.
39. Rannikko JH, Hollmen M. Clinical landscape of macrophage-reprogramming cancer immunotherapies. *Br J Cancer* 2024;131:627–640.
40. Hu WT, Li M, Ma PJ, et al. A silence catalyst: CCL5-mediated intercellular communication in cancer. *Arch Toxicol* 2025;99:2699–2712.
41. Thibault B, Ramos-Delgado F, Pons-Tostivint E, et al. Pancreatic cancer intrinsic PI3Kalpha activity

- accelerates metastasis and rewires macrophage component. *EMBO Mol Med* 2021;13:e13502.
42. Gupta S, Ramjaun AR, Haiko P, et al. Binding of ras to phosphoinositide 3-kinase p110alpha is required for ras-driven tumorigenesis in mice. *Cell* 2007;129:957–968.
 43. Baer R, Cintas C, Dufresne M, et al. Pancreatic cell plasticity and cancer initiation induced by oncogenic Kras is completely dependent on wild-type PI 3-kinase p110alpha. *Genes Dev* 2014;28:2621–2635.
 44. Wu CY, Carpenter ES, Takeuchi KK, et al. PI3K regulation of RAC1 is required for KRAS-induced pancreatic tumorigenesis in mice. *Gastroenterology* 2014;147:1405–1416.e7.
 45. Edling CE, Selvaggi F, Buus R, et al. Key role of phosphoinositide 3-kinase class IB in pancreatic cancer. *Clin Cancer Res* 2010;16:4928–4937.
 46. Torres C, Mancinelli G, Cordoba-Chacon J, et al. p110gamma deficiency protects against pancreatic carcinogenesis yet predisposes to diet-induced hepatotoxicity. *Proc Natl Acad Sci U S A* 2019;116:14724–14733.
 47. Kaneda MM, Cappello P, Nguyen AV, et al. Macrophage PI3Kgamma drives pancreatic ductal adenocarcinoma progression. *Cancer Discov* 2016;6:870–885.
 48. Hobbs GA, Baker NMOL/L, Miermont AM, et al. Atypical KRAS(G12R) mutant is impaired in PI3K signaling and macropinocytosis in pancreatic cancer. *Cancer Discov* 2020;10:104–123.
 49. Cintas C, Douche T, Dantes Z, et al. Phosphoproteomics identifies PI3K inhibitor-selective adaptive responses in pancreatic cancer cell therapy and resistance. *Mol Cancer Ther* 2021;20:2433–2445.
 50. Psakhye I, Jentsch S. Protein group modification and synergy in the SUMO pathway as exemplified in DNA repair. *Cell* 2012;151:807–820.
 51. Enserink JM. Sumo and the cellular stress response. *Cell Div* 2015;10:4.
 52. Sheng Z, Zhu J, Deng YN, et al. SUMOylation modification-mediated cell death. *Open Biol* 2021;11:210050.
 53. Zinzani PL, Wang H, Feng J, et al. CHRONOS-4: phase 3 study of copanlisib plus rituximab-based immunotherapy in relapsed indolent B-cell lymphoma. *Blood Adv* 2024;8:4866–4876.
 54. Damodaran S, Zhao F, Deming DA, et al. Phase II study of copanlisib in patients with tumors with PIK3CA mutations: results from the NCI-MATCH ECOG-ACRIN Trial (EAY131) Subprotocol Z1F. *J Clin Oncol* 2022;40:1552–1561.
 55. Velikkakam T, Gollob KJ, Dutra WO. Double-negative T cells: setting the stage for disease control or progression. *Immunology* 2022;165:371–385.
 56. Ahmed A, Tait SWG. Targeting immunogenic cell death in cancer. *Mol Oncol* 2020;14:2994–3006.
 57. Erdem S, Lee HJ, Shankara Narayanan JSN, et al. Inhibition of SUMOylation induces adaptive antitumor immunity against pancreatic cancer through multiple effects on the tumor microenviro nmol/Lent. *Mol Cancer Ther* 2024;23:1597–1612.
 58. Sivaram N, McLaughlin PA, Han HV, et al. Tumor-intrinsic PIK3CA represses tumor immunogenicity in a model of pancreatic cancer. *J Clin Invest* 2019;129:3264–3276.
 59. Carnevalli LS, Sinclair C, Taylor MA, et al. PI3Kalpha/delta inhibition promotes anti-tumor immunity through direct enhancement of effector CD8(+) T-cell activity. *J Immunother Cancer* 2018;6:158.
 60. Brahmer JR, Tykodi SS, Chow LQ, et al. Safety and activity of anti-PD-L1 antibody in patients with advanced cancer. *N Engl J Med* 2012;366:2455–2465.

Received February 19, 2025. Accepted August 12, 2025.

Correspondence

Address correspondence to: Günter Schneider, MD, Department of Surgery, University Medical Center Göttingen, Robert-Koch-Str. 40, 37075 Göttingen, Germany. e-mail: gunter.schneider@med.uni-goettingen.de; or Ulrich Keller, MD, Department of Hematology, Oncology and Cancer Immunology, Campus Benjamin Franklin, Charité - Universitätsmedizin Berlin, Hindenburgdamm 30, 12203 Berlin, Germany. e-mail: ulrich.keller@charite.de; or Matthias Wirth, PhD, Department of Surgery, University Medical Center Göttingen, Robert-Koch-Str. 40, 37075 Göttingen, Germany, and Department of Hematology, Oncology and Cancer Immunology, Campus Benjamin Franklin, Charité - Universitätsmedizin Berlin, Hindenburgdamm 30, 12203 Berlin, Germany. e-mail: matthias.wirth@med.uni-goettingen.de.

Acknowledgments

The authors thank Judith-Achler Galitzki, Konstandina Isaakidis, Gerhild Fiolka, and Jennifer Appelhaus for their excellent technical assistance and express their gratitude to the Sartorius Corporate Research Department for the support of this research. Illustrations were created with [BioRender.com](https://www.biorender.com). Part of results shown are based on data generated by The Cancer Genome Atlas Research Network (<https://www.cancer.gov/tcga>). The authors thank the fluorescence-activated cell sorter core facility of the University Medical Center Göttingen (DFG project number 63915960).

CRedit Authorship Contributions

Hazal Köse, MSc (Conceptualization: Supporting; Data curation: Equal; Formal analysis: Equal; Funding acquisition: Supporting; Investigation: Equal; Methodology: Lead; Validation: Lead; Visualization: Equal; Writing – original draft: Supporting)
 Christian Schneeweis, PhD (Data curation: Equal; Investigation: Equal; Methodology: Supporting; Validation: Equal)
 Philipp Putze, MSc (Formal analysis: Equal; Methodology: Equal)
 Constanza Tapia Contreras, PhD (Data curation: Supporting; Formal analysis: Supporting; Investigation: Equal)
 Laura Ferreira, MSc (Data curation: Supporting; Formal analysis: Supporting; Investigation: Supporting; Validation: Supporting)
 Leonie Witte, PhD (Data curation: Supporting; Formal analysis: Supporting; Investigation: Supporting; Validation: Supporting)
 Ilaria Deidda, MSc (Data curation: Supporting; Formal analysis: Supporting; Investigation: Supporting; Validation: Supporting)
 Frederik Herzberg, MD (Formal analysis: Supporting; Methodology: Supporting)
 Sophie Ebert, MSc (Investigation: Supporting; Validation: Supporting)
 Juraj Jakubik, PhD (Formal analysis: Supporting; Methodology: Supporting)
 Leoni Moldaner, MSc (Formal analysis: Supporting; Methodology: Supporting)
 Jovan Todorovic, MD (Formal analysis: Supporting; Methodology: Supporting)
 Isabelle Träger, MD (Investigation: Supporting; Validation: Supporting)
 Chuanbing Zang, PhD (Investigation: Supporting; Validation: Supporting)
 Uta M. Demel, MD (Validation: Supporting), Elisabeth Hessmann, MD (Resources: Equal)
 Marieluise Kirchner, PhD (Formal analysis: Supporting; Investigation: Supporting; Methodology: Equal; Resources: Equal)
 Simone Rhein, PhD (Formal analysis: Equal; Methodology: Equal)
 Jens Hoffmann, PhD (Resources: Equal)
 Zuzana Tatarova, PhD (Formal analysis: Supporting; Methodology: Equal; Resources: Equal)
 Michael Ghadimi, MD (Resources: Equal)
 Dieter Saur, MD (Methodology: Supporting; Resources: Supporting)
 Kai Kappert, MD (Investigation: Supporting; Methodology: Supporting; Resources: Supporting)
 Philip Mertins, PhD (Methodology: Equal; Resources: Supporting)
 Günter Schneider, MD (Conceptualization: Equal; Funding acquisition: Equal; Resources: Equal; Supervision: Equal; Writing – original draft: Equal)
 Ulrich Keller, MD (Conceptualization: Equal; Funding acquisition: Equal; Project administration: Equal; Supervision: Equal; Writing – original draft: Equal)

Matthias Wirth, PhD (Conceptualization: Equal; Data curation: Equal; Formal analysis: Equal; Funding acquisition: Equal; Investigation: Equal; Project administration: Equal; Resources: Supporting; Supervision: Equal; Visualization: Lead; Writing – original draft: Equal)

Conflicts of interest

These authors disclose the following: Ulrich Keller received reimbursement for advisory board function, speaker honorarium, and travel support from Takeda for content unrelated to this manuscript. Hazal Köse, Ulrich Keller, Günter Schneider, and Matthias Wirth have filed a patent application related to aspects of this work (application number EP25189303.8, pending). The remaining authors disclose no conflicts.

Funding

This work was supported by funding from Deutsche Forschungsgemeinschaft (WI 6148/1-1 project number 529255113 to Matthias Wirth, KE 222/10-1 project number 494535244, KE 222/11-1 project number 58460329, and

German Research Foundation Excellence Strategy - EXC 3118/1 - project number 533770413 to Ulrich Keller, and CRU5002 to Günter Schneider and Elisabeth Hessmann), German Cancer Aid (70115444 to Matthias Wirth and 700111944, 70114724, and 70116097 to Ulrich Keller), Hector-Stiftung (M2408 to Matthias Wirth), Wilhelm-Sander-Stiftung (2017.048.2 to Ulrich Keller, Günter Schneider, and Matthias Wirth), SPARK-BIH (to Hazal Köse, Ulrich Keller, and Matthias Wirth), and Stiftung Charité (Ulrich Keller) and The German Cancer Consortium (Zuzana Tatarova).

Data Availability

All data generated in this study provided within the article and its supplementary data files are available via online repositories or upon request. RNA sequencing and single nuclei RNA sequencing data are deposited at European Nucleotide Archive, accession number ENA ID: PRJEB83901; proteomics data are available via PRIDE ID: PXD059116. [Supplementary Table 1](#) CRISPR beta scores. [Supplementary Table 2](#) drug screening data. All other raw data are available upon request from the corresponding authors.